

H<sub>2</sub>/H<sub>∞</sub> MIXED ROBUST CONTROLLER SYNTHESIS FOR A FIN ACTUATION SYSTEM

A THESIS SUBMITTED TO  
THE GRADUATE SCHOOL OF NATURAL AND APPLIED SCIENCES  
OF  
MIDDLE EAST TECHNICAL UNIVERSITY

BY

TUNCAY UĞURLU ÖLÇER

IN PARTIAL FULFILLMENT OF THE REQUIREMENTS  
FOR  
THE DEGREE OF MASTER OF SCIENCE  
IN  
MECHANICAL ENGINEERING

JANUARY 2013



Approval of the thesis:

**H<sub>2</sub>/H<sub>∞</sub> MIXED ROBUST CONTROLLER SYNTHESIS FOR A FIN ACTUATION SYSTEM**

Submitted by **TUNCAY UĞURLU ÖLÇER** in partial fulfillment of the requirements for the degree of **Master of Science in Mechanical Engineering Department, Middle East Technical University** by,

Prof. Dr. Canan ÖZGEN  
Dean, Graduate School of **Natural and Applied Sciences**

Prof. Dr. Suha ORAL  
Head of Department, **Mechanical Engineering**

Prof. Dr. R. Tuna BALKAN  
Supervisor, **Mechanical Engineering Dept., METU**

Prof. Dr. Bülent E. PLATİN  
Co-Supervisor, **Mechanical Engineering Dept., METU**

**Examining Committee Members:**

Prof. Dr. Y. Samim ÜNLÜSOY  
Mechanical Engineering Dept., METU

Prof. Dr. R. Tuna BALKAN  
Mechanical Engineering Dept., METU

Prof. Dr. Bülent E. PLATİN  
Mechanical Engineering Dept., METU

Asst. Prof. Dr. Yiğit YAZICIOĞLU  
Mechanical Engineering Dept., METU

Dr. Bülent ÖZKAN  
Mechatronics Division, TÜBİTAK SAGE

**Date** : \_\_\_\_\_

**I hereby declare that all information in this document has been obtained and presented in accordance with academic rules and ethical conduct. I also declare that, as required by these rules and conduct, I have fully cited and referenced all material and results that are not original to this work.**

Name, Last name : Tuncay Uğurlu ÖLÇER

Signature : \_\_\_\_\_

## ABSTRACT

### H<sub>2</sub>/H<sub>∞</sub> MIXED ROBUST CONTROLLER SYNTHESIS FOR A FIN ACTUATION SYSTEM

Ölcer, Tuncay Uğurlu

M.S., Department of Mechanical Engineering

Supervisor : Prof. Dr. R. Tuna BALKAN

Co-Supervisor : Prof. Dr. Bülent E. PLATİN

January 2013, 99 pages

In fin actuation systems, the performance of classical linear control systems is not satisfactory due to uncertainty of the system parameters and disturbances of the working medium. For this reason, sliding mode, H<sub>2</sub> or H<sub>∞</sub> robust controllers are widely used in literature for such systems. However, use of such controllers results in very conservative system responses. Based on this fact, in this thesis, development of a more effective robust controller is aimed via integration of the optimum properties of the existent pure H<sub>2</sub> and H<sub>∞</sub> type robust controllers. To achieve this, during the controller synthesizing procedure, some of the optimization parameters are weighted according to H<sub>2</sub> norm minimization, and parameter uncertainties and other variables are weighted according to H<sub>∞</sub> theorem. First, the system set up to be controlled is physically constructed and performed system identification processes. Then, two different types of robust controllers H<sub>2</sub> and H<sub>∞</sub> controllers are designed and tested over both the real system and simulation. Finally an H<sub>2</sub>/H<sub>∞</sub> mixed type controller synthesized and the results are compared with the outputs of the robust controllers of the previous step.

**Keywords:** Fin actuation systems, robust control, H<sub>2</sub>/H<sub>∞</sub> mixed robust control, system identification, *h2hinfsyn*

## ÖZ

### BİR KANAT TAHRIK SİSTEMİ İÇİN $H_2/H_\infty$ TÜMLEŞİK GÜRBÜZ KONTROLCÜ SENTEZİ

Ölcer, Tuncay Uğurlu

Yüksek Lisans, Makina Mühendisliği Bölümü

Tez Yöneticisi : Prof. Dr. R. Tuna BALKAN

Ortak Tez Yöneticisi : Prof. Dr. Bülent E. PLATİN

Ocak 2013, 99 sayfa

Kanat tahrik sistemlerinde, sistem değişkenlerindeki belirsizlikler, bozucu etkiler ve ortamda var olan gürültüler sebebiyle, klasik doğrusal kontrol sistemlerinin başarımı yeterli olmamaktadır. Bu sebeple, bu sistemlerde, kayan kipli,  $H_2$  veya  $H_\infty$  tipi gürbüz kontrolcüler yaygın olarak kullanılmaktadır. Ancak bu kontrolcü mekanizmalarının kullanımı aşırı ihtiyatlı sistem cevapları ortaya çıkarmaktadır. Bundan dolayı bu çalışmada, var olan  $H_2$  ve  $H_\infty$  tipi gürbüz kontrolcülerin en iyi özelliklerinin ayrı ayrı alınarak tümleştirilmesi ve daha verimli bir kontrol sistemi geliştirilmesi amaçlanmıştır. Bu amaçla, kontrolcü tasarım çalışmalarında, birtakım eniyileme değişkenleri  $H_2$  normu üzerinden ağırlıklarılarak ele alınırken, diğer değişkenler ile sistem değişkenlerindeki belirsizlikler  $H_\infty$  teoremleri kullanılarak ağırlıklandırılmıştır. İlk olarak denetimi yapılacak sistem fiziksel olarak oluşturulmuş ve üretilip çalıştırılan bu sistem üzerinden sistem tanımlama çalışmaları gerçekleştirilmiştir. Daha sonra,  $H_2$  ve  $H_\infty$  olmak üzere iki tip gürbüz kontrolcü tasarlanarak hem gerçek sistem hem de benzetimler üzerinde denenmiştir. Son aşamada ise  $H_2/H_\infty$  tümleşik tip gürbüz kontrolcü sentezi yapılarak elde edilen sonuçlar bir önceki aşamada denenen kontrolcü çıktıları ile karşılaştırılmıştır.

**Anahtar kelimeler:** Kanat tahrik sistemleri, gürbüz kontrol,  $H_2/H_\infty$  tümleşik gürbüz kontrol, sistem tanımlama, *h2hiefsyn*

THIS WORK IS DEDICATED TO

**MUSTAFA KEMAL ATATÜRK**

**(1881-193<sup>∞</sup>)**

“Science is the most genuine guide in life.”

## **ACKNOWLEDGEMENTS**

I would like to express my appreciation to my supervisors Prof. Dr. R. Tuna BALKAN and Prof. Dr. Bülent E. PLATİN for their helpful criticism, guidance and patience in the progress and preparation of this thesis.

I want to send my thanks to my colleagues Dr. İ. İlker DELİCE, Dr. Alper AKMEŞE, Dr. G. Serdar TOMBUL, Mete AYDEMİR and my head of division Dr. Bülent ÖZKAN for their technical support and guidance, endless help and patience during the execution of experimental studies and the edition of this thesis. I also specially thank to Dr. Erdinç N. YILDIZ for his encouragements to this topic and advices on controller design.

The support and facilities of TÜBİTAK SAGE especially in the preparation and application of experimental studies are gracefully appreciated.

I am very grateful to all members of my family for their endless support not only during my thesis preparation, but also throughout my life.

Finally I would like to thank to my great love and future wife Özlem. She is the source of my all motivation and energy, I adore her. Without her endless support, I could not finish this work.

## TABLE OF CONTENTS

ABSTRACT .....	v
ÖZ .....	vi
ACKNOWLEDGEMENTS .....	viii
TABLE OF CONTENTS .....	ix
LIST OF FIGURES .....	xii
LIST OF TABLES .....	xiv
CHAPTERS .....	1
1. INTRODUCTION.....	1
1.1. AIM OF THE STUDY .....	1
1.2. DESCRIPTION OF PROBLEM AND SCOPE OF THE THESIS .....	1
1.3. BACKGROUND AND BASIC CONCEPTS.....	2
1.3.1. A Brief History of the Control Theory .....	2
1.3.2. Basic Concepts in Robust Control .....	3
1.3.2.1. Feedback Loop and Generalized Plant .....	3
1.3.2.1. Stability and Internal Stability.....	5
1.3.2.2. Norms of Signals and Systems .....	5
1.3.2.3. Sensitivity, Robustness and Disturbance Rejection .....	6
1.3.2.4. Plant Uncertainty and Small Gain Theorem.....	7
1.3.3. Problem Definitions and Solutions in State Space Form.....	8
1.3.3.1. $H_2$ Optimization Problem Definition .....	9
1.3.3.2. $H_\infty$ Optimization Problem Definition.....	9
1.3.3.3. $H_2/H_\infty$ Mixed Optimization Problem Definition .....	10
1.3.3.4. Solutions to Standard $H_2/H_\infty$ Mixed Robust Control Problems.....	11
1.4. REVIEW OF THE LITERATURE ON $H_2/H_\infty$ MIXED CONTROL .....	12
1.4.1. Literatures on Theory of $H_2/H_\infty$ Mixed Robust Control .....	13
1.4.2. $H_2/H_\infty$ Mixed Robust Control Applications from Literature.....	17
2. SYSTEM MODELING AND IDENTIFICATION .....	25
2.1. MODELING OF THE SYSTEM.....	25
2.1.1. Description of the Physical System .....	25
2.1.2. Mathematical Models of the Subcomponents.....	26
2.1.2.1. Motor.....	26
2.1.2.2. Sensor.....	28
2.1.2.3. Motion Transmission Mechanism and Calculation of Transmission Ratio.....	28
2.1.2.4. Calculation of Equivalent Moment of Inertia.....	30
2.1.3. Creation of Block Diagram for Controller Synthesis .....	31
2.1.3.1. External Loads and Disturbances .....	31
2.1.3.2. System Parameters and Uncertainties .....	32
2.1.3.3. Weighting Functions .....	32

2.1.3.4. Block Diagram.....	33
<b>2.2. SYSTEM IDENTIFICATION.....</b>	<b>35</b>
2.2.1. Real Time Data.....	35
2.2.1.1. Designation of Inputs .....	35
2.2.1.2. Evaluation of Outputs .....	37
2.2.2. Post Processing of Data in Time Domain.....	38
2.2.2.1. Time Domain Compatibility Comparison Using Parameter Estimation Method.....	38
2.2.2.2. Checking the “Goodness” of the Fits Using VAF Criterion .....	39
2.2.3. Post Processing of Data in Frequency Domain .....	40
2.2.3.1. Bode Diagram Fitting with Least Square Error Method .....	41
2.2.3.2. Experimental Creation of Bode Diagram.....	43
2.2.3.3. Checking the “Goodness” of the Results Using VAF Method.....	44
2.2.3.4. Simulating and Comparing the Results both in Time and Frequency Domain .....	45
2.2.4. Estimating the Uncertainty of the System Parameters .....	46
<b>3. SYNTHESIS OF ROBUST CONTROLLERS .....</b>	<b>49</b>
<b>3.1. REQUIREMENTS FOR THE CLOSED LOOP SYSTEM .....</b>	<b>49</b>
3.1.1. Motivation to $H_2/ H_\infty$ Mixed Control for Fin Actuation Systems.....	50
3.1.2. Selection of Weighting Functions .....	50
3.1.2.1. Weighting Function for Reference Signal $W_{ref}$ .....	52
3.1.2.2. Weighting Function for Cogging Torque $W_{cog}$ .....	53
3.1.2.3. Weighting Function for Aerodynamic Loads $W_{aero}$ .....	53
3.1.2.4. Weighting Function for Sensor Noise $W_{sens}$ .....	53
3.1.2.5. Penalty for Deviation from Ideal System $W_{perf}$ .....	53
3.1.2.6. Penalty for Controller Output $W_{act}$ (for Pure $H_2$ and $H_\infty$ Case) .....	54
3.1.2.7. Penalty for Controller Output $W_{act2}$ (for Mixed $H_2/H_\infty$ Case) .....	55
3.1.3. Creation of Generalized Plant .....	55
<b>3.2. SYNTHESIS OF PURE ROBUST CONTROLLERS .....</b>	<b>58</b>
3.2.1. $H_\infty$ Controller Synthesis .....	58
3.2.1.1. Simulation Results .....	62
3.2.2. $H_2$ Controller Synthesis .....	64
3.2.2.1. Simulation Results .....	67
<b>3.3. <math>H_2/H_\infty</math> MIXED CONTROLLER SYNTHESIS .....</b>	<b>69</b>
<b>4. DISCUSSION, CONCLUSION AND RECOMMENDATIONS .....</b>	<b>71</b>
<b>4.1. COMPARISON OF THE CONTROLLERS .....</b>	<b>71</b>
4.1.1. Comparison via Analytical Methods .....	71
4.1.2. Comparison via Simulation Results .....	76
4.1.3. Experimental Results.....	78
<b>4.2. CONCLUSION .....</b>	<b>82</b>
<b>4.3. FUTURE WORKS .....</b>	<b>83</b>
<b>REFERENCES .....</b>	<b>84</b>

APPENDIX.....	87
A.1.    State Space Matrices of Generalized Plants.....	87
A.2.    Alternative Weightings to Generate Better Controller.....	88
A.3.    System Identification Input-Outputs in Time Domain.....	89
A.4.    Frequency Spectrum of Input Signals.....	92
A.5.    Time Domain Comparison of Bode Estimations .....	96
A.6.    Photo of the System.....	99

## LIST OF FIGURES

### FIGURES

Figure 1. Tail controlled guided ammunition [1] .....	2
Figure 2. Basic classical feedback control system .....	4
Figure 3. Generalized plant control system.....	4
Figure 4. Bode magnitude plot and 2-norm of a system .....	5
Figure 5. Bode magnitude plot and $\infty$ -norm of a system .....	6
Figure 6. Unity feedback loop.....	6
Figure 7. Generalized plant with plant uncertainty .....	8
Figure 8. Extended generalized plant for mixed controller synthesis .....	10
Figure 9. Comparison of $H_2$ , $H_\infty$ and $H_2/H_\infty$ mixed performances [16] .....	14
Figure 10. Region $S(\alpha, r, \theta)$ .....	16
Figure 11. The location of the resultant closed loop poles of example of [22]. .....	17
Figure 12. Model of the control object [24] .....	18
Figure 13. Frequency and impulse response for $H_\infty$ control ( $\gamma_{\text{opt}} = 0.000356$ ) [24] .....	19
Figure 14. Frequency and impulse response for $H_2$ control ( $\eta_{\text{opt}} = 0.016$ ) [24].....	19
Figure 15. Frequency and impulse response for $H_2/H_\infty$ control ( $\gamma_{\text{opt}} = 0.0004$ $\eta_{\text{opt}} = 0.038$ ) [24] .....	19
Figure 16. Controller structure of [25] .....	20
Figure 17. $H_2/H_\infty$ standard problem for acceleration sensitivity control [28].....	21
Figure 18. Step response of mixed $H_2/H_\infty$ , $H_\infty$ , and $H_2$ 2 <sup>nd</sup> order system [29] .....	22
Figure 19. Step response of mixed $H_2/H_\infty$ , $H_\infty$ , and $H_2$ 2 <sup>nd</sup> order system with uncertainty [29].....	23
Figure 20. Step response of mixed $H_2/H_\infty$ , $H_\infty$ , and $H_2$ 3 <sup>rd</sup> and 4 <sup>th</sup> order system [29] .....	23
Figure 21. The full-car model of vehicle [30] .....	24
Figure 22. Schematic backside view of an ammunition and coordinate frame for a fin .....	26
Figure 23. Data from the motor characteristic test .....	27
Figure 24. Schematic diagram of the FAS as an inverted slider crank mechanism .....	28
Figure 25. Change of transmission ratio (N vs $\delta$ ) .....	30
Figure 26. Block diagram for controller synthesis .....	34
Figure 27. An input signal used in system identification as band limited white noise.....	36
Figure 28. An input signal used in system identification as PRBS .....	36
Figure 29. Frequency spectrum of inputs in Figure 27 and Figure 28 .....	37
Figure 30. Output to inputs in Figure 27 and Figure 28 .....	38
Figure 31. Block diagram in SIMULINK® for parameter estimation .....	39
Figure 32. Comparison of parameter estimation results with real outputs .....	39
Figure 33. Frequency characteristics of the experimental outputs .....	41
Figure 34. Fitted transfer function fittings on Bode diagram .....	42
Figure 35. $B_{eq}$ limits with frequency responses .....	43
Figure 36. The input and corresponding output to find Bode plot of the real system .....	43
Figure 37. Experimental frequency response data and fitted curve .....	44
Figure 38. Detailed view of a frequency domain curve fit.....	45
Figure 39. Overall view of goodness of fits .....	45
Figure 40. Time domain comparison between real and estimated models .....	46
Figure 41. Bode diagram of the ideal closed loop system.....	50
Figure 42. Typical shape of sensitivity function $S$ [6] .....	51
Figure 43. Typical shape of loop transfer function $L$ [6] .....	51
Figure 44. The plant in generalized plant notation.....	52
Figure 45. Magnitude plot of weighting function $W_{\text{ref}}(s)$ in frequency domain .....	53
Figure 46. Magnitude plot of cost function $W_{\text{perf}}(s)$ in frequency domain .....	54
Figure 47. Inverse of $W_{\text{act2}}(s)$ weighting function.....	55
Figure 48. Subsystem to simulate the mechanism and calculation of gear ratio N .....	57
Figure 49. Outermost block diagram used in simulation .....	58
Figure 50. Expansion of subsystem in Figure 49, the fin actuation system plant .....	58
Figure 51. Singular value plot of the sensitivity function in $H_\infty$ controlled case without uncertainty ..	59
Figure 52. Singular value plot of the open loop gain in $H^\infty$ controlled case without uncertainty ..	60

Figure 53. Bode plot of the closed loop response and corresponding bandwidth .....	60
Figure 54. Effect of uncertainty to singular value plots .....	61
Figure 55. Step response of the closed loop system including parameter uncertainties .....	61
Figure 56. Simulation response of the feedback system under external 40 N.m disturbance .....	62
Figure 57. Zooming of Figure 56 .....	63
Figure 58. Command generated by the $H_\infty$ controller .....	63
Figure 59. Simulated response of $H_\infty$ controlled plant to 12 Hz sinusoidal reference signal .....	64
Figure 60. Singular value plot of the sensitivity function in $H_2$ controlled case without uncertainty	65
Figure 61. Singular value plot of the open loop gain in $H_2$ controlled case without uncertainty .....	65
Figure 62. Bode plot of the closed loop response and corresponding bandwidth .....	66
Figure 63. Effect of uncertainty to singular value plots .....	66
Figure 64. Step response of the closed loop system including parameter uncertainties .....	67
Figure 65. Simulation response of the feedback system under external 40 N.m disturbance .....	68
Figure 66. Zooming of Figure 65 .....	68
Figure 67. Command generated by the $H_2$ controller .....	68
Figure 68. Simulated response of $H_2$ controlled plant to 12 Hz sinusoidal reference signal .....	69
Figure 69. Step response of the closed loop system including parameter uncertainties .....	70
Figure 70. Comparison of sensitivity functions .....	71
Figure 71. Comparison of open loop transfer functions .....	72
Figure 72. Comparison of controllers.....	72
Figure 73. Comparison of complementary singular values .....	73
Figure 74. Bode plot of closed loop transfer functions with corresponding bandwidth .....	74
Figure 75. Comparative step response characteristics.....	74
Figure 76. Frequency response comparison .....	75
Figure 77. Simulated response of closed loop systems. ....	77
Figure 78. Detailed view of responses to ramp input .....	77
Figure 79. Detailed view to sinusoidal input.....	77
Figure 80. Command tracking performance of real system .....	78
Figure 81. Detailed view of Figure 80 .....	79
Figure 82. Response to higher frequency input of real system.....	79
Figure 83. Detailed view of Figure 82 .....	80
Figure 84. Controller command during the reference tracking given in Figure 80 .....	80
Figure 85. Detailed view of Figure 84 .....	81
Figure 86. Controller command during the reference tracking given in Figure 82 .....	81
Figure 87. Detailed view of Figure 86 .....	82
Figure 88. System identification of input-outputs in time domain.....	92
Figure 89. Frequency spectrum of input signals. ....	95
Figure 90. Time domain comparison of estimation results. ....	99
Figure 91. Photo of the experimental set up including the plant .....	99

## LIST OF TABLES

### **TABLES**

Table 1. Norm definitions for signals and systems .....	5
Table 2. Comparison of Different Control Law Designs [10].....	18
Table 3. Gain and Phase Margins [29].....	22
Table 4. Performance and Robustness Comparison of Different Methods .....	24
Table 5. Value of system parameters .....	30
Table 6. Obtained $B_{eq}$ values by parameter estimation in kg.mm/s.....	39
Table 7. VAF values of the fittings via parameter estimation.....	40
Table 8. Performance requirements for the closed loop system.....	49
Table 9. Stabmarg fields descriptions .....	75
Table 10. Summary of comparison of controllers .....	82

## CHAPTER 1.

### INTRODUCTION

#### 1.1. AIM OF THE STUDY

Guided ammunition is a weapon system that can reach a distance away from the launching platform and hit a specific target precisely such that only the target is damaged. These types of systems are generally use aerodynamic principles to orient their route and movements. The most frequent method for creation of aerodynamic forces on a flying system is to make moving surfaces on the outer surface. Motion of the aerodynamic surfaces in a flying object induces forces on different axes. These aerodynamic surfaces can be placed on the tail, body or the nose part of the system. These aerodynamic surfaces are defined as fins and they are mechanically actuated by fin actuation systems.

In guided ammunition, the orientation of the fins is critical and must always be in the true angle such that the weapon could be oriented in the space at the desired position. Therefore, the positions of the fins always should be stable; the fins should follow the references and the response of the mechanical fin actuation system should not be affected by the external conditions. To be able to have all of these properties, the fin actuation system must be controlled and the controlled system should be robust against external perturbations. Also, in a mechanical system, inaccuracies in the mathematical models always exist due to manufacturing tolerances, nonlinearities and many other unpredicted effects. Since the task of the fin actuation system is very critical, these types of uncertainties should be handled. All of these requirements lead to a system that is properly controlled, precise and well performing. These kinds of problems require more powerful control techniques than classical and modern control. Robust control is a tool to attempt such problems and includes  $H_2$  and  $H_\infty$  techniques.

In this thesis, it is intended to design an  $H_2/H_\infty$  mixed type robust controller for a fin actuation system of guided ammunition such that the closed loop system is stable and responses occur in a manner as defined previously. The fin actuation system used here is an electromechanically actuated 4-link mechanism together with an encoder for position measurement. The actuated fins are positioned on the tail.

#### 1.2. DESCRIPTION OF PROBLEM AND SCOPE OF THE THESIS

The issued fin actuation in this text is placed inside of a tail controlled guided ammunition. The schematic drawing of such kind of system is given in Figure 1. In a guided platform, the autopilot gathers positions and accelerations data of the missile body from the inertial navigation units and any other available sensors and according to the planned route, it calculates the required angles that must be achieved via fin actuation system and then creates the position commands for actuators [1].

The task of the mechanical system behind the fins is to create the angle required by the autopilot according to a previously defined closed loop behavior. To achieve this, the mechanical system should overcome the all external loads and not be unstable under the effect of noise and perturbations.

In this thesis, the fin actuation system is modeled and identified to obtain the mathematical model of the plant. Using this mathematical model, three types of robust controllers are synthesized:  $H_2$ ,  $H_\infty$  and  $H_2/H_\infty$  mixed using MATLAB<sup>®</sup> and SIMULINK<sup>®</sup> tools. The controller models are uploaded to

a real system via an experimental setup. Then the outputs of the closed loop systems are analyzed and compared. In this manner, the studies of this paper are outlined below

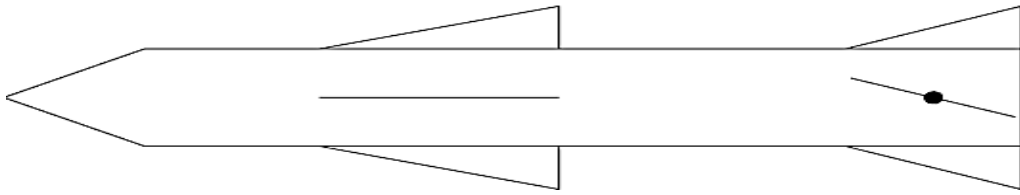


**Figure 1.** Tail controlled guided ammunition [1]

In Chapter 1, the general definition of the system and the aim of this text are given briefly. After that some basic concepts and required background information in modern and robust control theory is given. In the last part of this chapter, the literature about  $H_2/H_\infty$  mixed type control is abstracted.

In Chapter 2, the mechanical system to be controlled is explained in detail. Then the subcomponents of the mechanical system are introduced. All of the parts are mathematically modeled; then required formulations and transfer functions of the system are obtained. After that the block diagram of the overall system is created. In the second section of this chapter, the frequency domain system identification work done on the real system is shown by comparing the results with time domain responses and real data. Finally using these experimental results, the uncertainties of the parameters and the disturbances are described

In Chapter 3, the three types of robust controllers are designed and they are uploaded to the experimental setup. The performances of the closed loop systems, under an external load and plant uncertainties, is both measured and simulated. All of the obtained data are presented here.

In Chapter 4, the results are compared, the study is summarized and related future works are given.

### 1.3. BACKGROUND AND BASIC CONCEPTS

#### 1.3.1. A Brief History of the Control Theory

Since the beginning of the use of mechanisms, people started to use control techniques. Throughout the last two hundred years, technological developments have been growing and all of the machines have been becoming more complex and capable. To govern and utilize this complexity and capability, the machines must be fully controlled by a human or automatically. To achieve this, among the history, control theory is developed and this development have been still continuing.

The first examples of the automatic control arose in the last of the eighteenth century in parallel to development of huge spectacular mechanical systems, like the steam engine invention of James Watt. In nineteenth century, new mathematical tools had been developed and application of these theories to the mechanical area created big leaps in the human life.

The significant works in control theory were done especially in the late 1800s and earliest years of the twentieth century, by starting from Lyapunov; Minorsky, Hazen, Bode, Evans, Nyquist and many others. In 1892 Lyapunov gave a mathematical statement for the stability of the dynamic systems. In 1922, Minorsky developed automatic control systems for steering of the ships, via describing stability from the differential equations of the system. In 1932, Nyquist worked on a simpler method for deciding the stability of the closed loop systems using the frequency response characteristics of the open loop systems. In 1934 Hazen defined servomechanism term for position control of the mechanical systems. During the decade of the 1940s, with the effects of the war

technology due to 2<sup>nd</sup> World War, control system theory has found new wide application areas in the real systems especially for the aerospace applications. In this period, thanks to frequency response methods due to Bode, engineers become capable to design well performed closed loop systems. In following years, root locus method is found by Evans [2].

All of these frequency response and root locus methods are called the '*classical control theory*' today. Using these classical control theory methods, it is possible to have stabilized and satisfactorily performed closed loop systems in the case of single input, single output (SISO) linear systems. However, these methods do not give optimized controllers and applicable only in SISO systems. After the last 1950s, the main aim in the control theory field was to reach optimal controllers and control multi input multi output (MIMO) systems.

The space race during the 1960s was a very motivating ambition for the control engineers. The automatization of the manufacturing processes started in these years, as well as computer technology became available for complex calculations. In this decade, the '*modern control theory*' was developed and widely used in many industrial areas. The studies on optimal control and modern control approaches become widespread all over the industry, but the most advanced techniques and new methodologies were particularly encouraged by the applications in the space. In 1960, Kalman made one of the most important contributions to control area by introducing state space technique [3].

Since the late 1960s and up to the end of 1980s, the studies emphasized over the optimal theory for both linear and non-linear systems in addition to stochastic systems. Since the complexity of the systems raised, determinability of the systems decreased. This situation created new requirements that can be solved by using adaptive and robust techniques.

From 1990s to the present, the achievements in modern and optimal control theory, made researchers to focus on robust,  $H_\infty$ , fuzzy logic and similar techniques to deal with the uncertainties in mathematical models and perturbations in the systems. Also, since the computers are easily accessible devices, the applications in the control theory, now, can be easily projected into the daily life and spread to new areas.

### **1.3.2. Basic Concepts in Robust Control**

Most of the control engineering problems can be solved by using classical control theory. It is possible to obtain perfectly satisfactory solution in both frequency and time domains by using just proportional-integral-derivative (PID) type controllers, especially when the system is almost linear and its mathematical model is well-defined. Difficulties arise when the plant is complex, non-linear, poorly modeled, has external disturbances or/and the required performance specifications are very stringent. To solve these types of control problems, the designer needs more powerful tool than "classical" ones. The robust control theory is developed in this context as an extension to optimal and modern control methods. The aim in a robust controller synthesis problem is that the controlled closed loop system can give the satisfactorily "well" responses under the pre-defined "worst case" scenarios. [4]. In the following pages the basic concepts used in robust controller synthesis are provided.

#### **1.3.2.1. Feedback Loop and Generalized Plant**

A feedback control system is a closed structure including inputs, internal signals and outputs. There are three main components: plant, controller and sensor. A diagram of a feedback system is given in Figure 2. In this diagram,  $r$  is 'reference or command input',  $v$  is 'sensor output',  $u$  is 'actuating signal, controller output or input to plant',  $d$  is 'external disturbance',  $y$  is 'plant output and measured signal' and finally  $n$  is 'noise to sensor'. Here, the three signals from outside ( $r, d, n$ ) are called as *exogenous inputs*.

The performance of a closed loop system is best when the output  $y$  can follow  $r$  in a prescribed manner under the effects of noise, disturbances and plant uncertainties. Another performance

criterion is related with the actuator signal  $u$ . The controller should minimize the size of  $u$ . All of these objectives creates an optimization problem. To solve such a problem, engineers developed new methods and notations. One of these concepts is generalized plant approach and widely used in robust control theory.

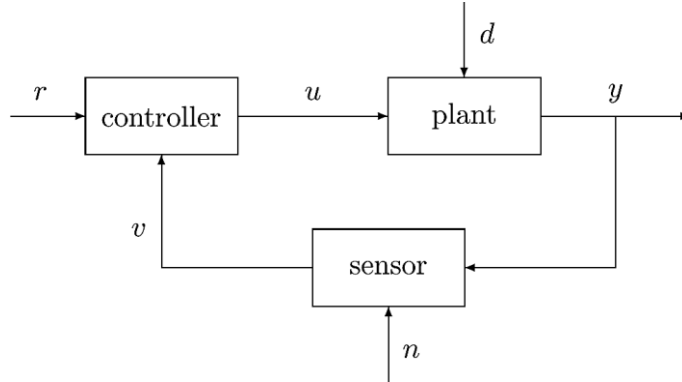


**Figure 2.** Basic classical feedback control system

The most general block diagram of a control system is shown in Figure 3. This schematic consists of everything that is required for the design and problem definition.  $P$  denotes the generalized plant matrix such that it includes all of the fixed and well-modeled physical properties of the real system to be controlled. In this matrix  $P$ , mathematical parameters of all subcomponents (actuators that generate inputs to the plant, dynamics of sensors, the plant itself and etc.) are placed in an appropriate manner.  $K$  denotes the linear controller to be synthesized and will be defined as a system matrix form that includes the controller properties. In real life,  $K$  is a controller device that may be an electrical circuit, computer software, PLC or any other device and it constitutes the output of the design procedure. The signal branches  $w$ ,  $z$ ,  $y$  and  $u$  are vector-valued functions of time. Here  $w$  carries all of the exogenous inputs (sensor noises, references, disturbances and so on) in its components. The vector  $z$  is called as ‘performance variables’ and contains all of the signals that would be controlled and penalized. These signals may be tracking errors between reference and plant outputs, limited actuator movements etc. The components of  $y$  are the outputs of the all sensors and feedback devices. Finally entries of  $u$  are the controlled inputs to the generalized plant [5].

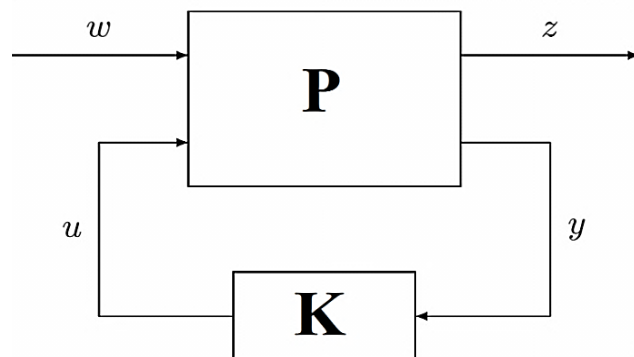


**Figure 3.** Generalized plant control system

### 1.3.2.1. Stability and Internal Stability

It is not possible to obtain an exact mathematical model of a physical system; therefore the control engineer always must be aware of how modeling errors and unpredictable factors might affect the performance of a closed loop system. Robustness of a system is parallel to its stability. So, to check the robustness of a system, the stability characteristics of the system should be examined.

*Stability* means, the system output  $y$  must not grow without bound due to a bounded input, initial condition or unwanted disturbance. For a linear time invariant (LTI) system, this is possible when there is no pole with positive real part i.e. there should be no poles (or eigenvalues) on the right half s-plane.

An LTI system is *internally stable* if all of the transfer functions from all internal signals to all exogenous outputs are stable.

### 1.3.2.2. Norms of Signals and Systems

The measure for the closed loop performance used in robust control is directly related with the norm of the system matrix of the closed loop transfer function from  $w$  to  $z$ . The general aim of the robust control is to minimize the norm of the signals and functions against all exogenous signals that have some limiting conditions. The controller design problem then becomes, find a controller  $K$  such that

$$\inf_{K \text{ stabilizing}} (\sup \|T_{zw}\|_q)$$

is minimized. Here  $\inf$  denotes ‘greatest lower bound’,  $\sup$  denotes ‘lowest upper bound’,  $q$  is the norm base. The widely used norms for robust control are 2 and  $\infty$ -norms. Also 1-norm of a signal is mathematically defined. These definitions of different norms for both signals and systems are given in Table 1 [5].

**Table 1.** Norm definitions for signals and systems

	Norms of signal $u(t)$	Norms of system $G_{zw}(s)$
1 - Norm	$\ u\ _1 = \int_{-\infty}^{+\infty}  u(t)  \cdot dt$	–
2 - Norm	$\ u\ _2 = \left( \int_{-\infty}^{+\infty} u(t)^2 \cdot dt \right)^{1/2}$	$\ G\ _2 = \left( \frac{1}{2\pi} \int_{-\infty}^{+\infty}  G(j\omega) ^2 \cdot d\omega \right)^{1/2}$
$\infty$ - Norm	$\ u\ _\infty = \sup_t  u(t) $	$\ G\ _\infty = \sup_\omega  G(j\omega) $

As seen from Table 1, 2-norm of a signal or a function is the total area (energy) under its Bode magnitude plot and  $\infty$ -norm of a signal is the peak (maximum response) point of the Bode magnitude plot of the system (Figure 4 and Figure 5).

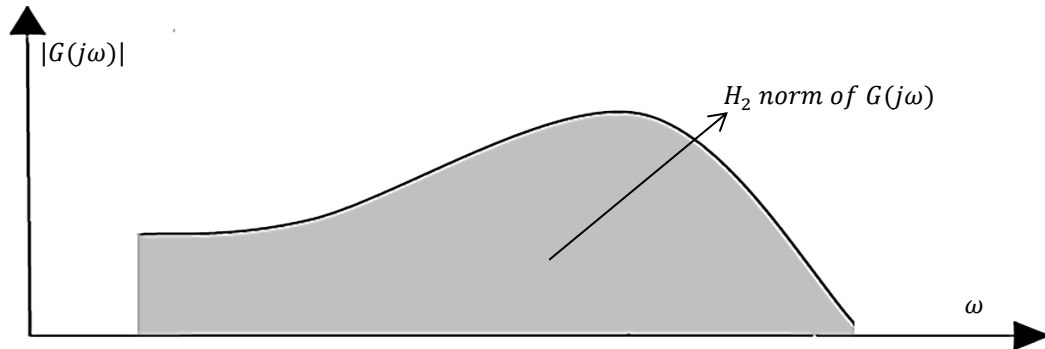


**Figure 4.** Bode magnitude plot and 2-norm of a system

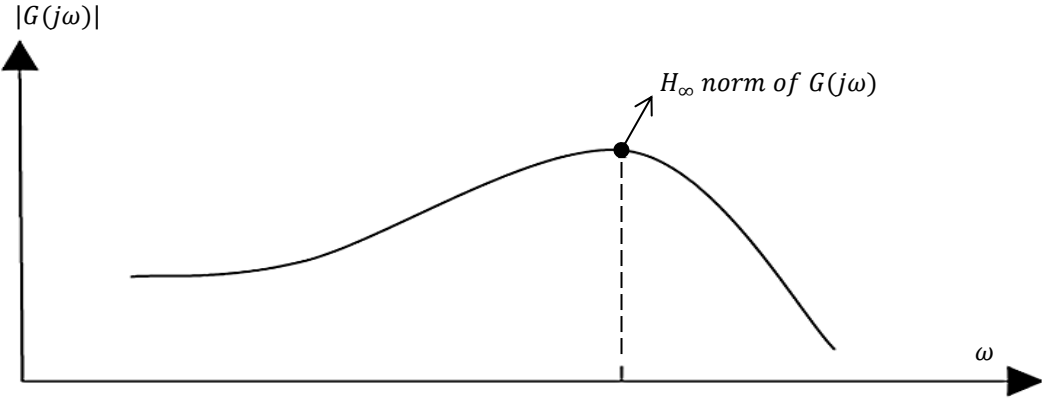


**Figure 5.** Bode magnitude plot and  $\infty$ -norm of a system

### 1.3.2.3. Sensitivity, Robustness and Disturbance Rejection

Assume a unity feedback loop given in Figure 6. Define  $L := PK$  as *loop transfer function*. Here and all over the text, ‘:=’ is the definition operator. Then, the transfer function from reference input  $r$  to  $e$  is called as the *sensitivity function* and given in equation (1.1) as,

$$S := \frac{1}{1 + L} \quad (1.1)$$

The *closed loop transfer function* of a system is the transfer function from  $r$  to  $y$ . Let  $T$  denote this function. Its formula is given by equation (1.2).

$$T := \frac{L}{1 + L} \quad (1.2)$$

Note that closed loop transfer function  $T$  also specifies how the output  $y$  is affected by the sensor noise  $n$ . Similarly, sensitivity function  $S$  also includes the effect of the disturbance input  $d$  in output  $y$ . [6]

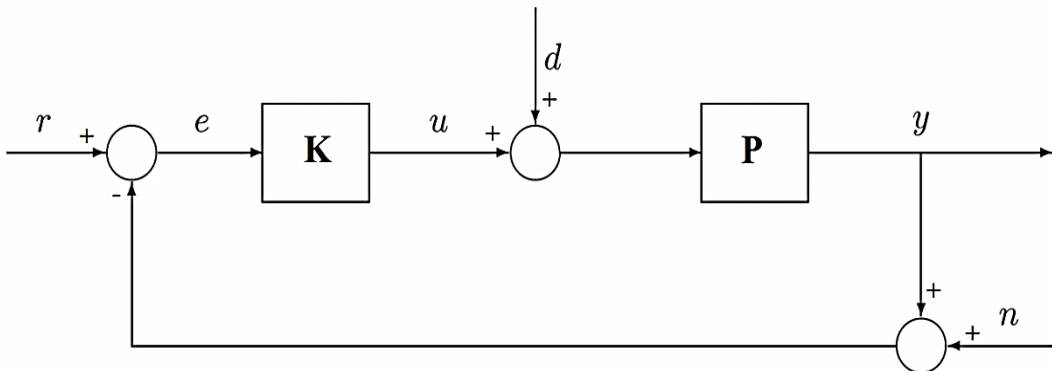


**Figure 6.** Unity feedback loop

The term ‘*sensitivity*’ comes from the idea that how much closed loop transfer function  $T$  changes from the variations in plant transfer function  $P$ . Take  $P$  and  $T$  as a variable and function respectively, and calculate the change of  $T$  for an infinitesimal change in  $P$ , i.e. :

$$\lim_{\Delta P \rightarrow 0} \frac{\Delta T/T}{\Delta P/P} = \frac{dT}{dP} \cdot \frac{P}{T} \quad (1.3)$$

One can easily see that the right hand side of the equation (1.3) is equal to function  $S$  given in equation (1.1) [5]. Thus, the *robustness* of a function can be measured using function  $S$ . Another important relation about  $T$  and  $S$  function is that:

$$S + T = 1 \quad (1.4)$$

Therefore the function  $T$  is also called *complementary sensitivity function*.

The requirements in a controller synthesis problem include stability, good command following, rejection of disturbances, attenuation of noises, robustness to modeling errors and minimization of control signal energy. For good command following and disturbance rejection, minimization of  $S$  is required and to reduce control sensitivity and increase robustness minimization of  $T$  is required (for more details please refer to [6]). Because of equation (1.4) is always must be satisfied, it is not possible to get both  $T$  and  $S$  near to zero over the whole frequency range. This tradeoff converts robust controller design problem to an optimization problem.

#### 1.3.2.4. Plant Uncertainty and Small Gain Theorem

To define “robustness” term in a mathematical manner, let first define a plant transfer function  $P$  is always member of a set  $\mathcal{P}$  which is a set of possible transfer functions. For example  $P \in \mathcal{P}$  such that;

$$\mathcal{P} = \left\{ \frac{1}{as^2 + bs + 1} : a_{min} \leq a \leq a_{max}, b_{min} \leq b \leq b_{max} \right\} \quad (1.5)$$

This  $\mathcal{P}$  is a structured set and it is parametrized by a finite number of parameters. But structured uncertainty is not necessarily parametrized explicitly. It may also be a discrete set of plants. However, unstructured sets are more important for control engineers, because it is not possible to have an “exact mathematical model” for complex real dynamic systems especially for high frequency dynamics [5]. There are some mathematical methods to analyze unstructured plant uncertainty and these makes possible to find solutions to controller synthesis problems with multiplicative disk uncertainty (a disk around any point of the Nyquist curve in s-plane). The robustness with respect to a characteristic of a plant is that; a controller  $K$  is *robust* to the selected characteristic of the plant for every plant selected from  $\mathcal{P}$ . The most important robustness characteristic is stability. A controller  $K$  provides *robust stability*, if it internally stabilizes all plants in  $\mathcal{P}$ .

To model plant uncertainty, the generalized plant control system in Figure 3 can be extended with an extra connection. This is given in Figure 7. Here,  $\Delta$  is an uncertainty model,  $P$  is nominal plant (modeled plant dynamics) and  $K$  is controller. Let  $M$  be the nominal closed loop system model.

Assume nominal closed loop system  $M$  is stable (check the eigenvalues of  $M$ ). If

$$\|M\|_\infty \cdot \|\Delta\|_\infty < 1$$

is satisfied, then the feedback interconnection is stable. This case yields,

$$\bar{\sigma}(\Delta) < \frac{1}{\bar{\sigma}(M)} \quad (1.6)$$

In (1.6),  $\bar{\sigma}$  is the maximum singular value of the matrix and equals to  $H_\infty$  norm of the transfer function matrix. The given theorem in (1.6) is very important in robust control theory and known as *small gain theorem* [7].

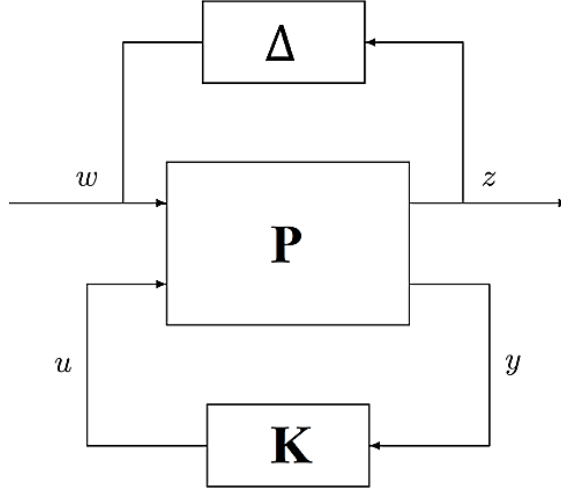


**Figure 7.** Generalized plant with plant uncertainty

### 1.3.3. Problem Definitions and Solutions in State Space Form

The general notation for widely used robust control spaces is standard. The Hardy space  $H_2$  is the space consists of square-integrable functions on the imaginary axis with the analytic continuation into the right-half-plane. The Hardy space  $H_\infty$  consists of bounded functions with analytic continuation into the right-half-plane [8].

For an LTI system given in Figure 3, the transfer function matrix can be shown as in equation (1.7).

$$G(s) = \begin{pmatrix} A & B \\ C & D \end{pmatrix} := C(sI - A)^{-1}B + D \quad (1.7)$$

Here the capital letters show the matrices and small letters are used to denote vectors. To give the problem definitions, let first introduce the notation. The system equations for a generalized plant  $P$  given in Figure 3 are given below in a state space form referring to notation of chapter 1.3.2.1 :

$$\begin{aligned} \dot{x} &= Ax + B_1w + B_2u \\ z &= C_1x + D_{11}w + D_{12}u \\ y &= C_2x + D_{21}w + D_{22}u \end{aligned} \quad (1.8)$$

The picking matrices  $P$  and  $K$ , for the generalized system and controller, respectively are:

$$P := \begin{pmatrix} [A] & [B_1 \quad B_2] \\ \begin{bmatrix} C_1 \\ C_2 \end{bmatrix} & \begin{bmatrix} D_{11} & D_{12} \\ D_{21} & D_{22} \end{bmatrix} \end{pmatrix} \quad K := \begin{pmatrix} A_f & B_f \\ C_f & D_f \end{pmatrix} \quad (1.9)$$

Using the notations in equation (1.9), the closed loop system matrix  $A_{cl}$  and picked matrix for closed loop system  $T_{cl}$  can be easily given as:

$$\begin{aligned} A_{cl} &:= \begin{pmatrix} A + B_2 D_f C_2 & B_2 C_f \\ B_f C_2 & A_f \end{pmatrix} \\ T_{cl} &:= \begin{pmatrix} [A + B_2 D_f C_2 & B_2 C_f] & [B_1 + B_2 D_f D_{21}] \\ [B_f C_2 & A_f] & [B_f D_{21}] \\ [C_1 + D_{12} D_f C_2 & D_{12} C_f] & [D_{11} + D_{12} D_f D_{21}] \end{pmatrix} \end{aligned} \quad (1.10)$$

To have a simpler controller synthesis problem,  $D_{22} = 0$  is assumed to have a strictly proper transfer function  $G_{22}(s)$ .  $D_{11} = 0$  is assumed in order to guarantee that the  $H_2$  and  $H_\infty$  problem is properly posed and finite [9].

### 1.3.3.1. $H_2$ Optimization Problem Definition

The  $H_2$  control problem is to find an admissible controller  $K$  (as in the form given in (1.9)) which internally stabilizes the plant  $P$  and minimizes the energy of the controlled output  $z$ . This is equal to minimizing the 2-norm of the closed loop transfer function  $T_{cl}$ .

$$\inf_{K \text{ admissible}} \|z\|_2 = \inf_{K \text{ admissible}} \|T_{cl}\|_2 \quad (1.11)$$

The controller  $K$  is unique and the order of it is equal to the order of the nominal plant plus the order of weights. To have an admissible controller, in addition to assumptions at chapter 1.3.3 the following assumptions are required.

- i.  $(A, B_2)$  is stabilizable and  $(C_2, A)$  is detectable.
- ii.  $D_{12}^T D_{12}$  is full rank;  $D_{21}^T D_{21}$  is full rank.
- iii.  $\begin{bmatrix} A - j\omega I & B_2 \\ C_1 & D_{12} \end{bmatrix}$  has full column rank for all  $\omega \in \mathbb{R}$ .
- iv.  $\begin{bmatrix} A - j\omega I & B_1 \\ C_2 & D_{21} \end{bmatrix}$  has full column rank for all  $\omega \in \mathbb{R}$ .

For existence of a stabilizing controller, assumption (i) is required. (ii) must be satisfied to avoid singularities. The last two conditions guarantee the existence of stabilizing solutions to the *algebraic Riccati equation* that are used for the solution of  $H_2$  problem [10].

### 1.3.3.2. $H_\infty$ Optimization Problem Definition

Similar to the  $H_2$  case, the  $H_\infty$  control problem is to find an admissible controller  $K$  (as in the form given in (1.9)) which internally stabilizes the plant  $P$  and minimizes the peak of the frequency response of the closed loop transfer function. In this condition,  $z$  is under the effect of a deterministic disturbance signal with bounded but unknown energy. This is equal to minimizing the  $\infty$ -norm of the closed loop transfer function  $T_{cl}$  from error  $e$  to disturbance signal  $d$ . (Please refer to Figure 6.)

$$\inf_{K \text{ admissible}} \sup_{\|d\|_2 \leq 1} \|e\|_2 = \inf_{K \text{ admissible}} \|T_{cl}\|_\infty \quad (1.12)$$

The optimal controller  $K$  yields  $\|T_{cl}\|_\infty = \underline{\gamma}$  and is not unique.  $K$  is a member of a family of suboptimal controllers such that  $\|T_{cl}\|_\infty < \underline{\gamma}$  can be defined,  $\underline{\gamma} < \gamma$ . The order of controller  $K$  is equal to the order of the nominal plant plus the order of weights. To have an admissible controller, in addition to assumptions at chapter 1.3.3 the following assumptions are required.

- i.  $(A, B_2)$  is stabilizable and  $(C_2, A)$  is detectable.
- ii.  $D_{12}^T D_{12}$  is full rank;  $D_{21}^T D_{21}$  is full rank.
- iii.  $\begin{bmatrix} A - j\omega I & B_2 \\ C_1 & D_{12} \end{bmatrix}$  has full column rank for all  $\omega \in \mathbb{R}$ .
- iv.  $\begin{bmatrix} A - j\omega I & B_1 \\ C_2 & D_{21} \end{bmatrix}$  has full column rank for all  $\omega \in \mathbb{R}$ .

For existence of a stabilizing controller, assumption (i) is required. (ii) must be satisfied to avoid singularities. The last two conditions guarantee that the solutions exist for the  $H_\infty$  problem [10].

#### 1.3.3.3. $H_2/H_\infty$ Mixed Optimization Problem Definition

In standard  $H_2$  or  $H_\infty$  problems, the objective is to design a controller  $K$  such that  $H_2$  or  $H_\infty$  norm of the closed loop transfer function is minimized as mentioned in previous sections. In combined  $H_2$  and  $H_\infty$  optimization technique, the exogenous inputs  $w$  and performance variables  $z$  are separated according to their optimization condition. In this manner, generalized plant in Figure 3 is extended as in Figure 8 and the state space equations (1.8), (1.9) and (1.10) are revised as following.

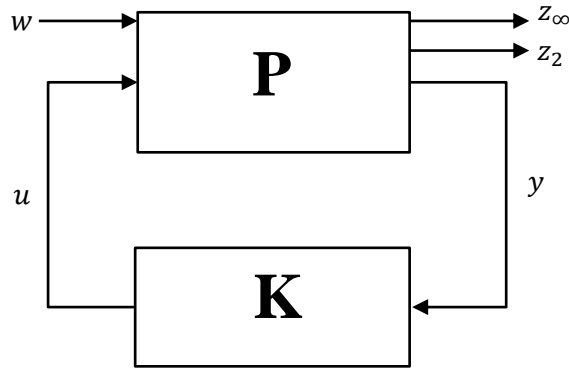


*Figure 8. Extended generalized plant for mixed controller synthesis*

$$\begin{aligned}\dot{x} &= Ax + Bw + B_u u \\ z_\infty &= C_\infty x + D_\infty w + D_{\infty u} u \\ z_2 &= C_2 x + D_2 w + D_{2u} u \\ y &= C_y x + D_y w + D_{yu} u\end{aligned}\tag{1.13}$$

The picking matrices  $P$  and  $K$  for the generalized system in Figure 8 and controller respectively:

$$\begin{aligned}P &:= \begin{pmatrix} [A] & [B & B_u] \\ \begin{bmatrix} C_\infty \\ C_2 \\ C_y \end{bmatrix} & \begin{bmatrix} D_\infty & D_{\infty u} \\ D_2 & D_{2u} \\ D_y & D_{yu} \end{bmatrix} \end{pmatrix} \\ K &:= \begin{pmatrix} A_f & B_f \\ C_f & D_f \end{pmatrix}\end{aligned}\tag{1.14}$$

Using the notations in equation (1.9) and (1.14), the closed loop state space equations are given below:

$$\begin{aligned}\dot{x}_{cl} &= A_{cl}x_{cl} + B_{cl}w \\ z_\infty &= C_{cl\infty}x_{cl} + D_{cl\infty}w \\ z_2 &= C_{cl2}x_{cl} + D_{cl2}w\end{aligned}\tag{1.15}$$

Let  $T_\infty$  is closed loop transfer function from  $w$  to  $z_\infty$  and  $T_2$  is closed loop transfer function from  $w$  to  $z_2$  of plant  $P$  in Figure 8. Then the mixed  $H_2/H_\infty$  problem definition is to find an output feedback controller  $u = Ky$  such that it internally stabilizes the plant  $P$  and maintains following conditions [10], [11]:

- i.  $\|T_\infty\|_\infty < \gamma_o$  and  $\|T_2\|_2 < \nu_o$ ;  $\gamma_o, \nu_o > 0$
- ii. Minimizes the tradeoff criterion

$$\alpha \|T_{wz_\infty}\|_\infty^2 + \beta \|T_{wz_2}\|_2^2 > 0 \text{ with } \alpha, \beta > 0\tag{1.16}$$

To have an optimal or sub-optimal stabilizing multi-objective  $H_2/H_\infty$  mixed controller  $K$ , the discrete  $H_2$  and  $H_\infty$  problems must be solvable. Therefore, to have an admissible mixed type controller, the conditions for  $H_2$  and  $H_\infty$  problems are combined and the following statements arise as necessities [10], [12].

- i. To have finite  $\|T_2\|_2 \rightarrow D_f = 0$ .
- ii. Since all real systems are proper  $\rightarrow D_{yu} = 0$ .
- iii.  $H_2$  and  $H_\infty$  problems must be independent.
- iv.  $(A, B_u)$  is stabilizable and  $(C_y, A)$  is detectable.
- v.  $D_{\infty u}^T D_{\infty u}$  is full rank and  $D_y D_y^T$  is full rank.
- vi.  $D_{2u}^T D_{2u}$  is full rank.
- vii.  $\begin{bmatrix} A - j\omega I & B_u \\ C_2 & D_{2u} \end{bmatrix}$  and  $\begin{bmatrix} A - j\omega I & B_u \\ C_\infty & D_{\infty u} \end{bmatrix}$  has full column rank for all  $\omega \in \mathbb{R}$ .
- viii.  $\begin{bmatrix} A - j\omega I & B \\ C_y & D_y \end{bmatrix}$  has full row rank for all  $\omega \in \mathbb{R}$ .

#### 1.3.3.4. Solutions to Standard $H_2/H_\infty$ Mixed Robust Control Problems

In output feedback case, the controller has its own dynamics and states. Let  $\xi$  denote states of the controller  $K$ . Then, the state space equations for the controller becomes;

$$\begin{aligned}\xi &= A_f \dot{\xi} + B_f y \\ u &= C_f \xi + D_f y\end{aligned}\tag{1.17}$$

The solution procedure for both  $H_2$  and  $H_\infty$  problems are firstly given by Doyle et. al. in [8] at 1989. Then, many other methods are developed based on this paper and using Riccati equations. Additionally there are many textbooks to find solutions and method for different type of  $H_2$  and  $H_\infty$  problems (For further details, refer to the textbooks [3], [4], [5], [13]).

Regarding the solution for multiobjective type  $H_\infty$  problems (i.e. mixed  $H_2/H_\infty$  problem) there is not many methods. The approach used in this study is the method proposed by Mathworks Corporation in MATLAB® software. This software tool uses linear matrix inequalities (LMI)

approach for the solution as summarized below. The detail of the algorithm and theory behind the application can be found on [12]. Also other theoretical approaches and applications of multiobjective type robust control are given in the subsequent section of this chapter.

For an output feedback controller case as in equation (1.18), in LMI technique, mixed  $H_2/H_\infty$  type problem is formulated as two parts that have  $H_2$  and  $H_\infty$  performance bounds and these two problems are given as inequalities. Then, these two inequalities generate a convex optimization problem and the solution can be obtained via simultaneous solution of two distinct constraints.

- $H_\infty$  Performance

The closed loop root mean square (RMS) gain for  $T_\infty$  does not exceed  $\gamma$  if and only if there exist a symmetric matrix  $\chi_\infty$  such that:

$$\begin{bmatrix} A_{cl}\chi_\infty + \chi_\infty A_{cl}^T & B_{cl} & \chi_\infty C_{cl\infty}^T \\ B_{cl\infty}^T & -I & D_{cl\infty}^T \\ C_{cl\infty}\chi_\infty & D_{cl\infty} & -\gamma^2 I \end{bmatrix} < 0 \quad (1.18)$$

$$\chi_\infty > 0$$

- $H_2$  Performance

The closed loop  $H_2$ -norm of  $T_2$  where ( $\|T_2\|_2^2 = \text{Trace}(C_{cl2}Q C_{cl2}^T)$ ) does not exceed  $v$  if and only if  $D_{cl2} = 0$  there exist two symmetric matrices  $\chi_2 > 0$  and  $Q$  such that:

$$\begin{bmatrix} A_{cl}\chi_2 + \chi_2 A_{cl}^T & B_{cl2} \\ B_{cl2}^T & -I \end{bmatrix} < 0 \quad (1.19)$$

$$\begin{bmatrix} Q & C_{cl2}\chi_2 \\ \chi_2 C_{cl2}^T & \chi_2 \end{bmatrix} > 0 \text{ and } \text{trace}(Q) < v^2$$

If  $\chi = \chi_\infty = \chi_2 = \chi_p$  (simultaneous solution of inequalities (1.18) and (1.19)) give solution to multiobjective optimality problem in equation (1.16). In (1.16) if,

- i.  $\alpha = 0; \beta = 1$  yields an  $H_2$  problem
- ii.  $\alpha = 1; \beta = 0$  yields an  $H_\infty$  problem
- iii.  $0 < \alpha < 1; 0 < \beta < 1$  yields  $H_2/H_\infty$  mixed problem.

The method mentioned here is quoted from [12]. In MATLAB® software, ‘*hinfmix*’ (replaced by ‘*h2hinfsyn*’ in r2012a) command runs this algorithm.

#### 1.4. REVIEW OF THE LITERATURE ON $H_2/H_\infty$ MIXED CONTROL

Starting from the late 1970s, there have been many developments on control theory area in parallel to developments on numerical solution techniques. Numerical methods provide an invaluable tool for treating difficult mathematical problems, especially for differential equations and matrix type inequalities. The question arose in robust controller synthesis are also an application area for the numerical techniques.

As previously mentioned, robust controller problems generally include  $H_2$  and  $H_\infty$  type problems. The theory behind these question techniques is very detailed and can be found in textbooks and lecture notes related with robust control theory. Some examples are [3], [4], [5], [7] and [14]. In this section, the theoretical approaches and applications related with mixed type  $H_2/H_\infty$  synthesis problems will be summarized using studies and descriptions from literature.

### 1.4.1. Literatures on Theory of $H_2/H_\infty$ Mixed Robust Control

In a MIMO feedback system, the controller can work using state feedback data or only output feedback data. The first techniques in robust control attempted to state feedback case, because of its relative simplicity. After the state space techniques become available, in 1989 Doyle et. al. created a basic theory for the solution of both standard  $H_2$  and  $H_\infty$  type control problems in state space [8]. In this paper, they separated robust control problems as full information, full control, disturbance feed-forward and output estimation. All of the following solution methods in robust control are based on this theory. They use generalized plant approach and the solutions are based on the algebraic Riccati equation in (1.20).

$$A^T X + X A + X R X - Q = 0 \quad (1.20)$$

As previously mentioned; the  $H_\infty$  criterion corresponds to design for the worst exogenous signal that has a deterministic disturbance model with bounded power and unknown spectrum. Similarly,  $H_2$  optimization is based on a stochastic noise disturbance model with fixed spectral density. Use of LQG ( $H_2$ ) technique utilizes quadratic cost problem while  $H_\infty$  theory seeks to minimize the worst case attenuation.

In many real-world applications, standard  $H_\infty$  synthesis cannot adequately capture all design specifications. Noise attenuation or regulations against random disturbances are more naturally expressed in LQG terms. Similarly, pure  $H_\infty$  synthesis only enforces closed loop stability and does not allow for direct placement of the closed loop poles in more specific regions of the left-half plane. Since the pole location is related to the time response and transient behavior of the feedback system, it is often desirable to impose additional damping and clustering constraints on the closed loop dynamics. This makes multi-objective synthesis highly desirable in practice [12]. Therefore the mixed  $H_2/H_\infty$  control problem has attracted much attention in recent years. There is an abstract of the some related works from the literature in the next paragraphs.

In 1989, Bernstein and Haddad developed the first Riccati based method for the mixed  $H_2/H_\infty$  problem using  $H_\infty$  - constrained LQG control problem in state feedback case [15]. They also give illustrative examples using numerical methods in the same study.

In 1990, Zhou et. al. published a paper that the first time use of “mixed  $H_2/H_\infty$ ” term. In this work, they introduce a theory that directly handles both  $H_2$  and  $H_\infty$  performance objectives at the same time. They also state that, in a mixed robust control problem  $H_2$  objective usually makes more sense for performance and  $H_\infty$  is better for robustness to plant perturbations [16]. Projecting this fact to a general plant with structured plant uncertainty, they generate the first mixed control problem statement by considering the general plant provided in Figure 8. Given the plant  $G$ , a constant  $\gamma$ , find a controller  $K$  such that it provides internal stability and is the solution of the (1.21).

$$\min_{K \text{ admissible}} \sup_{\omega_1 \in \mathcal{P}} \{ \|z\|_P^2 - \gamma \|\omega_1\|_P^2 \} \quad (1.21)$$

Using this problem definition, Zhou et. al. designed a mixed  $H_2/H_\infty$  type controller using numerical techniques and drew the Bode plot of the closed loop system to compare the results with the pure  $H_2$  and  $H_\infty$  controllers as given in Figure 9.

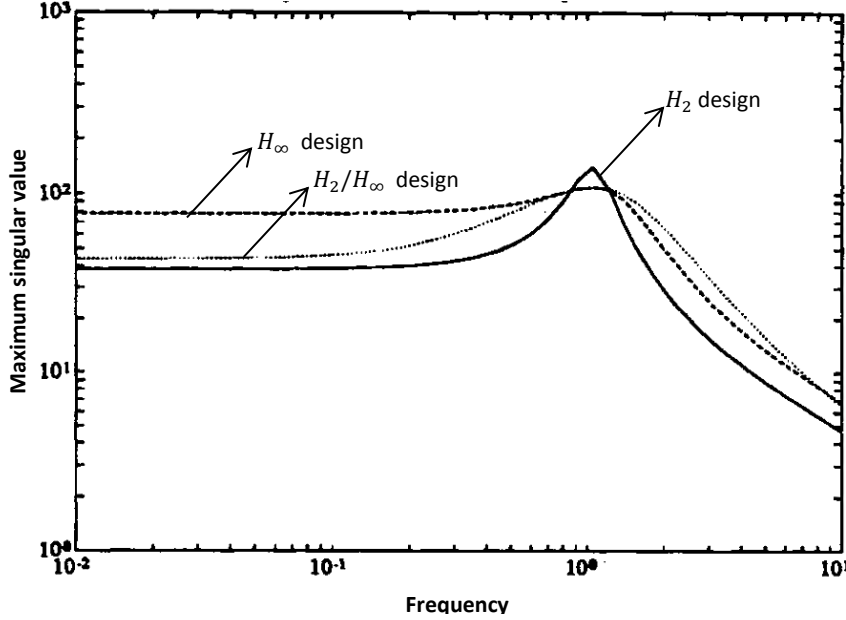


**Figure 9.** Comparison of  $H_2$ ,  $H_\infty$  and  $H_2/H_\infty$  mixed performances [16]

Although the problem stated, there was no generic analytical solution until the work of Rotea and Khargonekar at 1991. They have not only developed a new problem definition as  $H_2$  optimal control with an  $H_\infty$  constraint but also introduced an analytical solution method for state feedback case. In this document, they also separate mixed controller problem to two types: *Problem A: Minimal  $H_2$  norm subject to an  $H_\infty$  constraint* and *Problem B: Simultaneous  $H_2/H_\infty$  optimal control* [17]. These two forms are given below in (1.22), (1.23).

$$\text{Problem A: } \inf\{\|T_1(K)\|_2 : K \text{ admissible and } \|T_2(K)\|_\infty < 1\} \quad (1.22)$$

$$\text{Problem B: } \inf\{\|T_1(K)\|_2 : K \text{ admissible}\} \text{ and such that } \|T_2(K)\|_\infty < 1 \quad (1.23)$$

Problem A is very similar to the Bernstein and Haddad problem (see [15]). However, Rotea and Khargonekar give analytic solution as an improvement to previous numerical methods by using small gain theorem and matrix based Riccati equation. Problem B is an  $H_2$  unconstrained version of problem A. Rotea et. al. give necessary and sufficient conditions for the existence of a solution to problem B. Since problem B is generalized form of A, the requirements for the existence of a solution to problem A becomes also available [17].

Up to this point, the referenced studies were about the “state feedback case” for controller and examined relatively “simple” problems. In July 1991, Khargonekar and Rotea gave a method to reduce the mixed  $H_2/H_\infty$  problem to a convex optimization problem over a bounded set of real matrices. The bounded subset include a  $q \times n$  and  $n \times n$  symmetric real matrices, where  $q$  is the dimension the control input and  $n$  is dimension of the states. Using this convex optimization approach, they deliver a global solution to general output feedback problem. To obtain a suboptimal controller,  $H_\infty$  estimation filter is used to convert output feedback problem to a state feedback problem. They also govern a theorem that there is always an output feedback controller solves the mixed type problem with dimension no larger than that of the generalized plant [18].

Since  $H_2$  and  $H_\infty$  robust controllers started to find new application areas in the beginning of 1990s, people wanted to know which controller synthesis method is better. To answer this question, Zhou has made a research to compare  $H_2$  and  $H_\infty$  controllers. In reference [9], he has shown that the

$H_\infty$  performance ratio for the one block problem between an  $H_2$  controller and an  $H_\infty$  controller is bounded by the number of some subsystem right half plane zeros. Assume that, a generalized  $m$ -th order plant  $G$  that satisfies the conditions of  $H_\infty$  admissible controller (see chapter 1.3.3.2 and conditions i-iv of this thesis), and let  $K_2$  be the optimal  $H_2$  controller,  $K_\infty$  be the optimal  $H_\infty$  controller and  $\mathcal{F}$  denote the closed loop transfer function. Then, in document [9], Zhou proofs that:

$$\beta = \frac{\|\mathcal{F}(G, K_2)\|_\infty}{\|\mathcal{F}(G, K_\infty)\|_\infty} \geq 1 \text{ and } \beta \leq 2k \quad (1.24)$$

where  $k = z_{12} + z_{21}$

In (1.24),  $z_{12}$  is the number of right half plane zeros of the transfer function between control signal and controlled output. Similarly  $z_{21}$  is the number of the right half plane zeros of the transfer function between disturbance and measurement. Note that the upper bound given in (1.24) is very conservative; Zhou shows that there are some plants that can actually have the ratio arbitrarily close to the upper bound. Also, this condition yields that for most practically motivated systems which have very few right half plane zeros, the performance ratio  $\beta$  will be relatively small. Although this result leads someone to think that for such kind of systems,  $H_2$  controller can perform as well as an  $H_\infty$  controller, it should be noted that  $H_2$  theory has not equal power with  $H_\infty$  to overcome the plant uncertainties [9]. Therefore the use of mixed type  $H_2/H_\infty$  technique may be required to obtain a simplified and well performed system between  $H_2$  and  $H_\infty$ .

In August 1994, Zhou et. al. published two successive papers. In the first one they introduced methods for analysis of robust performance of mixed  $H_2/H_\infty$  controlled systems. The paper deals with the systems have disturbances in white noise or non-white noise form and structured and unstructured plant uncertainty. The method developed here is also valid for the systems that their mixed norms cannot be expressed explicitly (For further details see [19] ).

The second document considers the analysis and synthesis of optimal mixed  $H_2/H_\infty$  controller. They collect the necessary and sufficient conditions to obtain mixed type optimal controller (given also in section 1.3.3.3 of this text) and gives the explicit state space formula for the optimal controller [20]. These two papers together with [18] create a guideline for mixed optimal controller design for further methods. Also the papers bring tools for testing the robustness and performance of the designed controller in mathematical manner.

One of the most important studies on the mixed  $H_2/H_\infty$  controller synthesis is the paper of Chilali and Gahinet in March 1996. In this manuscript, they handle mixed control problem together with pole placement constraints and they serve an LMI based method to find the optimal output or state feedback control. The procedure is as follows: Firstly a convex region for poles is defined using performance properties and desired characteristics of the closed loop system. The clustering regions for pole are on the left half-plane and using transient response characteristic of a second order system with poles  $\lambda = -\zeta\omega_n \pm j\omega_d$  with  $\omega_n$  is undamped natural frequency,  $\zeta$  is damping ratio and  $\omega_d$  is damped natural frequency. One can put on the specific bounds on these characteristics to ensure a satisfactory transient response. Regions of pole clustering include an  $\alpha$ -stability regions on the left half plan such that  $Re(s) \leq -\alpha$ , vertical strips, disks, conic sectors or any convex geometry [21]. Another interest in region is  $S(\alpha, r, \theta)$  of complex numbers  $x + jy$  such that:

$$x < -\alpha < 0, \quad |x + jy| < r, \quad \tan(\theta).x < -|y| \quad (1.25)$$

The region of equation (1.25) is given in Figure 10. If all of the closed loops are in the shaded region  $S$ , one can guarantee that a minimum decay rate is  $\alpha$ , a minimum damping ratio is  $\zeta = \cos(\theta)$  and a maximum undamped natural frequency is  $\omega_d = r \cdot \sin(\theta)$ . It is known that these values bound the maximum percent overshoot, the frequency of the oscillatory modes in transient response, the delay time, the rise time and the settling time.

After convex region  $S(\alpha, r, \theta)$  is defined, the mixed  $H_2/H_\infty$  problem can be easily formulated in LMI (linear-matrix-inequality) form [21]. Then the obtained problem can be solved extended

Lyapunov theorem. In this study, the main improvement according to preceding methods, it eliminates Riccati based approaches and proposes a simpler algorithm for computer programs. The theory behind the well-known MATLAB® software LMI Control Toolbox (the toolbox includes *hinfmix* command) is this paper. Here, Chilali and Gahinet give the details of the solution for both state and output feedback controllers. They also apply the method to a benchmark problem in robust control and provide the results. For further details see [21]. Also document [12] of MATLAB® software includes details and algorithms of this LMI technique.

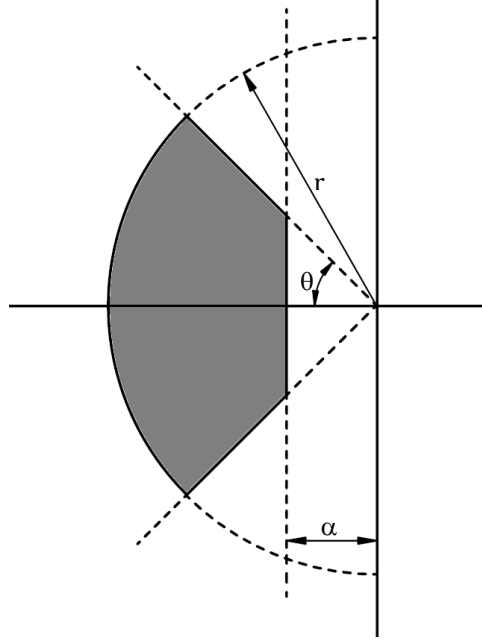


**Figure 10.** Region  $S(\alpha, r, \theta)$

In 2003, Wu and Lee examine the problems in mixed  $H_2/H_\infty$  control and they extend the previously developed methods, especially the technique of Chilali and Gahinet to the problems with non-convex regional pole constraints using Kroenecker product and barrier method. They apply their procedure to a state feedback case. Additionally they state that the procedure is valid also for output feedback case. The closed loop pole region of an example problem is given in the paper and Figure 11 [22]. Note that, the all of poles lie inside of a non-convex constraint region.

The theories covered up until now handle the problems in linear-time-invariant systems. In 1995, Scherer proposes a solution to the mixed  $H_2/H_\infty$  problem for time varying systems and discusses various specializations to linear parametrically varying and time invariant systems. The theory in this text is also valid for pure  $H_2$  and  $H_\infty$  problems [23]. However, the theory is based on the state feedback case and the extension to the output feedback case for varying systems is still a hot topic.

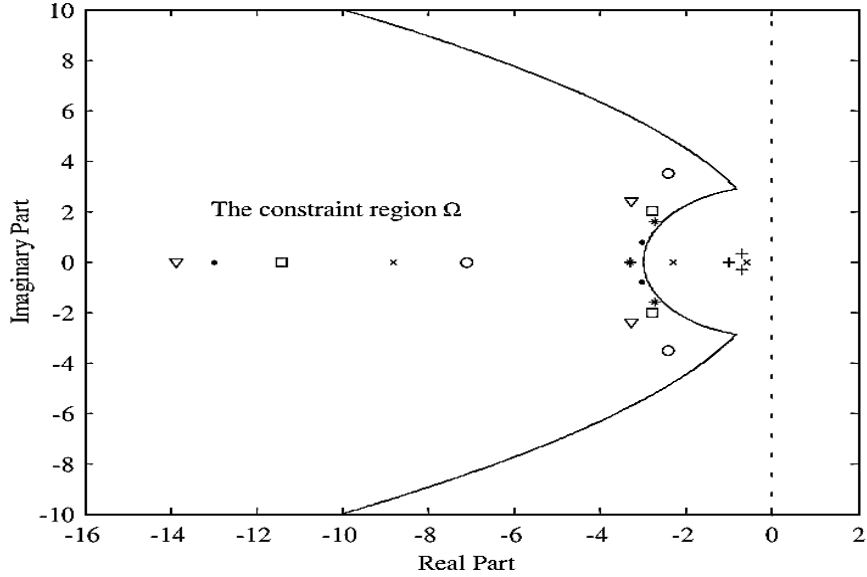


**Figure 11.** The location of the resultant closed loop poles of example of [22].

#### 1.4.2. $H_2/H_\infty$ Mixed Robust Control Applications from Literature

Parallel to the developments on the theories and computational capabilities, mixed robust control techniques started to find application areas in early 1990s especially in aerospace and defense industries due to strict requirements on complex systems. Large portion of the applications found in literature include use of MATLAB® software and/or advanced numerical methods.

One of the first mixed controller application is the master thesis of Kusnerek in 1991. In this thesis, the author uses a numerical algorithm coded in Fortran to solve the matrix equations and use MATLAB® to visualize the system responses. The purpose of the study is to demonstrate the use of mixed solution and compare the results with the pure  $H_\infty$  controller for firstly a single input single output (SISO) and a single input two outputs (SI2O). In the final part, an  $H_2/H_\infty$  mixed controller was designed and the controller was applied to a physical system with two inputs two outputs (2I2O). Here Kusnerek find a solution to a non-conservative optimization problem such that 2-norm of one transfer function subject to an  $\infty$  norm bound using the theory of Bernstein-Haddad. Then he obtains that the mixed controlled system response is 5% better in a specific SISO example, 27% better in a specific 2I2O example compared to pure  $H_\infty$  controlled version of same examples [11].

Another outstanding study as a multiobjective robust controller application is the thesis of Ullauri in 1994. In the document a general mixed  $H_2/H_\infty$  output feedback optimal controller with multiple  $H_\infty$  constraints synthesized on two types of systems. One of the controlled plants is a SISO system that models the normal acceleration of an F-16 aircraft. The other system is a MIMO system which is the benchmark problem of MATLAB®; mathematical model of the longitudinal HIMAT aircraft example of NASA. To solve the multiobjective control problem, the author developed software using a special numerical method. After that, the method is validated over SISO system. Then mixed type controller for the MIMO plant is designed using same algorithm. The obtained results proofs that it is possible to obtain a nominal performance and robust stability simultaneously by using  $H_2/H_\infty$  mixed controller. Table 2 summarizes the results of the study [10].

**Table 2.** Comparison of Different Control Law Designs [10]

	$H_2$	$H_\infty$	$\mu$ (D-K)	Mixed $H_2/H_\infty$
Handle white Gaussian Noise (WGN)	x			x
Robust Stability, Nominal Performance (RS,NP)		x	x	x
Robust Performance			x	
Tradeoff between RS and NP freely				x
WGN and RS, NP				x
Reduced order controller				x

In 1996, Nonami and Sivrioglu have made active vibration control of a flexible body model; using LMI based convex optimization technique of Chilali and Gahinet. They applied the theory both for state feedback and output feedback situations and compared the closed loop system response of mixed controlled system with the previously designed pure  $H_2$  and  $H_\infty$  controllers [24]. The aim of the study is to regulate and damp the external vibrations on the plant given in Figure 12. In this figure  $m_i, k_i, c_i$  is the mass, stiffness and damping of the body, respectively.  $x_i$  is the displacement of each mass and also the system states,  $u$  is control signal and  $w$  is the external disturbance. The physical system is non-linear. However to obtain a robust controller the system is linearized and the system matrices and norm constraints are given in reference [24]. Using these constraints and reference [21] as a guide, they obtain an optimal  $H_2/H_\infty$  mixed controller.

The frequency and impulse responses of 4th mass with these three distinct types of controller are given in Figure 13, Figure 14 and Figure 15. The optimal controller for an LTI system is not unique. They obtain the optimal plant by using trial and error and iterative methods on  $H_2$  norm constraint  $\eta$  and  $H_\infty$  norm constraint  $\gamma$ . The design progress can be seen from the reference [24]. Note that the frequency response performance of the  $H_\infty$  control in Figure 13 is better than the performance of  $H_2$  in Figure 14 especially for low frequency range. Similarly, the time response performance of the  $H_2$  control in Figure 13 is better than the performance of  $H_\infty$  in Figure 14. Therefore one can take a tradeoff between these two controllers and can obtain a good closed loop response in both domains. Using LMI based  $H_2/H_\infty$  mixed controller synthesis, Nonami and Sivrioglu achieve a good result as given in Figure 15 [24].

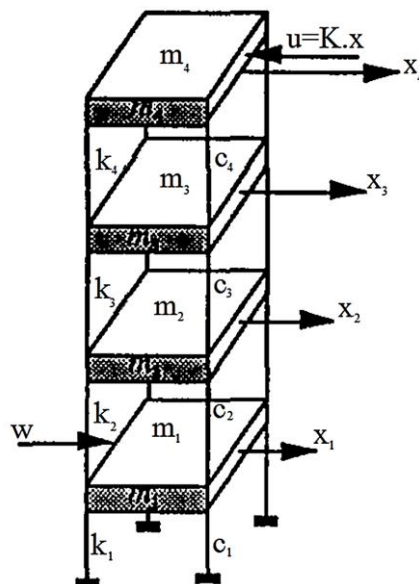


**Figure 12.** Model of the control object [24]

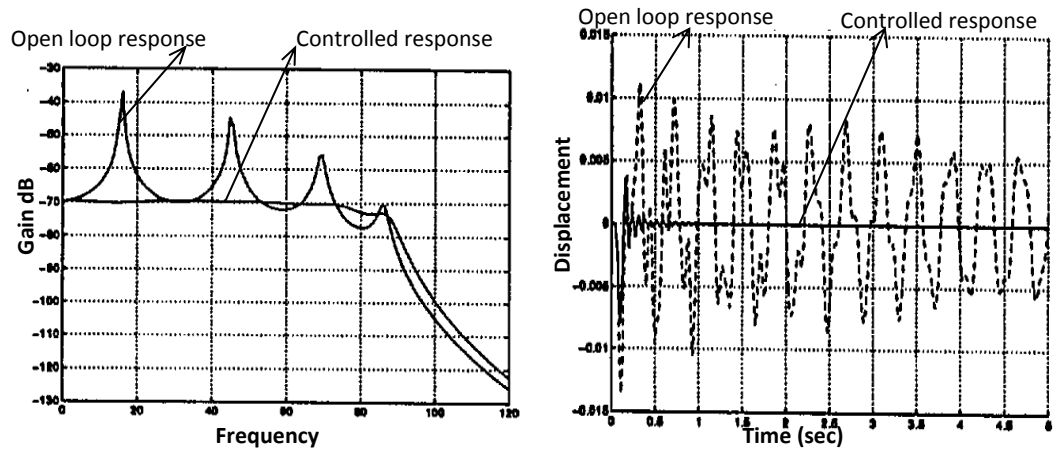


**Figure 13.** Frequency and impulse response for  $H_\infty$  control ( $\gamma_{opt} = 0.000356$ ) [24]

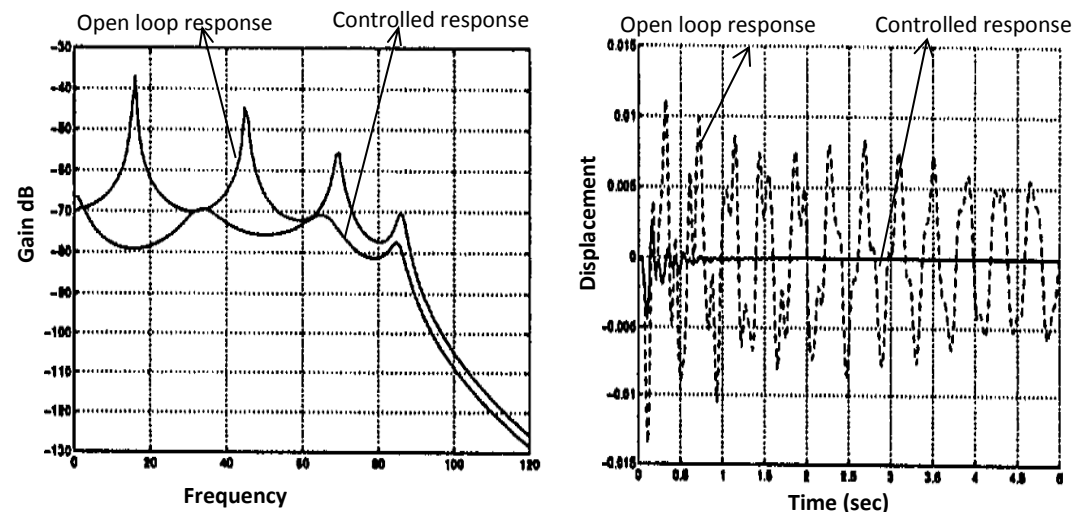


**Figure 14.** Frequency and impulse response for  $H_2$  control ( $\eta_{opt} = 0.016$ ) [24]

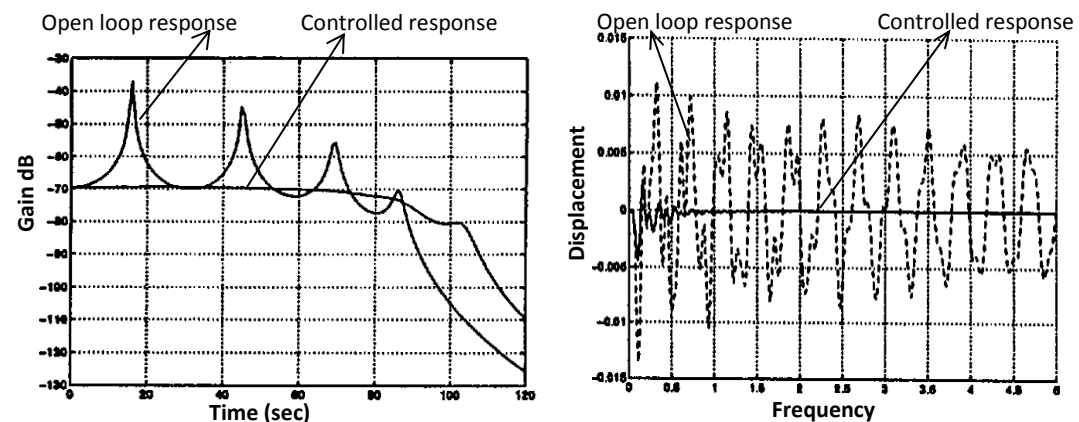


**Figure 15.** Frequency and impulse response for  $H_2/H_\infty$  control ( $\gamma_{opt} = 0.0004$   $\eta_{opt} = 0.038$ ) [24]

In 2004 Yoo et. al. bring another approach to mixed type control systems other than  $H_2/H_\infty$  type. They want to control an electromechanical fin actuation system of a guided missile. In their study, they claim that the conventional systems using a linearized model do not guarantee the satisfactory performance for a fin actuation servo system, therefore they advise to use a robust controller. Use of  $H_\infty$  technique satisfies robust stability, however a degree of freedom on robust performance is also required. To achieve this, Yoo et. al. propose a two degree of freedom controller using  $H_\infty$  and a disturbance observer [25]. Here the controller structure used in paper is given in Figure 16. In feed forward path, they use an  $H_\infty$  controller to overcome robustness issues. The disturbance observer in feedback path includes three components: a time delay estimation algorithm part, an anti-filtering compensator part and a low pass filter part. The effectiveness of this design is shown in the document via both simulation and experiment.

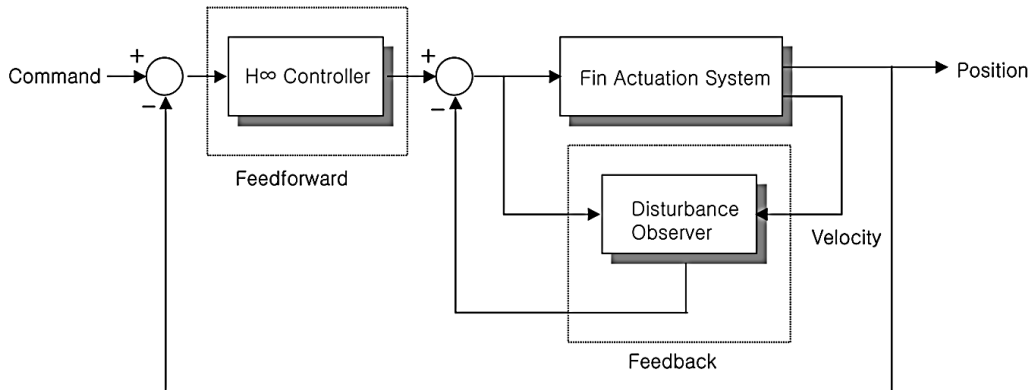


**Figure 16.** Controller structure of [25]

In the last few years, some new approaches as an extension to LMI techniques to solve mixed  $H_2/H_\infty$  problem have been developed. One of the motivation of a such kind of search is that, since the optimal controller is not unique, sometimes, solution obtained via LMI method may not achieve best values for two norms. The algorithm may also fail to find a controller even if one solution exists. Popov attacked to this phenomenon and propose a new algorithm to find the optimal  $H_2/H_\infty$  mixed controller especially in the base of the minimization of both norms. In the project [26] that presented at 2005, the problem formulation in LMI form for state and output feedback cases distinctly is given firstly. After that, the solutions for two cases of controllers (state feedback and output feedback) obtained in two different ways: via LMI toolbox of MATLAB® and using a numerical method developed by the author that uses genetic algorithm approach. Finally, Popov shows that, the controllers created by genetic algorithm suggested in the study, provides better and less conservative results than “classical” LMI convex optimization method, especially for dynamic output feedback situation. Additionally, the algorithm can find a controller such that it has similar performance and less order than LMI output. However this method requires much more computational effort than LMI methods [26].

$H_2/H_\infty$  mixed controllers find another application area in the load frequency control (LFC) of interconnected electrical power systems, because such systems have highly non-linear and hard to model dynamics. On the other hand, LFC system requirements are to minimize the transient errors of the frequency and tie-line power, and to ensure zero state errors of these quantities. Regarding these issues, Bensemouci and Ghany presented a paper on LMI based design of an output feedback control for multi-area load frequency control in 2007 [27]. As similar to the other works on literature, to solve the multiobjective design problem with regional pole constraint, they use embedded MATLAB® functions to attempt to output feedback problem. The results of the simulations are summarized and can be seen in [27].

As previously stated, LMI solvers do not guarantee the derived controller is the “best” in the optimization criteria. These common tools run a numerical algorithm. Although these methods are invaluable tools for the loop-shaping of complex systems, it is possible to obtain better closed loop responses and simpler controller architecture for some mixed control problems which can be solved explicitly. In this manner, Alazard et. al. suggest an analytical method to attempt multiobjective state feedback control problems related with mechanical systems used in aerospace engineering [28]. The linearized mechanical systems are generally described by a second order differential equation form:

$$M\ddot{q} + D\dot{q} + Kq = Fu \quad (1.26)$$

In (1.26),  $q \in \mathbb{R}^n$  is the vector of the  $n$  degrees of freedom,  $M, D, K$  are respectively the  $n \times n$  mass, damping and stiffness matrices.  $u \in \mathbb{R}^n$  is the vector of the  $n$  control signals and  $F$  is the  $n \times n$  input matrix. In this study, it is assumed the all of the states are measured and controller  $K$  is static state feedback controller. To obtain optimal mixed  $H_2/H_\infty$  controller, the acceleration sensitivity function  $P$  is weighted by a second order frequency-domain weighting function. Then the block diagram of the system is provided in Figure 17, where  $z_1$  is the performance variable to be minimized by  $H_\infty$  criterion and  $z_2$  is the performance variable to be minimized by  $H_2$  criterion.

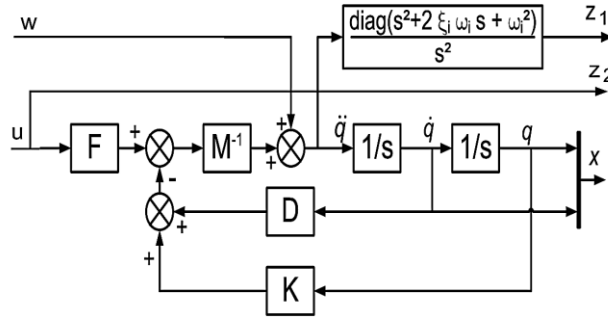


**Figure 17.**  $H_2/H_\infty$  standard problem for acceleration sensitivity control [28]

After the problem definition is stated using an objective function for optimization, they obtain generalized plant and present a detailed analytical procedure to reach to the optimal mixed controller for state feedback (full information) case both in one degree of freedom and multi-variable situations. They compare their results with the outputs of the well-known “hinfmix” macro function of MATLAB® (which uses LMI method) and underline that their analytical method gives better results in the terms objective function. For further details, see [28]. Although the analytical method gives the best controller, note that this method is available only for full information (state feedback) case. But in many real systems, it is not possible to measure all of the states.

In 2009, Akbar et. al. applied a mixed  $H_2/H_\infty$  controller to a continuous time singularly perturbed system with linear state variable feedback [29]. The control law is derived using auxiliary cost minimization approach for continuous LTI singularly perturbed system. In this paper, the writers solve the  $H_2/H_\infty$  mixed type controller by using iteratively gain independent coupled Riccati equations method different than the previous LMI techniques. After mixed type controller, they also synthesize pure LQG ( $H_2$ ) and pure  $H_\infty$  controllers in 2<sup>nd</sup>, 3<sup>rd</sup> and 4<sup>th</sup> order. They compare the performance and robustness of these different control systems via using time response to a unit step input and analyzing phase and gain margins. These results are given in the paper and presented in Figure 18, Figure 19, Figure 20 and Table 3. The results in this paper indicate that the developed mixed  $H_2/H_\infty$  type controller performs fairly better than  $H_2$  and  $H_\infty$  based controllers in both time response and robustness measures [29].

The last research to be discussed in this chapter is the  $H_2/H_\infty$  mixed controller application to a case study on full vehicle suspension. The paper is published by Türkay and Akçay in 2011 [30]. In this work, the authors develop two procedures for multi-objective control of a full vehicle suspension model excited by random road disturbances. The schematic of the controlled plant is given in Figure 21. They formulate the control problem as in the form of  $H_2/H_\infty$  mixed synthesis and find the output feedback type controller using conventional LMI method for convex optimization. This method yields a controller that has the same order with the generalized plant. To obtain a reduced order controller, they re-formulate the multi-objective control as a non-convex and non-smooth optimization problem. Next, they propose a solution method to new formulation via fixed-order optimization. The simulations using these two different methods show that, the lower order controllers can also have similar performance enhancement to LMI design. They also state that, both of the obtained controllers are good alternative to LQG based ones.

The cited literatures show that the basic performance properties of the different types of control methods can be summarized as in Table 4.

**Table 3. Gain and Phase Margins [29]**

System	2 <sup>nd</sup> order	2 <sup>nd</sup> order (uncert.)	3 <sup>rd</sup> order	4 <sup>th</sup> order
$H_2/H_\infty$	GM=∞ PM=∞	GM=∞ PM=∞	GM=∞ PM=95.8°	GM=∞ PM=88.07°
LQG	GM=∞ PM=84.5°	GM=∞ PM=81.4°	GM=∞ PM=77.0°	GM=∞ PM=61.01°∞
$H_\infty$	GM=∞ PM=95.1°	GM=∞ PM=94.5°	GM=∞ PM=103°	GM=∞ PM=62.7°

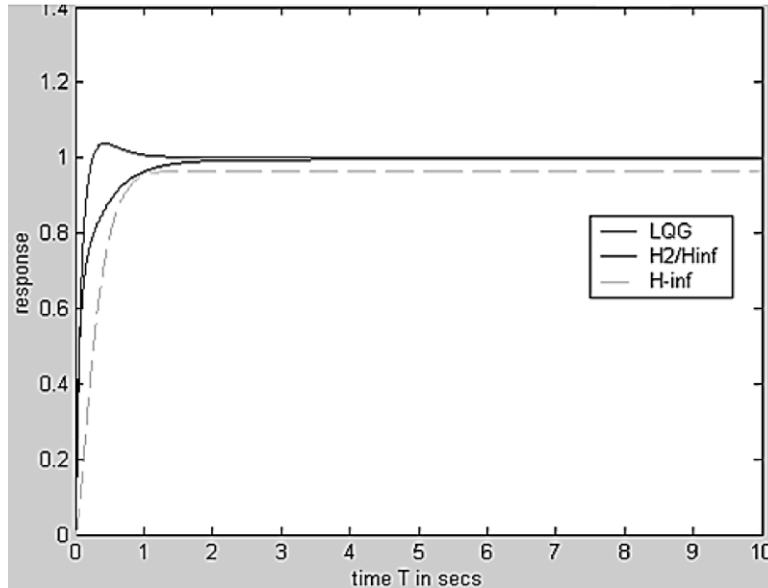


**Figure 18. Step response of mixed  $H_2/H_\infty$ ,  $H_\infty$ , and  $H_2$  2<sup>nd</sup> order system [29]**

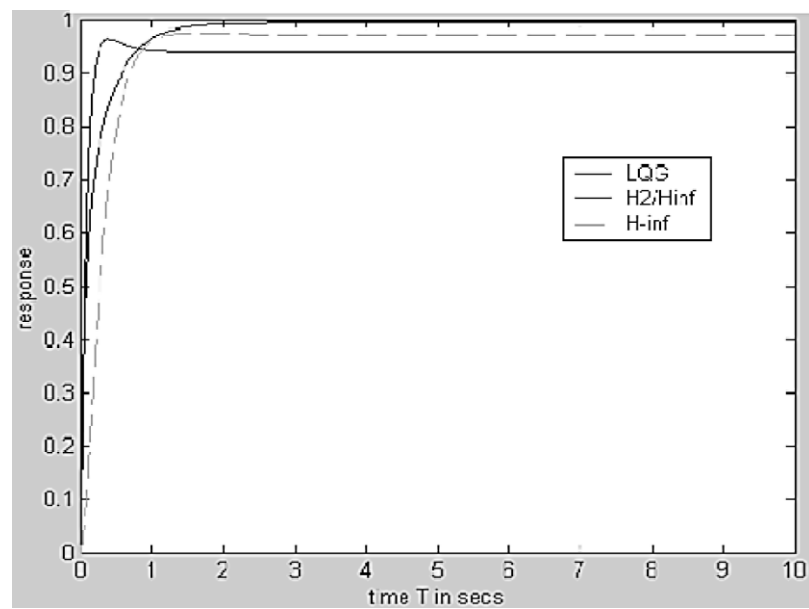


**Figure 19.** Step response of mixed  $H_2/H_\infty$ ,  $H_\infty$ , and  $H_2$  2<sup>nd</sup> order system with uncertainty [29]

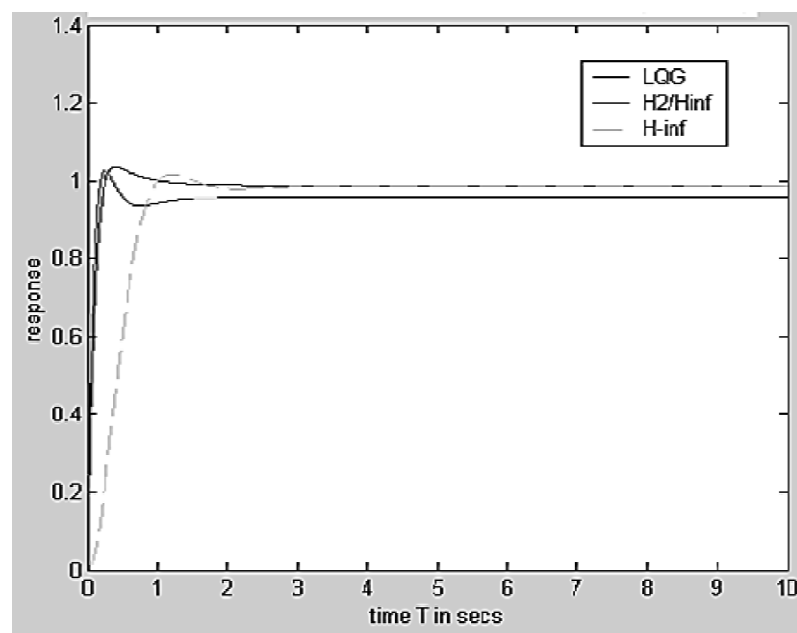


**Figure 20.** Step response of mixed  $H_2/H_\infty$ ,  $H_\infty$ , and  $H_2$  3<sup>rd</sup> and 4<sup>th</sup> order system with uncertainty [29]

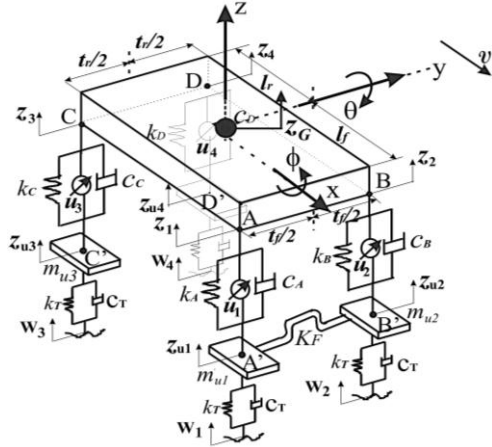


**Figure 21.** The full-car model of vehicle [30]

**Table 4.** Performance and Robustness Comparison of Different Methods

	$H_2$ (LQG) Controller	$H_\infty$ Controller	$H_2/H_\infty$ Mixed
Transient Response Performance	Very Good	Moderate	Good
Robustness to Plant Uncertainty	Moderate	Very Good	Very Good
Robustness to Exogenous Noise	Good for known frequency spectrum	Good for known bounded power	Good for both types of noises

## **CHAPTER 2.**

### **SYSTEM MODELING AND IDENTIFICATION**

#### **2.1. MODELING OF THE SYSTEM**

The task of the fin actuation system in a guided aerial platform is to implement the required angular positional fin deflection that comes from the guidance autopilot. To satisfy position of the missile platform such that it precisely follows a route previously planned; angular fin deflection data are derived by guidance autopilot using aerodynamics principles and acceleration data read by gyros. To increase the precision level of the ammunition, other type of sensors, for example infrared imaging, laser distance measurers etc. can also be used. The instant data of the overall missile is obtained using inertial measurement units. The autopilot calculates required positional rates in yaw, pitch and roll rates of the body and converts this data to fin deflections in the light of the all sensor information. When the position command is generated by the autopilot, the mission of the fin actuation system (FAS) starts.

##### **2.1.1. Description of the Physical System**

The back side view of a missile and corresponding positive direction of force and moment vectors at each control surface are shown Figure 22. During the flight of the missile, forces and torques on the control surfaces occur due to aerodynamics of the system. The control surface should overcome these loads and conserve their orientation to make the required maneuver. All of the forces and torques other than hinge moment can be carried by the bearings of the fin shaft; the hinge moment  $M_y$  must be overwhelmed by FAS. To achieve this, use of a mechanism is inevitable. In this manner, an inverted slider crank mechanism is connected to the control surfaces. The explanation and detailed mathematical model of the mechanism is given in section 2.1.2.3.

In this study, the handled fin actuation plant is an electromechanical system. In this plant, there are a brushless DC servo motor coupled to the outer fins of the missile via a transmission mechanism connected on the shaft and a sensor as a feedback element for to measure position. The output of the system is the actual fin deflection; however, due to physical restrictions of the missile, the position sensor cannot be placed to the fin, instead placed to the motor shaft. Nonetheless, since the mathematical model of the transmission can be well defined, one can easily derive the real fin angle using motor position.

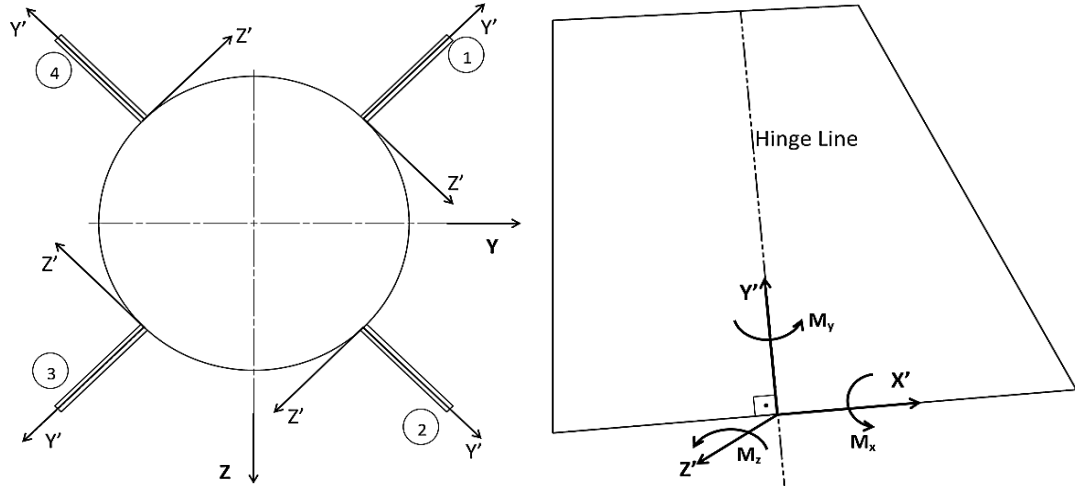


**Figure 22.** Schematic backside view of an ammunition and coordinate frame for a fin

### 2.1.2. Mathematical Models of the Subcomponents

#### 2.1.2.1. Motor

Servo motor is a device that converts electrical energy to mechanical torque. The input to a servo motor is current and it produces torque directly related to the input current. The servo motor assumed to have a linear characteristics and the its constitutional equation is given in equation (2.1) where  $T_m$  is the total torque produced by the motor at the motor shaft,  $K_t$  is motor torque constant and  $I$  is the input current to the motor.

$$T_m = K_t \cdot I \quad (2.1)$$

The constant  $K_t$  is the characteristics of the motor and ideally it is defined as a constant in room temperature. According to the related technical documents of the component, the value can have small variations (less than 5%) in operating conditions. However, to hold the system linear during the modeling and control, this value will be assumed as constant.

To identify the value of torque constant, a dynamometer set-up is used as a resistive load to test the motor. The dynamometer is directly coupled to motor shaft and the generated torque by motor is measured in static condition. The obtained data visualized in Figure 23 as in the form of torque versus current. Here the obtained linear fit to data by least square method indicates that the motor constant (the slope of the fitted curve) is about  $45000 \frac{\text{kg} \cdot \text{mm}^2}{\text{s}^2 \cdot \text{A}}$  with a coefficient of determination (R-squared) value of 0.99. However,  $K_t$  of the motor is given in the technical document of the motor as

$K_t = 48000 \frac{\text{kg} \cdot \text{mm}^2}{\text{s}^2 \cdot \text{A}}$ . This means there is 5% deviation in the value of torque constant as calculated in equation (2.2). This deviation is also provided in the datasheet of the motor as the same value. During the controller design and system identification procedure, the nominal value of torque constant will be assumed as in the datasheet of the motor.

$$\Delta K_t = \frac{48000 - 45000}{48000} \times 100 \approx 5\% \quad (2.2)$$

Another important point that can be observed from Figure 23 is that, the motor is able to start to generate mechanical torque after 0.35 A. The source of this loss is the phenomenon of *cogging*.

*Cogging torque* in a brushless DC motor is the torque due to interaction between the permanent magnets on rotor and slots of the coils on the stator. The cogging phenomenon induces a dead zone dynamics. It is undesirable and can be seen on only “infinitesimal motion” of the shaft. Actually, the overall  $0.35\text{ A}$  loss in the current does not only originated by cogging; but also the frictional effects on the bearings of the motor shafts contributes to this value. The detailed modeling of this dead zone is another issue and is not covered in this thesis, because in this system the motor will bear against higher loads and also will make relatively larger amplitude motions. Therefore, this torque loss due the cogging will be assumed to be as constant dead zone loss. This dynamics will be taken into consideration during calculations and simulations. Using equation (2.1), one can obtain the corresponding total torque loss is  $T_{cog} = 17\text{ N}\cdot\text{mm}$  as shown in equation (2.3).

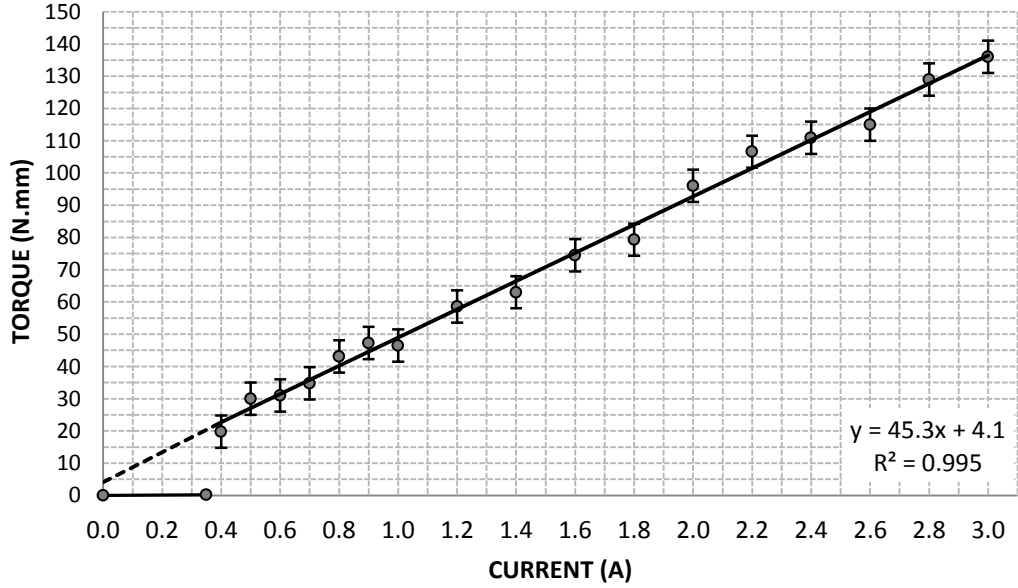


**Figure 23.** Data from the motor characteristic test

$$T_{cog} = K_t \cdot I = 48000 \times 0.35 = 17\text{ N}\cdot\text{mm} \quad (2.3)$$

The net torque at the output of the motor shaft drives a mechanical rotational system that has a general equation of motion as in equation (2.4) [31].

$$T_{net} = J_{eq} \ddot{\theta}_m + B_{eq} \dot{\theta}_m + T_{hinge} \quad (2.4)$$

In equation (2.4),  $J_{eq}$  is the total equivalent inertia at the motor side,  $\theta_m$  is the angular position of motor shaft,  $B_{eq}$  is equivalent viscous damping coefficient and  $T_{hinge}$  is the external torques (aerodynamic hinge moments on fin) coming from outside of the body as disturbance. Here  $T_{net}$  is net torque output of the motor and given in (2.5).

$$T_{net} = T_m - T_{cog} \quad (2.5)$$

Other parameters and variables in equations (2.4) and (2.5) will be explained in detail in the following sections.

### 2.1.2.2. Sensor

In a control system, the most critical component is the sensor that measures the plant output. In a FAS the output is the angular position of the fin as an aerodynamic control surface. As previously mentioned, in the FAS of this study, due to some geometrical, physical and financial limitations, an incremental encoder is used as a position sensor that measures the rotation of the motor shaft. The sensor used is a digital type sensor; therefore it is robust to noise in electrical signals. The encoder works in 11-bit resolution. This means that the count of the signal increments 2048 ( $= 2^{11}$ ) times for one revolution of the motor shaft. The data from the encoder are taken at 1 kHz. Although the system is digital, there may occur errors on digital reading values. The experiments show that in some noisy media, the last bit of the encoder data may have fault. This situation will be considered in the controller synthesis part as a criterion in weighting selection.

### 2.1.2.3. Motion Transmission Mechanism and Calculation of Transmission Ratio

The physical system behind the fin is an inverted slider crank mechanism as an example of 4-link mechanisms. The schematic diagram of the mechanism with positive directions is given in Figure 24. The input to the mechanism is the stroke of the slider  $s$ . The output is fin deflection angle  $\delta$ . The plant is shown at APPENDIX A.6 with a photo.

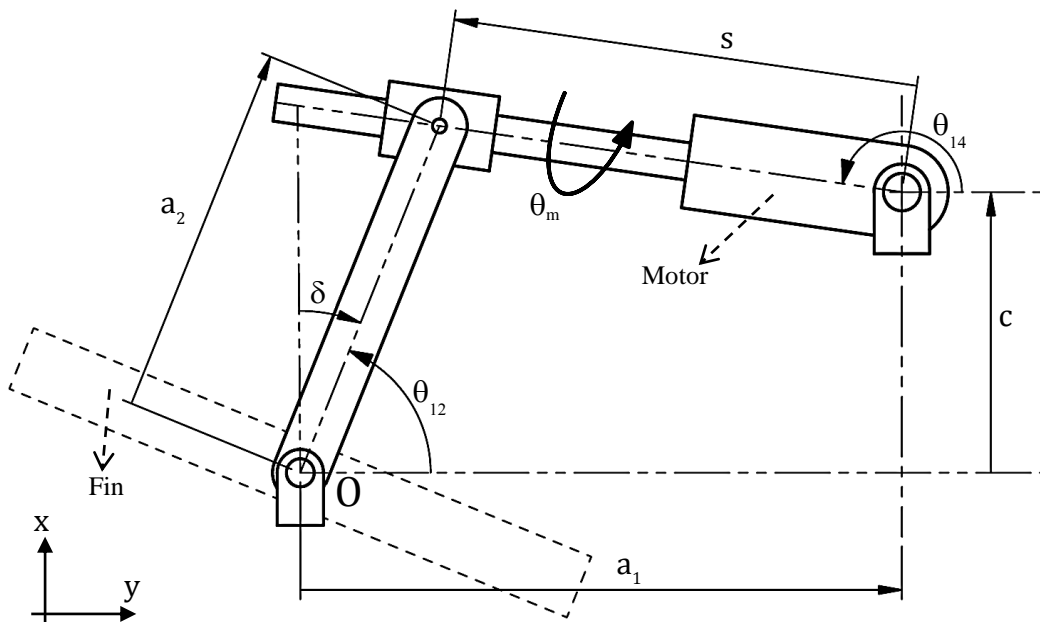


**Figure 24.** Schematic diagram of the FAS as an inverted slider crank mechanism

Sliding motion is obtained using a ballscrew directly connected to the motor shaft. Ballscrew is a mechanical component that can directly convert rotary motion to linear motion via a nut going on the screw path of the ballscrew shaft. The fins of the missile are directly connected to link  $a_2$  from the pivot point.

To obtain mathematical model of the mechanism, let us first achieve the position analysis using loop closure equation (LCE), take point O as origin and positive directions as in Figure 24.

$$a_2 \cdot e^{i\theta_{12}} = a_1 + c \cdot i + s \cdot e^{i\theta_{14}} \quad (2.6)$$

where  $i = \sqrt{-1}$ . Decompose equation (2.6) into  $x$  and  $y$  axes:

$$\begin{aligned}
x - \text{axis} \quad & a_2 \cdot \cos(\theta_{12}) = a_1 + s \cdot \cos(\theta_{14}) \\
y - \text{axis} \quad & a_2 \cdot \sin(\theta_{12}) = c + s \cdot \sin(\theta_{14})
\end{aligned} \tag{2.7}$$

Note that, in Figure 24 the rotation of the motor shaft is  $\theta_m$  and this rotation is converted to linear stroke  $s$  by a ballscrew. The ballscrew is a mechanical component that has a helical raceway for ball bearings can roll over it such that with an appropriate threaded nut assembled onto shaft; rotary motion of the screw can be converted to linear sliding motion. The pitch of the thread on the ballscrew forms mathematical relation between the motor revolution and stroke. The pitch of the ballscrew in this application is  $p = 2$  mm per revolution. In this manner,  $\rho = \frac{p}{2\pi} = 0.3183 \frac{\text{mm}}{\text{rad}}$  is the transmission ratio between motor rotation and linear movement  $s$ . This is given in equation (2.8) where  $s_o$  is constant and the minimum value of stroke.

$$s = s_o + \rho \cdot \theta_m \tag{2.8}$$

Now, in this system, the output is the fin deflection  $\delta$ . As seen from Figure 24, the equation for fin deflection can be obtained as in equation (2.9).

$$\delta = 90^\circ - \theta_{12} \tag{2.9}$$

The FAS here is capable to deflect the control surfaces to  $\delta = \pm 20^\circ$ . This yields;

$$70^\circ \leq \theta_{12} \leq 110^\circ \tag{2.10}$$

Statement (2.10) indicates that  $\theta_{12}$  can be used as independent variable to calculate the mathematical model of the overall mechanism. The mechanism is a transmission device that increases torque by reducing the speed of the actuating source. The actuator is DC motor whose position is given by  $\theta_m$  parameter. The transmission ratio ( $N$ ) between motor torque and hinge moment of control surface is equal to the ratio of the speed of the motor shaft and fin deflection. Since the parameter  $\theta_{12}$  is used as independent variable, one can obtain the transmission ratio  $N$  by using time derivatives of equations in (2.7) and (2.8). To simplify the calculations, first eliminate the parameter  $\theta_{14}$  which is also function of  $\theta_{12}$ . Rewriting of equations (2.7):

$$\begin{aligned}
s \cdot \cos(\theta_{14}) &= -a_1 + a_2 \cdot \cos(\theta_{12}) \\
s \cdot \sin(\theta_{14}) &= -c + a_2 \cdot \sin(\theta_{12})
\end{aligned} \tag{2.11}$$

Take square of both equations in (2.11) and apply summation to each side, by using identity of  $\sin^2(\theta) + \cos^2(\theta) = 1$ :

$$s^2 = a_1^2 - 2 \cdot a_1 \cdot a_2 \cdot \cos(\theta_{12}) + a_2^2 - 2 \cdot c \cdot a_2 \cdot \sin(\theta_{12}) + c^2 \tag{2.12}$$

Now, to obtain velocity relation, take time derivative of equation (2.12);

$$2 \cdot s \cdot \dot{s} = 2 \cdot a_1 \cdot a_2 \cdot \sin(\theta_{12}) \cdot (\dot{\theta}_{12}) - 2 \cdot c \cdot a_2 \cdot \cos(\theta_{12}) \cdot (\dot{\theta}_{12}) \tag{2.13}$$

Similarly time derivative of equation (2.8) returns;

$$\dot{s} = \rho \cdot \dot{\theta}_m \tag{2.14}$$

Replace  $\dot{s}$  in equation (2.14) and  $s$  in equation (2.12) to equation (2.13). After simplification one can obtain the transmission ratio  $N$  as an explicit function of independent variable  $\theta_{12}$  as:

$$\begin{aligned}
N(\theta_{12}) &:= \frac{\dot{\theta}_m}{\dot{\theta}_{12}} = \frac{T_{hinge}}{T_m} \\
&= \frac{a_2(a_1 \cdot \sin(\theta_{12}) - c \cdot \cos(\theta_{12}))}{\rho\sqrt{a_1^2 - 2 \cdot a_2 \cdot a_1 \cdot \cos(\theta_{12}) + c^2 - 2 \cdot a_2 \cdot c \cdot \sin(\theta_{12}) + a_2^2}}
\end{aligned} \tag{2.15}$$

The values of the system parameters are given in Table 5. Substitution of these values into equation (2.15) gives the value of  $N$  for each  $\theta_{12}$  value. Since the fin deflection angle is system output, the function of  $N$  is plotted with respect to  $-20^\circ \leq \delta \leq 20^\circ$  and given in Figure 25.

**Table 5.** Value of system parameters

$a_1$	100 mm
$a_2$	45 mm
$\rho$	$0.32 \frac{\text{mm}}{\text{rad}}$
$c$	43 mm

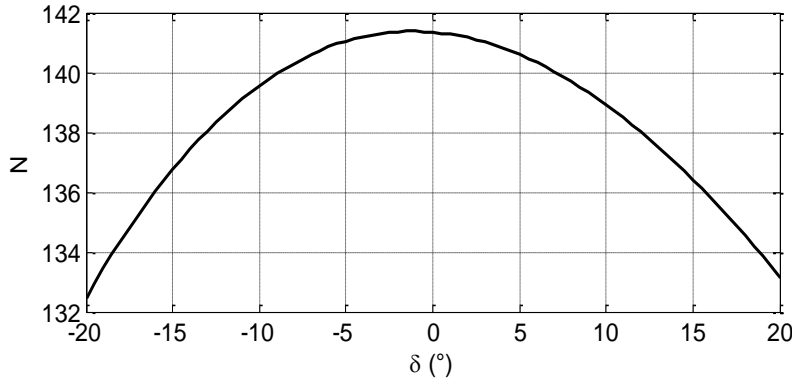


**Figure 25.** Change of transmission ratio ( $N$  vs  $\delta$ )

As seen from the Figure 25, the transmission mechanism has nonlinear characteristics. The maximum and minimum values of the transmission ratio are 141.4 and 132.4 respectively. To be able to have a linearized system model, the transmission ratio will be assumed as constant. Since the system will generally work on the vicinity of  $0^\circ$  deflection angle,  $N = 141.4$  will be used as the value of the function. However, after the linear model based controller is obtained, during the experiment and simulations, the actual value of  $N$  that depends on the fin deflection and provided in equation (2.15) will be used as a conversion factor both for motor position ( $\theta_m$ ) to fin deflection ( $\delta$ ) and motor output torque ( $T_m$ ) to hinge moment ( $T_{hinge}$ ).

#### 2.1.2.4. Calculation of Equivalent Moment of Inertia

The differential equation of motion the FAS is given in equation (2.4). Here, note that all of the moving parts are considered that has the same angular speed with the motor,  $\dot{\theta}_m$ . The rotation axes of some components of mechanism are different than motor shaft. Therefore, to be able to have appropriate model, all of the moment of inertia must be projected onto rotary axis of motor shaft. Formula for the total equivalent moment of inertia is given in equation (2.16)

$$J_{eq} = J_{nut}^{eq} + J_{ballscrew} + J_{rotor} + J_{crank}^{eq} \tag{2.16}$$

In this assembly, the shaft of the ballscrew is directly connected to rotor of the motor and behaves like the motor shaft. The moment of inertia of the  $J_{ballscrew} = 1.36 \text{ kg} \cdot \text{mm}^2$  is given by manufacturer. The moment of inertia of the rotor of the motor  $J_{rotor} = 3.22 \text{ kg} \cdot \text{mm}^2$  is provided in the datasheet of the motor. In equation (2.16)  $J_{eq}^{crank}$  is the equivalent moment of inertia of the link  $a_2$  that is connected to aerodynamic control surfaces. The projected value of the inertia can be calculated by using transmission ratio of the mechanism. It is known that, in a mechanical system the ratio of the projected moment of inertia equals to square of the gear ratio. In this manner, the moment of inertia of the crank with respect to its own rotation axis (the pivot axis at point O of Figure 24) can be derived from the 3D model of the FAS as  $J_{crank} = 229.4 \text{ kg} \cdot \text{mm}^2$ . Then using equation (2.17)

$$J_{crank}^{eq} = \frac{J_{crank}}{N^2} = \frac{229.4}{141.4^2} = 0.01 \text{ kg} \cdot \text{mm}^2 \quad (2.17)$$

The equivalent moment of inertia of the nut can be derived from kinetic energy equation for both frames, because it has translational motion. The velocity of the nut  $v_{nut}$  is equal to  $\dot{s}$ ,  $m_{nut} = 0.042 \text{ kg}$  is given by manufacturer and by using equation (2.14)

$$\begin{aligned} \frac{1}{2}m_{nut} \cdot v_{nut}^2 &= \frac{1}{2}J_{nut}^{eq} \dot{\theta}_m^2 \\ m_{nut} \dot{s}^2 &= J_{nut}^{eq} \dot{\theta}_m^2 \rightarrow m_{nut} \cdot (\rho \cdot \dot{\theta}_m)^2 = J_{nut}^{eq} \dot{\theta}_m^2 \\ J_{eq}^{nut} &= m_{nut} \cdot \rho^2 = 0.042 \cdot 0.3183^2 \\ &= 0.004 \text{ kg} \cdot \text{mm}^2 \end{aligned} \quad (2.18)$$

Now, replace corresponding parameters in (2.16) with the equations (2.17) and (2.18):

$$J_{eq} = 4.6 \text{ kg} \cdot \text{mm}^2$$

### 2.1.3. Creation of Block Diagram for Controller Synthesis

In section 2.1.2, the required mathematical models are derived. Using equations (2.1), (2.4) and (2.5) one can draw the entire block diagram. To have a block diagram in a system, system should be taken as linear, to achieve this; the value of the function  $N$  in (2.15) will be taken constant as previously mentioned.

#### 2.1.3.1. External Loads and Disturbances

The external loads on the system are  $T_{hinge}$  and  $T_{cog}$  as torques due to aerodynamic effects and the total torques due to dry friction and cogging, respectively. The value of  $T_{cog}$  is found to be as  $17 \text{ N} \cdot \text{mm}$  experimentally as previously mentioned in section 2.1.2.1 and equation (2.3). The value of  $T_{hinge}$  is described from aerodynamic simulations and provided that at the fin side, the maximum possible value for total external aerodynamic load is  $40 \text{ N} \cdot \text{m}$  as a design requirement. Since all of the formulations and equations are defined on motor rotary axis (in terms of  $\theta_m$ ), using the linearized value of transmission ratio  $N = 141.4$ , this magnitude can be projected onto motor rotary axis. In this manner;

$$\begin{aligned} |T_{hinge}| &\leq \frac{40 \cdot 10^3}{141.4} \\ |T_{hinge}| &\leq 283 \text{ N} \cdot \text{mm} \end{aligned} \quad (2.19)$$

It is assumed that  $T_{hinge}$  randomly varies between the values described at (2.19) in a uniform manner. The absolute sign here is used to show that, the direction of the external torque also changes.

On top of external torques, the system also has sensor noise as a disturbance entry as previously stated in section 2.1.2.2.

### 2.1.3.2. System Parameters and Uncertainties

The linearized model of the system can be obtained using the equations of the system given in (2.1), (2.4) and (2.5). Taking Laplace transform of differential equation (2.4) and simple manipulations yield the transfer function of the plant from control signal  $I(s)$  to system output  $\theta_m(s)$  as in (2.20).

$$\frac{I(s)}{\theta_m(s)} = \frac{K_t}{s(J_{eq}s + B_{eq})} \quad (2.20)$$

In equation (2.20),  $K_t$  is defined with its uncertainty in section 2.1.2.1 using technical documents and experiments. Value of  $J_{eq}$  is derived in section 2.1.2.4. The only unknown parameter here is  $B_{eq}$ . This parameter cannot be directly defined using mathematical methods and will be found experimentally via system identification techniques.

### 2.1.3.3. Weighting Functions

In robust controller design, weighting functions are used to shape the performance and robustness characteristics of a closed loop system. With the aid of the weighting functions, the robust control problem can be converted into an optimization problem. In this section, the required weighting functions and the notations will be introduced. The content and property of the weighting functions will be given in controller synthesis chapter in detail.

In the system studied here, there are 3 disturbance signals introduced in section 2.1.3.1 and summarized here:  $d_1$  = external torques due to cogging effect,  $d_2$  = external torques due to aerodynamic loads  $d_3$  = disturbances due to sensor noise. Weighted disturbances will be used as loop shaping paradigms for robust controllers.

There is 1 exogenous input other than disturbances, namely  $\delta_{ref}$  = reference command for fin deflection.

Required performance variables (costs) are  $z_1$  = the difference between the system output  $\delta$  and required idealized system behavior and  $z_2$  = the weighted value of controller output. In mixed controller design case. An additional  $z_3$  variable is defined to use in mixed  $H_2/H_\infty$  case as cost to the control signal in  $H_2$  manner.

The output of the plant is  $\theta_m$  = angular position of motor and will be converted to fin deflection  $\delta$  using transmission ratio  $N$  as previously stated.

To tune the controller such that it meets the design requirements, the parameters should be shaped in design space. Following notations will be used for weighting functions.

- $W_{ref}$  : For reference command signal, related to  $\delta_{ref}$
- $W_{cog}$  : For losses due to cogging torque  $T_{cog}$ , related to  $d_1$
- $W_{aero}$  : For external aerodynamic loads  $T_{hinge}$ , related to  $d_2$
- $W_{sens}$  : For sensor noise, related to  $d_3$
- $W_{perf}$  : To penalize deviation from ideal closed loop system, related to  $z_1$
- $W_{act}$  : To penalize controller output (actuation input to the plant), related to  $z_2$
- $W_{act2}$  : To penalize controller output (used in mixed controller case)

#### 2.1.3.4. Block Diagram

Using the derived equations and given functions up to here the block diagram of the system is drawn and provided in Figure 26. Here, all of the notations other than  $G_{ideal}(s)$  that denotes the ideal closed loop response characteristics, are previously defined. The figure summarizes the system to be controlled. The controller  $K(s)$  is shown as shaded and will be synthesized. The dashed lines are used to separate the uncertainty blocks. The uncertainty bound for  $K_t$  is previously gotten, the uncertainty bound of  $B_{eq}$  will be determined after system identification. In this diagram, the reference input to system is fin actuation angle in degrees; therefore it is converted to radians using conversion factor  $\frac{\pi}{180}$ .

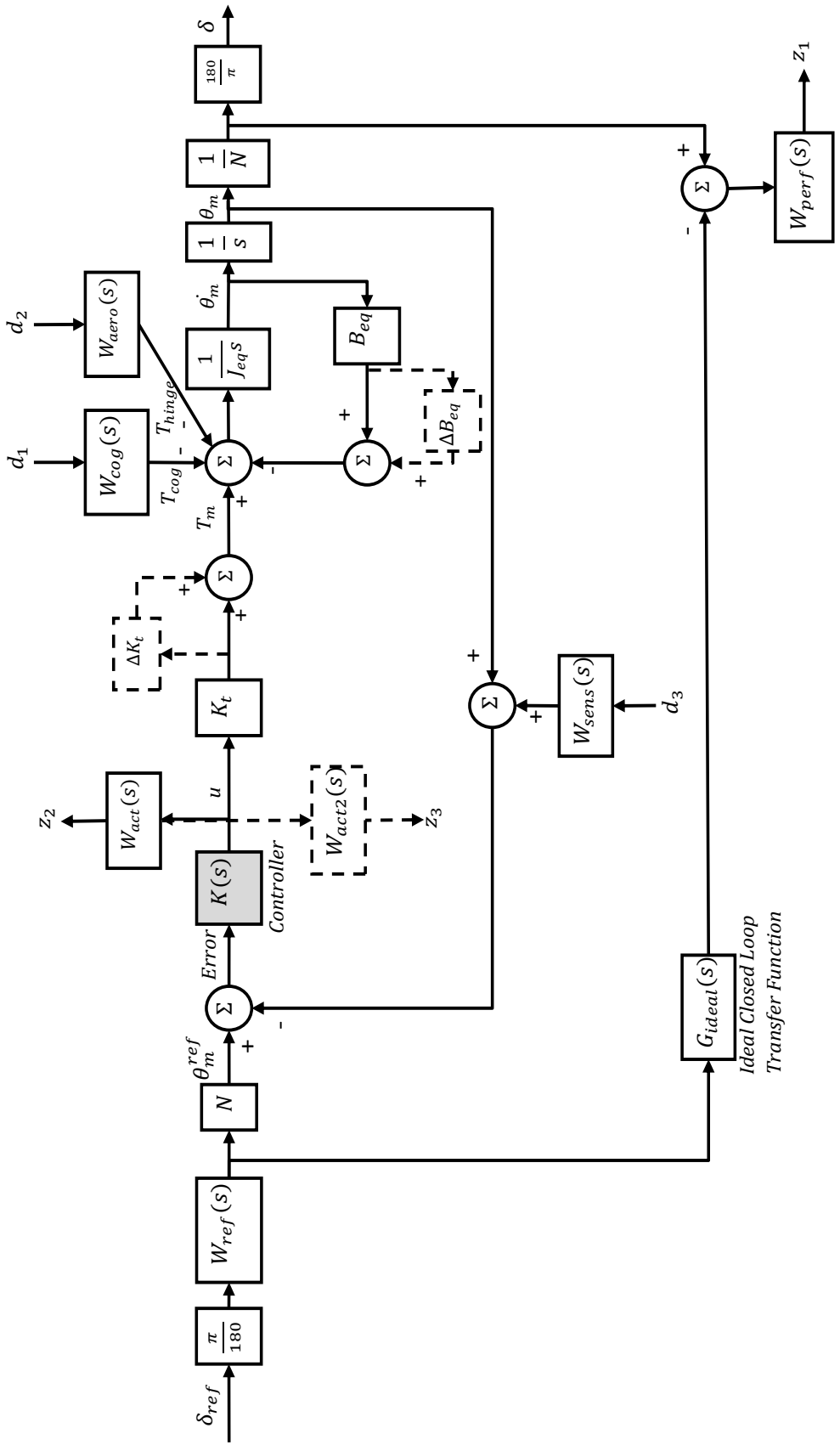


Figure 26. Block diagram for controller synthesis

## 2.2. SYSTEM IDENTIFICATION

System identification is the generation of dynamic system models from experimental data. The purpose of identification tests is to excite the plant and to collect relevant information about the process dynamics and its disturbances. The process inputs are generally random manipulating commands such that as many as possible modes of the dynamic system are stimulated.

In section 2.1 the mathematical model of the system is derived and it is demonstrated that the system is a typical 2<sup>nd</sup> order system with one integrator (type 1 system). System parameters are defined and the available values are provided. Since the system dynamics is known, the system identification will be made for a grey box model. The experimental data will be used to estimate the average value and uncertainty of  $B_{eq}$ , which is the equivalent viscous damping coefficient of the FAS. Although the modeled system is 2<sup>nd</sup> order, of course the real system has characteristics and modes in larger degree of freedom. The effects and influences of unmodeled dynamics will be inevitable in the output data of the identification experiments. However, the constraints for controller design states that, the closed loop transfer function should behave similar to a second order ideal system characteristic with 12 Hz bandwidth. As will be explained in further part of this section, the frequency content of the generated random input signals to the dynamic system can excite the system modes until 30 Hz. Therefore the system model up to 30 Hz can be obtained using these signals. In this manner, the higher frequency modes ( $> 30$  Hz) of the plant can be neglected and this lower order model of the system is sufficient to shape the closed control loop.

### 2.2.1. Real Time Data

The reference input and output of FAS is fin deflection angle. However, in this specific set-up the output of the system is the position of the motor shaft due to available position of the feedback element. Therefore, the inputs for identification are in terms of motor rotation. There are physical limits on the mechanical system. The angular rotation is saturated at  $\pm 23^\circ$  for fin deflection due to physical constraints. If the inputs to the motor shaft is large, system become saturated at these physical points.

In this system identification experiments, a MATLAB® equipped real time xPC Target® module is used as signal generator and data collector. The generated signals are directly match the current input of the motor in terms of amperes. The collected output data are the angular position of the motor read by the incremental encoder in terms of radians. The all input and corresponding output sets are given graphically in APPENDIX A.3.

#### 2.2.1.1. Designation of Inputs

The most commonly used signal types in system identification are PRBS (*pseudorandom binary sequence*) and white noise signals. The mean value of the all generated identification signals is tuned to be zero. A pseudorandom binary sequence is a signal that shifts between two levels in a certain fashion and is a periodic signal. When creating PRBS data as input to the system, the two shifting levels (gain of the signal), the period and switching time of the signal should be chosen by user. The switching time is the minimal number of sampling intervals after which the sequence is allowed to shift [32]. The main advantage of PRBS is that it can easily be generated by digital (discrete) systems.

White noise is a sequence of independent and identically distributed random variables of zero mean. Theoretically, the frequency content of white noise signal covers all frequencies with equal power. But in real systems, this is impossible due to limited energy. Hence, the band limited white noises can only be realized. In this case, the signal contains some frequency components with high magnitude within a bandwidth. The main advantage of band limited white noise is that an ideal white noise signal makes possible to stimulate all modes of a system within the bandwidth of the signal. However, for digital systems there will be some loss in frequency content of the signal due to sampling [32].

The PRBS and band limited white noise type inputs are used for excitation of the system. Meanwhile the system has saturation at  $\pm 23^\circ$ , some of the inputs induces flatness on the maximum or minimum positions of the system output. The mathematical model of the system is assumed to be linear and possible saturations annihilate the linearity. Saturation also occurs when the amplitude of the input signal is note large enough to overwhelm  $T_{cog}$ . Note that PRBS and white noise input signals are created by software tools and the requirements for signal generation are the switch time, period and amplitude of the signal. The period of the signals are chosen to be as constant and to avoid nonlinearities, switch times and amplitudes of the signals are changed until obtain satisfactorily “well” outputs that have no saturation by a trial and error method. Finally 26 datasets are generated as input signals and two examples of these signals given in Figure 27 and Figure 28 as band limited white noise and PRBS. Using these inputs, the response of the system is saved as output for post processes. To see all of the datasets used in system identification, please refer to APPENDIX A.3.

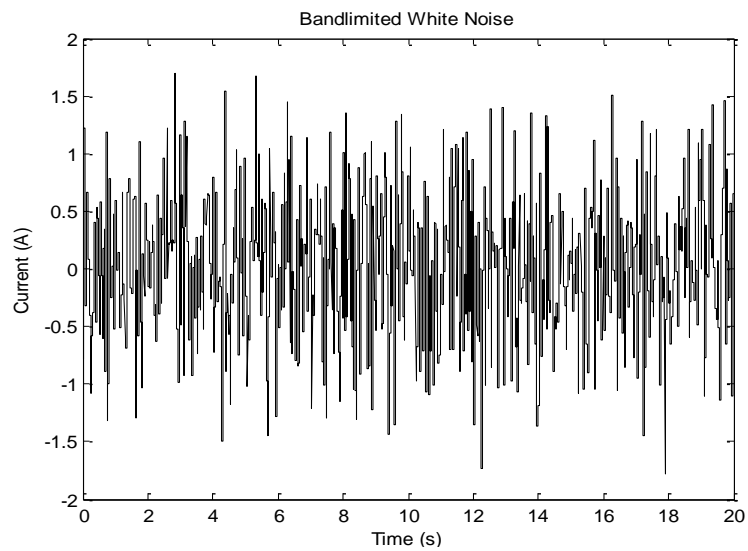


**Figure 27.** An input signal used in system identification as band limited white noise

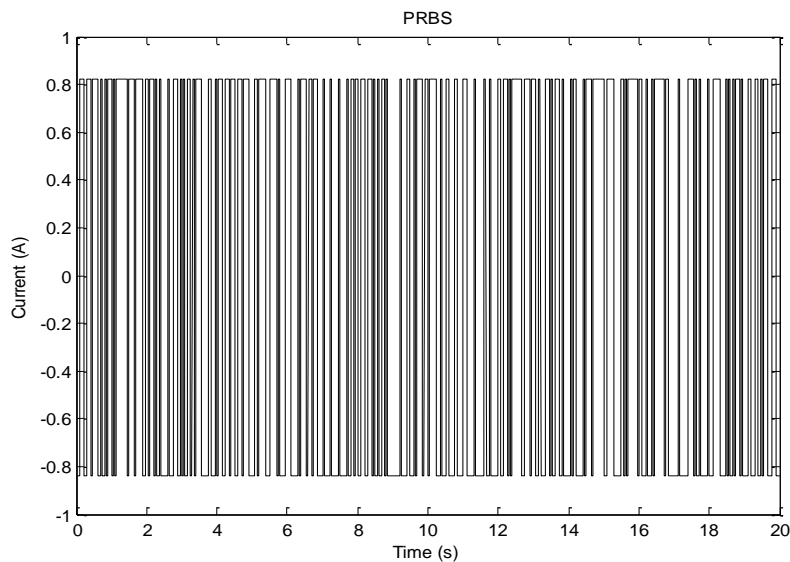


**Figure 28.** An input signal used in system identification as PRBS

Another motivation in system identification is that the input signals should excite as many possible modes as on the frequency response of the system. To get the most precise and correct mathematical model, the frequency content of the input data should be large enough to stimulate the frequencies larger than the interested region [33]. In Figure 29 the frequency content of the same input data are given by using a fast Fourier transform (FFT) algorithm. The sampling frequency of the data is 1 kHz. Therefore the maximum frequency is limited at 500 Hz. As observed in Figure 29 and APPENDIX A.4, in the most of the signals, the amplitude of the frequency content decreases after 20 Hz and the signals also have large magnitude on 30-35 Hz. After this frequency value; the excitement of the plant decreases rapidly. Nonetheless characteristic of the system up to 12 Hz is critical for controller design. Consequently, the stimulations on these inputs are sufficient to identify the low frequency dynamics to design a controller.

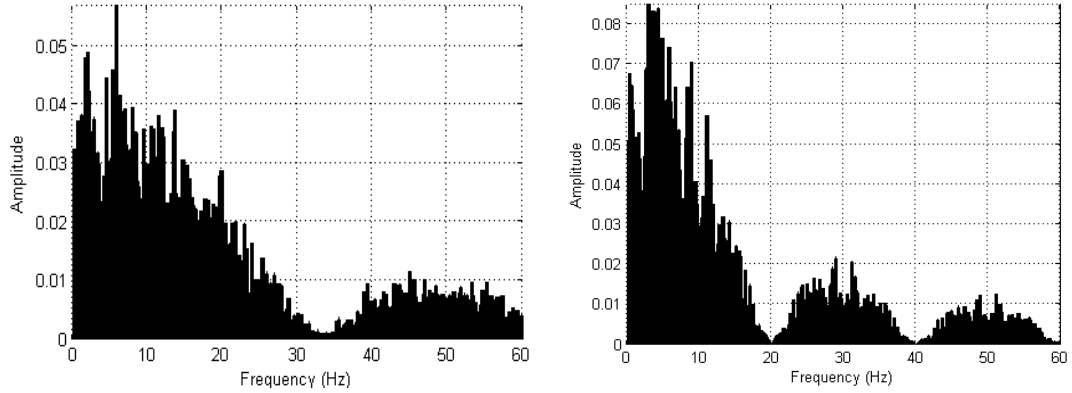


**Figure 29.** Frequency spectrum of inputs in Figure 27 and Figure 28

### 2.2.1.2. Evaluation of Outputs

The individual input signals are supplied to the plant and corresponding outputs in terms of  $\theta_m$  are recorded in time domain. Two samples of these output (to the inputs shown in section 2.2.1.1) data are given in Figure 30. As explained in section 2.2.1.1, the inputs are tuned such that there is no saturation exists on the plant output. The mathematical model of the plant assumes that the system is linear; on the other hand a drift to one side occurs during excitation. This phenomenon can be seen in Figure 30. During the post process for system fitting procedure, to eliminate this drift, the mean of the data is subtracted from the actual values. Another point in the outputs is that, the data include effects of higher frequencies. So the time domain data are filtered before using in system identification algorithm by using a low-pass filter with 30 Hz cutoff frequency, because the dynamics of lower frequencies is more important as previously mentioned.

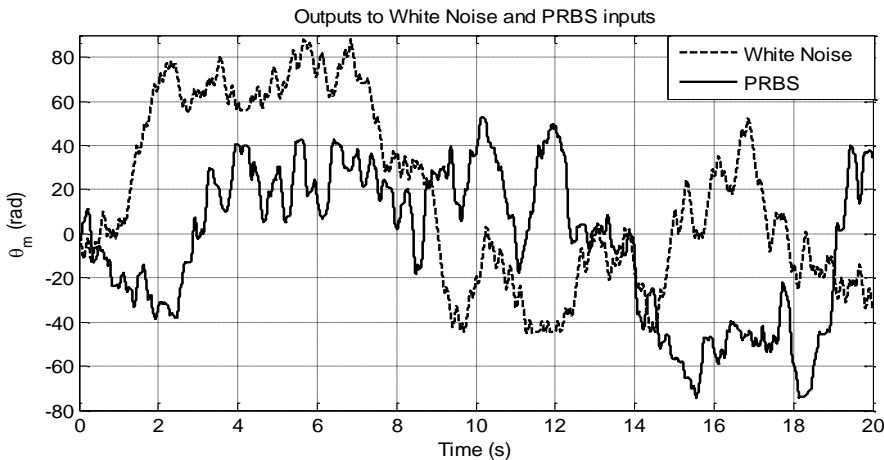


**Figure 30.** Output to inputs in Figure 27 and Figure 28

### 2.2.2. Post Processing of Data in Time Domain

In this section, the system fitting studies in time domain will be summarized. Although the data fed into system are produced to describe the frequency response characteristics of the system, the time domain processing will be achieved to have some predictions and make a simple first check for the goodness of the mathematical model obtained in section 2.1. All of the calculations, estimations and analyses are done using MATLAB® r2012a software.

The first available tool in MATLAB® is the graphical user interface of system identification tool and can be run by using ‘*ident*’ command. However in this tool the algorithm works for previously defined grey box model. As described in section 2.1 and the system is a second order system with free integrator and the form is given equation (2.20). The most similar model available in MATLAB® system identification tool is ‘Process Model’ that has the form given in (2.21).

$$G(s) = \frac{K_p}{s(1 + T_{p1}s)} \quad (2.21)$$

However, here, note that two fitting parameters  $K_p$  and  $T_p$  include the system parameters  $K_t, J_{eq}$  and  $B_{eq}$  in coupled form as in equation (2.22). Hence, it is not possible to search  $B_{eq}$  directly.

$$K_p = \frac{K_t}{B_{eq}} \text{ and } T_p = \frac{J_{eq}}{B_{eq}} \quad (2.22)$$

#### 2.2.2.1. Time Domain Compatibility Comparison Using Parameter Estimation Method

The parameter to be defined after system identification is  $B_{eq}$ , however the graphical user interface of MATLAB® system identification toolbox does not allow the isolated search for  $B_{eq}$  as indicated previously. To overcome the coupling phenomenon that given in equation (2.24); “Parameter Estimation” tool of MATLAB® SIMULINK® is used for isolated search of  $B_{eq}$ . The block diagram given in Figure 31 is drawn and the available values of  $K_t = 48000 \frac{kg \cdot mm^2}{s^2 \cdot A}$  and  $J_{eq} = 4.6 kg \cdot mm^2$  are placed. Then the available experimental inputs and outputs are uploaded to model using the graphical user interface (GUI) of “Parameter Estimation” tool. The options for searching algorithms are set to their default value. The parameter to be estimated assigned as  $B$  and using least square error method, the software has found the appropriate values as presented in Table 6. Then

using the obtained  $B_{eq}$  values for each individual sets, the outputs of simulation and the measured ones are tabulated in Figure 32. Note that the obtained average value for  $B_{eq} = 234.7 \frac{kg\cdot mm}{s}$ .

**Table 6.** Obtained  $B_{eq}$  values by parameter estimation in kg.mm/s

Dataset	$B_{eq}$
DataY4	263.5
DataY9	265.5
Data9	130.1
Ident5	246.6
DataY6	268
<b>Average</b>	<b>234.7</b>

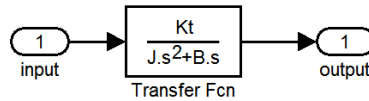


**Figure 31.** Block diagram in SIMULINK® for parameter estimation

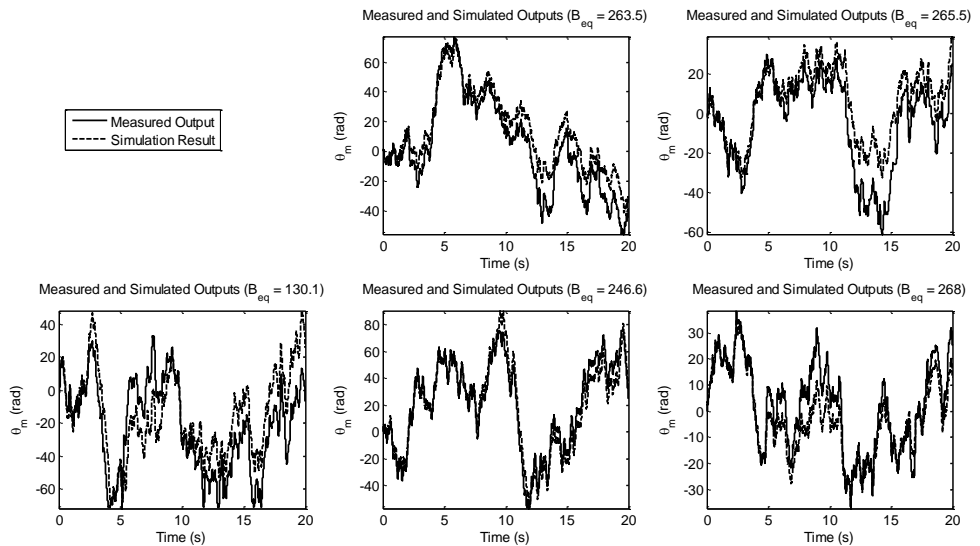


**Figure 32.** Comparison of parameter estimation results with real outputs

### 2.2.2.2. Checking the “Goodness” of the Fits Using VAF Criterion

There are some available goodness of fitting standards available in the literature related to measure the quality of the fitting. In 1998, Babuska introduced a criterion to measure the validation performance of a system identification procedure [34]. This criterion called as VAF (Variance Accounting For) and makes it possible to evaluate expressed as a percentage, quality of a model by comparing the standardized variation of the variance between two signals. This method is very well specialized to system identification. It gives comparably more meaningful results than previous statistical methods, especially when one compares the modeled and real data in visual way. The optimal value is 100% if two signals are equal. If the trend of the data generated by identification is

similar and parallel to the experimental data, VAF criteria produces a result very near to 100%. However this case is not true for other statistical methods, for example normalized mean square error method or others. The expression for VAF criterion is given in (2.23) where  $y$  is the output of the real system (measured) and  $y_m$  is the output of the model prediction.

$$VAF = 100\% \left( 1 - \frac{var(y - y_m)}{var(y)} \right) \quad (2.23)$$

The calculation in equation (2.23) is achieved in MATLAB using the following script:

```
VAF= diag(100*(eye(size(Y))-cov(Y-Ymodel)./cov(Y)));
```

VAF criterion applied to both function fittings from system identification and parameter estimation. The VAF compatibility of the system identification toolbox functions are as follows: The simulated outputs of the datasets and functions of Table 6 are given in Figure 32. Note that the simulation outputs are very similar to the real outputs such that the VAF values vary between 96.5 – 96.8%. Although the calculated goodness values of the same function changes for different datasets, some of the data creates very compatible results, for example VAF values vary 91.6 – 94.3% for different  $B_{eq}$  values and this similarity level is very sufficient for controller design.

To analyze the goodness for the fits of parameter estimation look at Figure 32. Note that some simulations yields better results. The corresponding VAF compatibility values of these functions are given in Table 7 with consecutive  $B_{eq}$  values in order from right to left and from upper to lower at Figure 32.

**Table 7.** VAF values of the fittings via parameter estimation

Dataset	$B_{eq}$	VAF
DataY4	263.5	94%
DataY9	265.5	84.4%
Data9	130.1	57.7%
Ident5	246.6	94.7%
DataY6	268	88.2%

VAF calculations in this section are achieved using the MATLAB® scripts provided above. The VAF compatibility values changes for different datasets and different functions. If the “quality” of the stimulating data is better, the excellence level of the parallel function fitting becomes much higher.

### 2.2.3. Post Processing of Data in Frequency Domain

Input to stimulate the system modes are fed into set-up in time domain and corresponding system outputs are collected. After that, some system identification methods are applied in time domain. According to these results, the system suits well to a second order continuous transfer function. The amount of the uncertainty in parameters cannot be obtained appropriately, because it is not possible to evaluate all time domain data together since the time domain characteristics of the inputs are different.

One of the bad features of time domain identification is that, the output of the system is very dependent to initial conditions, besides the suitable initial conditions of fitting functions are not easily be predictable. Therefore, in some cases, even though the trends of both outputs (the modeled and measured) are the same, the quality of fitting may be bad due to initial condition differences. Another issue in time domain response is that, the simulation results of fitted function do not provide direct prudence for frequency response of the real system. But, generally the frequency response characteristics of the model is more important. Even if the fitted functions have satisfactory VAF values, to verify the quality of the functions especially in compatibility of frequency response,

fitting procedure in frequency domain is also necessary. The post processes and verification in frequency domain are presented in this section.

Since there is not any direct frequency domain system identification tool, some algorithms are created and carried out by using the built-in functions of MATLAB®. In this manner, all of the time domain data converted to frequency domain by using “*tfeestimate*” built-in function of MATLAB®. Using this script, the frequency response characteristics of the all experimental data are obtained together and plotted in Figure 33 as Bode diagram. Each colored solid line denotes the output of different dataset.

Note that in Figure 33 all of the outputs show a general behavior and their general trend is the same. Another important observation is that, there are indistinguishable and randomized characteristics after about 200 rad/s ( $\approx 30$  Hz) for all datasets. This case is originated by the nonlinearities and higher modes of the system. As explained before, the excitation of the input signals rapidly decreases after 30 Hz (look at the figures of frequency spectrum of inputs in APPENDIX A.4); therefore the characteristics obtained at larger frequencies are not guaranteed to belong to real dynamic system. Due to controller performance necessities, examination of the dynamics up to 30 Hz will be enough. In the following sections, the identification procedures will be applied to 0 – 30 Hz frequency range. Hence, these high frequency modes will be neglected, only the linear portion of the data will be taken into account.

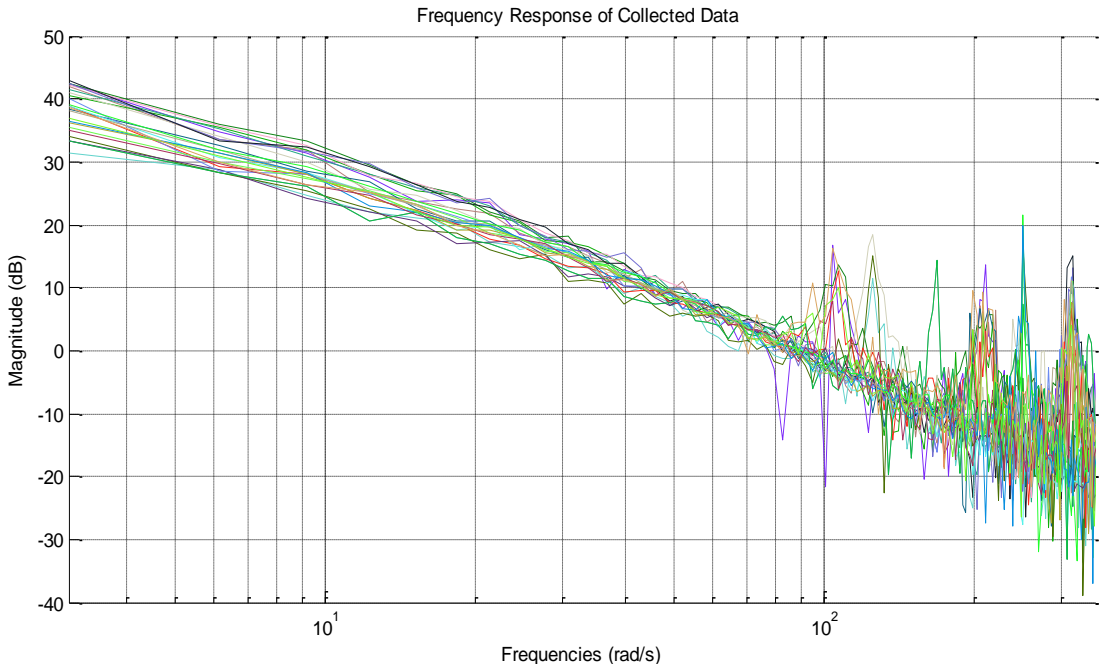


**Figure 33.** Frequency characteristics of the experimental outputs

#### 2.2.3.1. Bode Diagram Fitting with Least Square Error Method

As seen from Figure 33, the Bode diagram of the experimental data is compatible to a second order system with free integrator as given in equation (2.20). Using this model an algorithm developed to find the unknown parameter  $B_{eq}$ . The script is based on least square error method and the aim is to find the ‘best’ fitting curve in frequency domain data. Since the general trend of the data is known,  $B_{eq}$  will be assigned as varying parameter and corresponding ‘best’ value will be recorded for each individual dataset. By this method, it is possible evaluate multiple datasets together. When the

algorithm finishes, not only the value of  $B_{eq}$  for each dataset but also the limits for the unknown parameter will be found. Using this limits and the mean value of parameter, amount of uncertainty is determined.

The scripts for transfer function fittings are created by using “*lsqnonlin*” built-in command of MATLAB® to fit a second order function to experimental data in the form of  $\frac{K_t}{J_{eq} \cdot s^2 + B_{eq} \cdot s}$ . Firstly the frequency response of the initial transfer function is calculated and then changing the value of  $B_{eq}$  and taking the other parameters as constant, the results are compared until the nonlinear least square curve fitting problem is solved. The form of nonlinear curve fitting problem is given in equation (2.24).

$$\min_x \|f(x)\|_2^2 = \min_x (f_1(x)^2 + f_2(x)^2 + \dots + f_n(x)^2) \quad (2.24)$$

In the algorithm generated here, the  $f(x)$  in (2.24) is the frequency response of the estimated transfer function. These function fits are shown in Figure 34. Note that, all of the responses can be squeezed into a bound. The corresponding  $B_{eq}$  values are listed as in the order of datasets given in APPENDIX A.3.

$$B_{eq} = \{125.3; 133.2; 141.4; 118.8; 144.5; 134.1; 120.4; 129.3; 123.6; 362.2; 196.2; 340.4; 314.2; 199.3; 321.9; 191.7; 340.4; 176.7; 250.1; 200.2; 232.6; 177.4; 224.8; 266.6; 222.3; 197.3\}$$

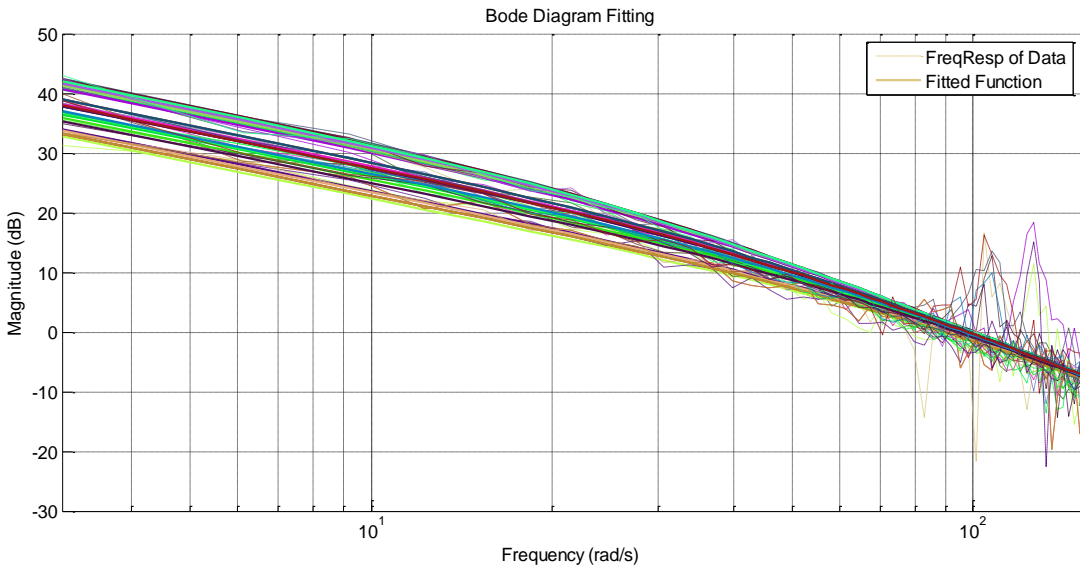


**Figure 34.** Fitted transfer function fittings on Bode diagram

These results will be evaluated at section 2.2.3.3 in quality manner. Corresponding equivalent viscous friction coefficient varies between  $B_{eq}^{max} = 362.2 \frac{kg \cdot mm}{s}$  and  $B_{eq}^{min} = 118.8 \frac{kg \cdot mm}{s}$ . The mean value is  $B_{eq}^{mean} = 207.1 \frac{kg \cdot mm}{s}$ . These extremes create a band on the Bode diagram and this case is plotted in Figure 35.

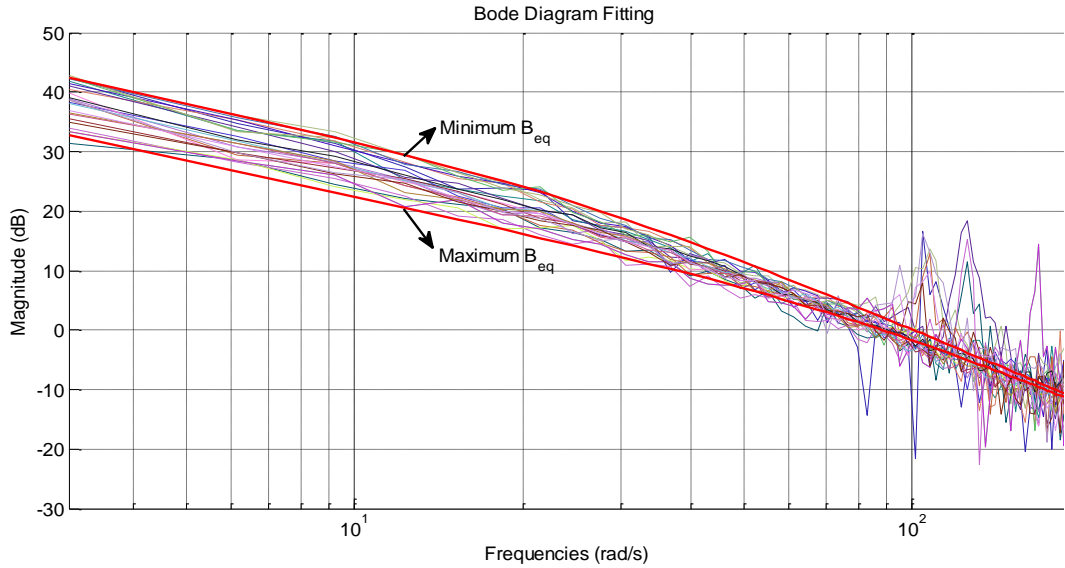


**Figure 35.**  $B_{eq}$  limits with frequency responses

#### 2.2.3.2. Experimental Creation of Bode Diagram

In section 2.2.3.1, the time domain data are transferred into frequency domain and the Bode diagram fitting procedures are applied. The frequency response of the real system can be measured experimentally and these results can be used for the confirmation of the system identification told in previous sections. On this aim, the real system stimulated by sinusoidal inputs and corresponding sinusoidal outputs are saved. One example of these inputs-outputs is given in Figure 36.

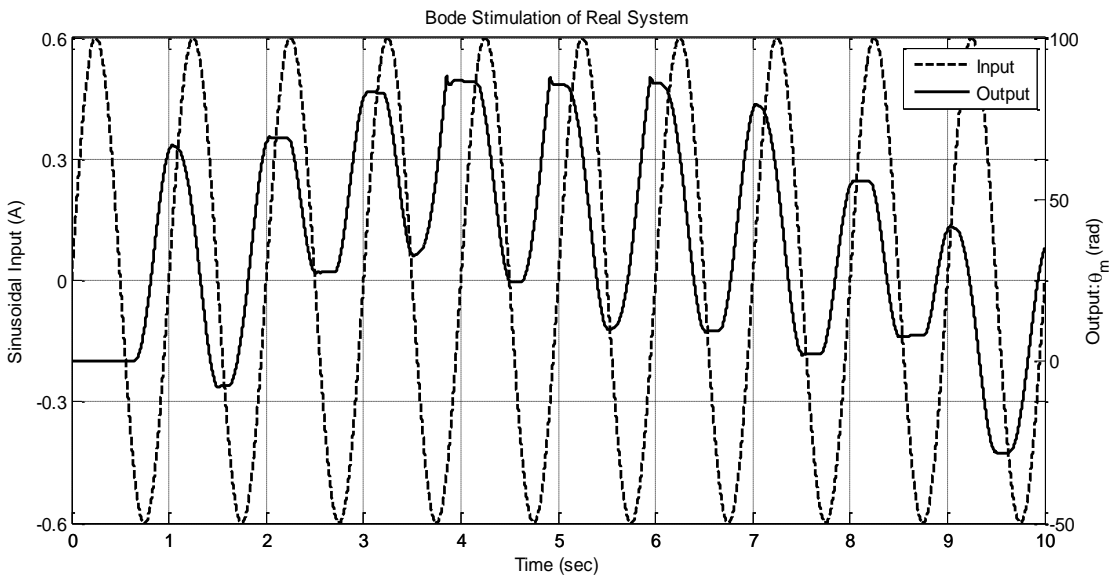


**Figure 36.** The input and corresponding output to find Bode plot of the real system

Note that in Figure 36, the output not only have amplitude and phase difference, but also there is drift; because of nonlinearity. However one can remove this trend via post process of data. Another important observation from the figure is that, there also exists some straightness on top of the sinusoidal responses. The reason for this saturation is cogging. Note that at these regions, the value of the incoming current is below than 0.35 A. After the trend in the data is eliminated via post processing; the ratios between the amplitude of output and input at each frequency is recorded. Then using the same method with section 2.2.3.1, a curve that has the form of second order transfer function with free is fitted. The obtained results are shown graphically at Figure 37.

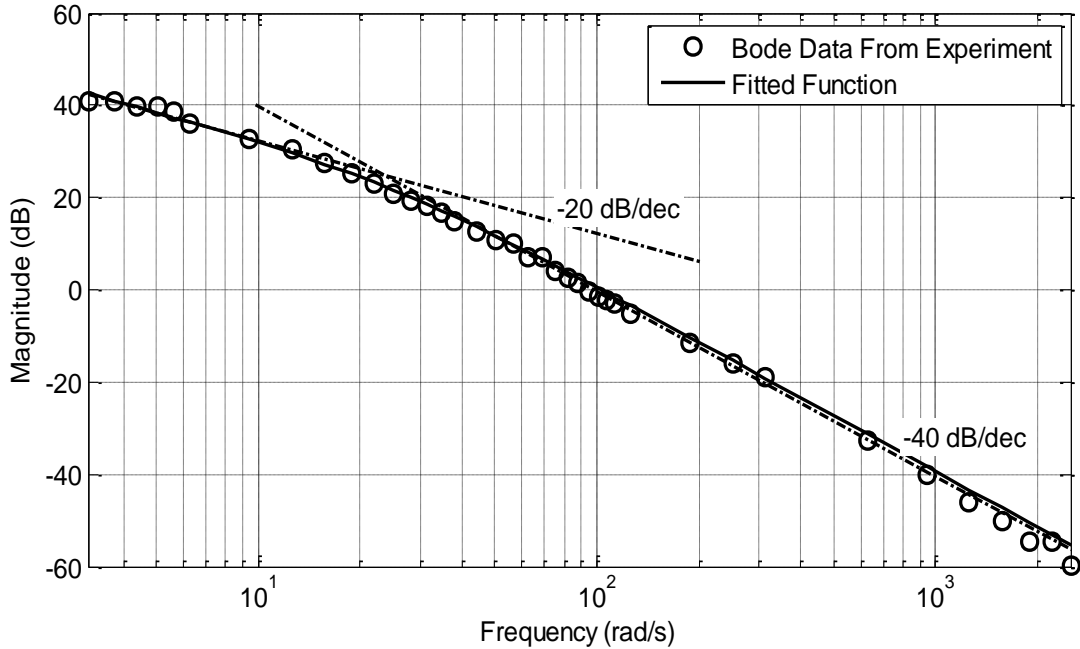


**Figure 37.** Experimental frequency response data and fitted curve

The slope of the fitted function starts from  $-20 \text{ dB/decade}$  and after a corner frequency the decay rate skips to  $-40 \text{ dB/decade}$ . This is the typical characteristics of 2<sup>nd</sup> order type 1 continuous time system. This algorithm finds the best fitted function as (by taking  $J_{eq} = 4.6 \text{ kg} \cdot \text{mm}^2$  as constant):

$$G_{fit}(s) = \frac{49690}{4.6 \cdot s^2 + 117 \cdot s} \quad (2.25)$$

Goodness of this fit can be checked and this yields  $VAF = 99\%$ . Note that the curve shown in Figure 37 is included by the interval shown on Figure 35. By this way, these identification models have become confirmed experimentally.

#### 2.2.3.3. Checking the “Goodness” of the Results Using VAF Method

Inside the frequency domain system identification algorithm, after the end of frequency domain fitting, the goodness' of the fits are also checked via calculation of VAF value of each individual fit. The detailed view of one data sample is presented in Figure 38.

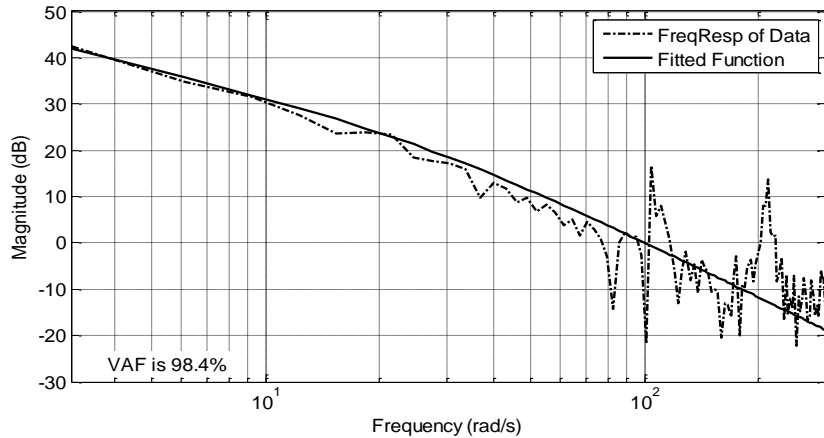


**Figure 38.** Detailed view of a frequency domain curve fit

The fitted continuous time transfer functions whose Bode diagram that shown in Figure 34 yields the following VAF values with the same order of the datasets given in APPENDIX A.3. This list is visualized on Figure 39. One can easily observe that the fittings are very good such that all of the compatibility values are larger than 80% and even larger than 90% except three datasets. The goodness values are consistent for different datasets in frequency domain. In the next section, the quality of these transfer function fittings will be tested in time domain by comparing the simulation outputs with the experimental ones.

$$VAF = \{98.4; 98.1; 99.5; 99.4; 84.5; 97.4; 98.1; 94.6; 95.1; 83.7; 99.2; 96.6; 81.6; 97.1; 99.5; 90.8; 96.6; 91.7; 95.8; 95.1; 97.5; 95.2; 95.5; 99.2; 99.4; 96.8\}$$

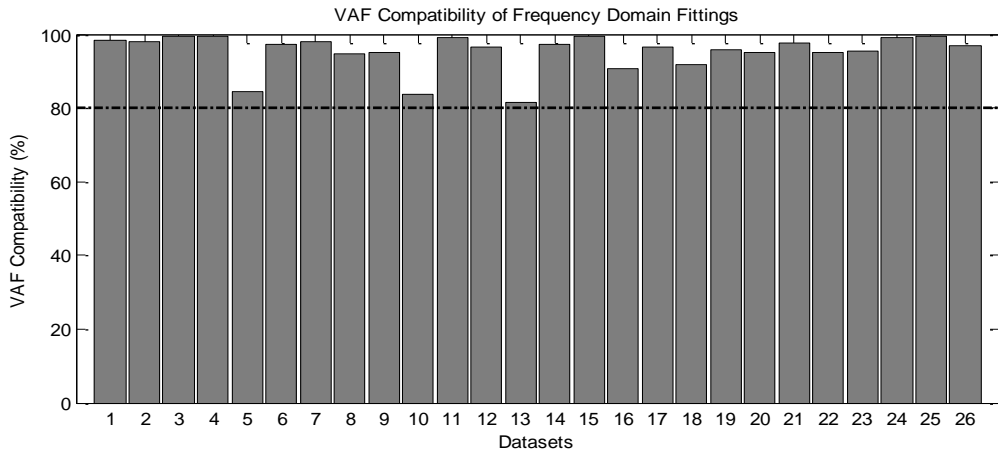


**Figure 39.** Overall view of goodness of fits

#### 2.2.3.4. Simulating and Comparing the Results both in Time and Frequency Domain

To measure the time domain performance of the fittings in frequency domain, the outputs of these models are compared with the real outputs. Each dataset simulated individually by using transfer functions have the form given in equation (2.26) with their corresponding  $B_{eq}$  values of section 2.2.3.1. The simulations are done by the help of built-in MATLAB function “*lsim*”.

$$G_{fit}(s) = \frac{48000}{4.6 \cdot s^2 + B_{eq} \cdot s} \quad (2.26)$$

One example of these simulations is provided in Figure 40. Here  $B_{eq} = 224.8 \frac{kg \cdot mm}{s}$  and corresponding time domain VAF compatibility is found as 93.9%. This means that the frequency content of the input signal is good such that it can excite the distant modes of the system.

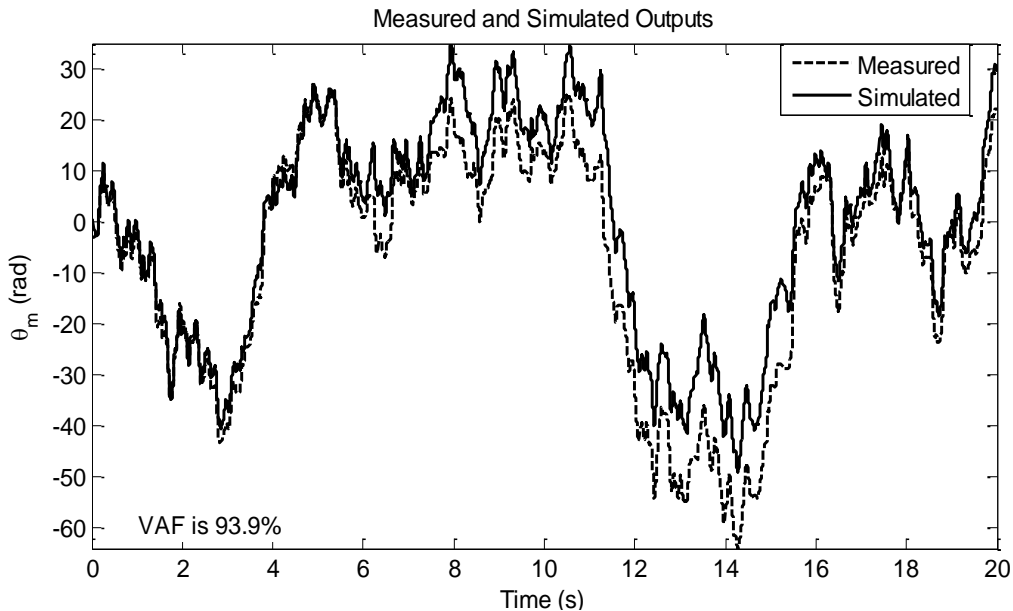


**Figure 40.** Time domain comparison between real and estimated models

Time domain simulation is done for all datasets. The corresponding results are plotted together with the real time domain outputs and provided in APPENDIX 0. Individual VAF quality is obtained by comparing simulated and experimental time domain outputs and displayed on every plot. According to these results, the datasets 3,13,16,18,19,20,21,22,23 and 25 show VAF compatibility larger than 70% also in time domain. If the Fourier characteristics of these inputs are examined (see APPENDIX A.4.), one can see that these inputs can excite wider frequency range because they have larger magnitudes on frequency contents. These signals emphasized by light green color in plots of APPENDIX A.4.

In the lights of these observations, one can claim that the applied system identification is successful and the unknown parameter  $B_{eq}$  is defined.

#### 2.2.4. Estimating the Uncertainty of the System Parameters

During section 2.2, the system identification to determine one unknown  $B_{eq}$  which denotes the equivalent viscous friction and cannot be directly specified by experimental methods, is accomplished both in time and frequency domain. Finally the founded value for  $B_{eq}$  can be summarized as  $B_{eq}^{mean} = 207.1 \frac{kg \cdot mm}{s}$  and  $118.8 < B_{eq} < 362.2$ . Reason for this uncertainty is that, the equivalent viscous friction can change according to environmental conditions, working duration of the real system, lubrication conditions etc. Therefore to have a satisfactory closed loop performance, this uncertainty can be regarded in controller synthesis. Using the given values of  $B_{eq}$ ,

the amount of uncertainty can be obtained as  $\Delta B_{eq} = 75\%$  and the calculation is given in equation (2.27).

$$\Delta B_{eq} = 100 \cdot \frac{\max((362.2 - 207.1), (207.1 - 118.8))}{207.1} \quad (2.27)$$

$$\Delta B_{eq} \approx 75\% \text{ and } B_{eq} = 207.1 \frac{kg \cdot mm}{s}$$

Another uncertain parameter in the system is the torque constant of DC motor  $K_t$ . This value can change according to load conditions and environmental issues. To identify the uncertainty of this parameter, all of the system identification in this chapter repeated by using two unknown parameters  $K_t$  and  $B_{eq}$ . However, the fitting functions yielded worse performance than one parameter case according to VAF compatibility measure. Therefore the default value of  $K_t$  is not make changed; and used as told in section 2.1.2.1. Then the value of torque coefficient is repeated in equation (2.28) to finalize the system identification.

$$\Delta K_t \approx 5\% \text{ and } K_t = 48000 \frac{kg \cdot mm^2}{s^2 \cdot A} \quad (2.28)$$



## CHAPTER 3.

### SYNTHESIS OF ROBUST CONTROLLERS

#### 3.1. REQUIREMENTS FOR THE CLOSED LOOP SYSTEM

In the previous chapter, the linear system model for the plant has been obtained and the corresponding controller design structure has been built. This block diagram is given in Figure 26. As explained in the previous chapter, the system parameters have uncertainties and there are external disturbances as aerodynamic loads and sensor noise to the system. Apart from the modeling errors, (recall that the system modeled up to 30 Hz) system has some nonlinearity. In this system, there are three sources for nonlinear behaviors. The first one is the saturation limit on the physical system, the fin deflection angle cannot be larger than  $\delta = \pm 23^\circ$ . Second nonlinearity source is that, the current input to the system cannot be larger than  $\pm 15 A$  which causes a saturation on the control signal. The final source is the previously mentioned cogging phenomenon. In the start of the motion from the zero speed, in the actuator the cogging torque  $T_{cog} = 17 N \cdot mm$  induces. This torque is always opposed to the motion regardless of the direction. Another important characteristic about the system is the limit on the angular speed. Due to capacity of the actuator, the system cannot reach to higher angular speed than  $150^\circ/s$  at the fin shaft  $|\dot{\delta}| \leq 150^\circ/s$ . All of these conditions will be taken into account in controller design to define the required weighting functions.

The plant is well defined up to this point. Now, the robust controller design procedure will be handled. The first step in the controller design procedure is to define the expected closed loop behavior of the system. It is desired that the low frequency response of the closed loop system at should be similar to an ideal transfer function given in equation (3.1) where  $\omega_n = 12 Hz$  and  $\xi = 0.707$ . The Bode plot of the ideal system is given in Figure 41. Additionally, the characteristics of the closed loop (while exposed to disturbances and uncertainties) should satisfy the conditions given in Table 8. Another important factor to be considered in the control design of a fin actuation is the minimization of control effort, because in an ammunition there is limited power supply and the total energy consumed by the plant is critical.

$$G_{ideal}(s) = \frac{\omega_n^2}{s^2 + 2\xi\omega_n s + \omega_n^2} \quad (3.1)$$

Using these criteria the weighting functions and performance variables will be defined to use in controller synthesis.

**Table 8.** Performance requirements for the closed loop system

Maximum percent over shoot	$\leq 5\%$
Settling Time	$\leq 0.06$ seconds
Bandwidth for $\pm 1^\circ$ amplitude signal (due to speed restriction of the actuator)	$\geq 12 Hz$ $= 75.4 rad/s$
Steady state error	$\leq 0.1^\circ$

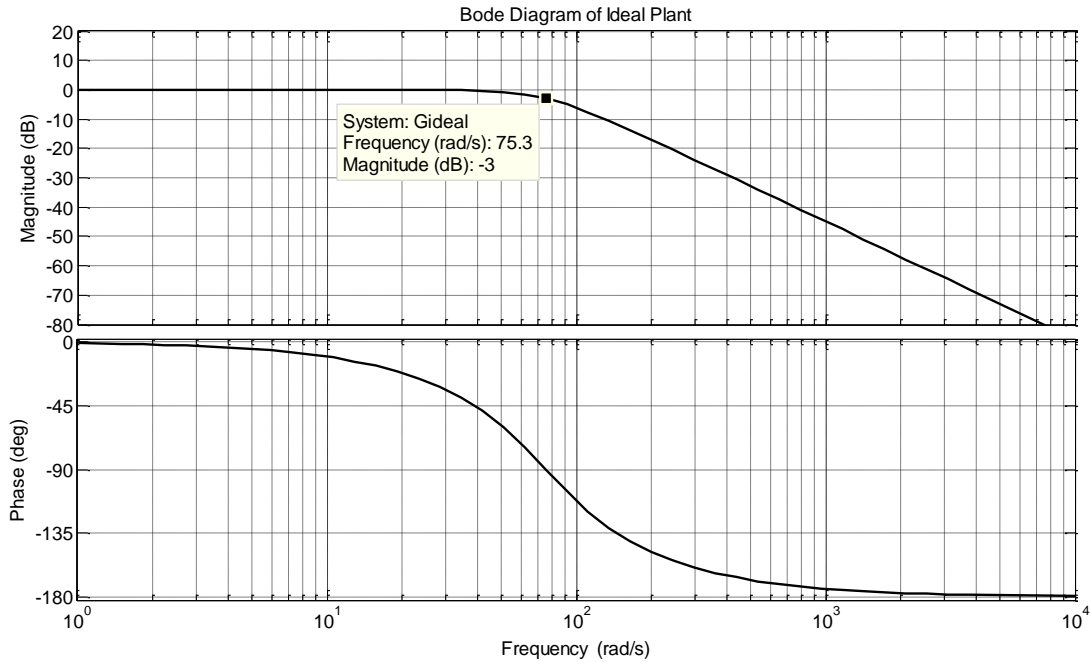


**Figure 41.** Bode diagram of the ideal closed loop system

### 3.1.1. Motivation to $H_2/H_\infty$ Mixed Control for Fin Actuation Systems

The main advantage of the  $H_2/H_\infty$  mixed controller is that, one can use distinct methods for optimization of distinct performance parameters. As mentioned in literature survey section of this text (section 1.4), to satisfy robustness and disturbance rejection, the performance variables related with the measured output should be penalized according to  $H_\infty$  criterion. Similarly to minimize the total energy of the performance parameters,  $H_2$  criterion can be used. Generally  $H_\infty$  performance is convenient to enforce robustness to model uncertainty. Recall that, according to small gain theorem (given at section 1.3.2.4) the system is stable for all uncertainties which satisfy the norm bound  $\|\Delta\|_\infty \leq 1$  if and only if the nominal closed loop transfer function  $T$  is stable and  $\|T\|_\infty \leq 1$ .  $H_\infty$  control is also useful to express frequency domain specifications such as bandwidth and low frequency gain. Additionally, some tracking performance can be best captured by  $H_\infty$  technique.  $H_2$  criterion is useful to express noise insensitivity and energy optimization [35]. The performance and robustness requirements are described in previous section. Thanks to  $H_2/H_\infty$  mixed design methods, this multiobjective optimization problem becomes solvable.

### 3.1.2. Selection of Weighting Functions

The weighting functions are frequency dependent transfer functions to use the shape of the closed loop transfer functions in robust controller synthesis. These weightings should be tuned such that the feedback control system should be stable and additionally exhibit good command following, disturbance rejection, sensor noise attenuation, control sensitivity minimization and robustness to modeling errors. To achieve these statements, previously mentioned *loop transfer function L* and *sensitivity function S* (please refer to section 1.3.2.3) of the feedback system must have the predefined typical shapes in frequency response as given in Figure 42 and Figure 43 [6].

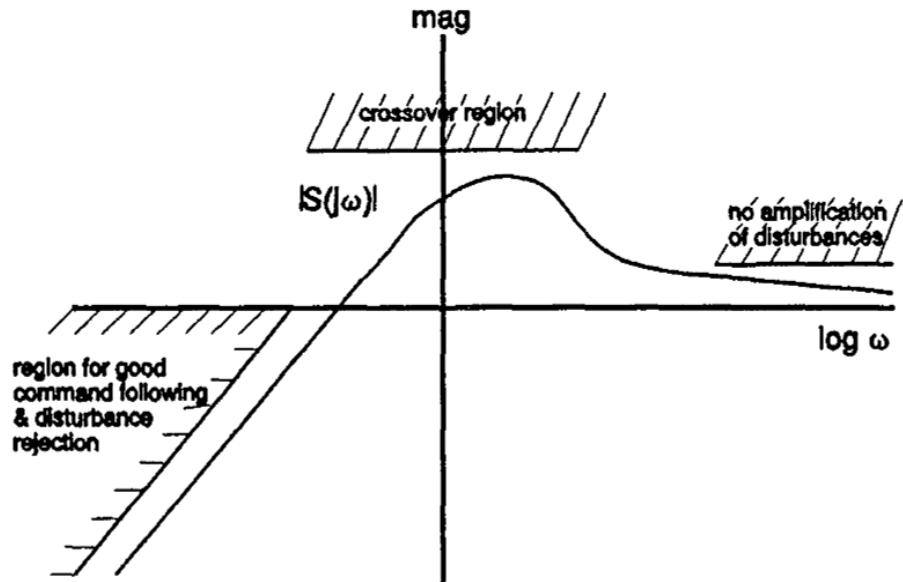


*Figure 42. Typical shape of sensitivity function  $S$  [6]*

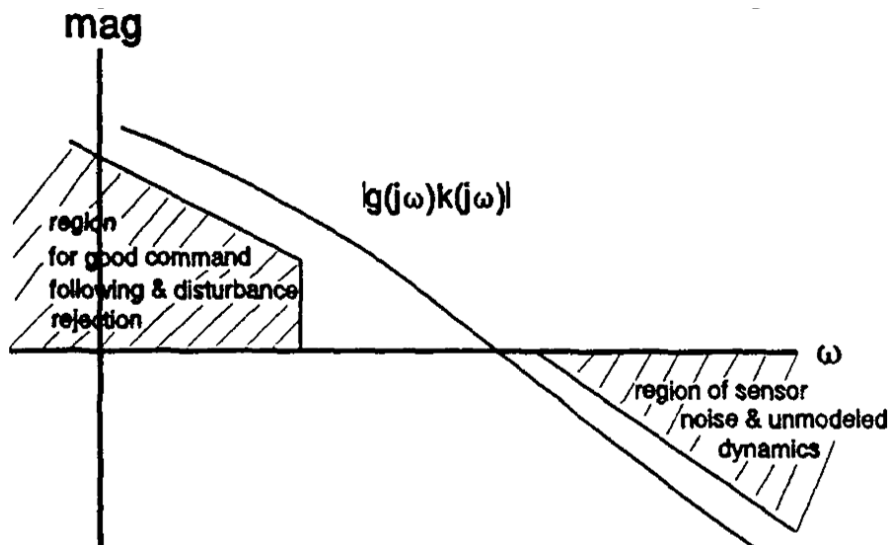


*Figure 43. Typical shape of loop transfer function  $L$  [6]*

There is not any straight forward method to define the weighting functions. However, there are some rule of thumbs and these methods are available in literature (for examples [6] [5] [13] [36] [37]). One of the factors regarded in the weighting function tuning is the properties of the plant and the expected behavior of the closed loop system.

Consider a generalized plant model at Figure 3. The controller synthesis block diagram of this thesis is given in Figure 26 can be projected into this generalized block diagram. The input and outputs of the system can be seen in Figure 44. The details of the variables are given in section 2.1.3.4. In robust controller design, all of the input and outputs of generalized plant are scaled to unity such that the robust controller  $K$  is calculated and optimized by regarding the inputs and outputs are unity [13]. By using this fact, the weighting functions at the input side should be shaped as the scaling up

and the output weightings (called as also ‘*cost functions*’) should be shaped as the scaling down to penalize their inputs. Apart from this, the  $H_\infty$  controller search algorithm minimizes the RMS of the input and output signals in consistent with the weightings. Therefore the desired magnitudes of the frequency response of the weightings are also scaled down by a factor of  $\sqrt{2}$ . In the following section, the weighting functions will be given. The order of the synthesized robust controller ( $H_2$ ,  $H_\infty$  and  $H_2/H_\infty$ ) will be equal to total degree of each function used in design.

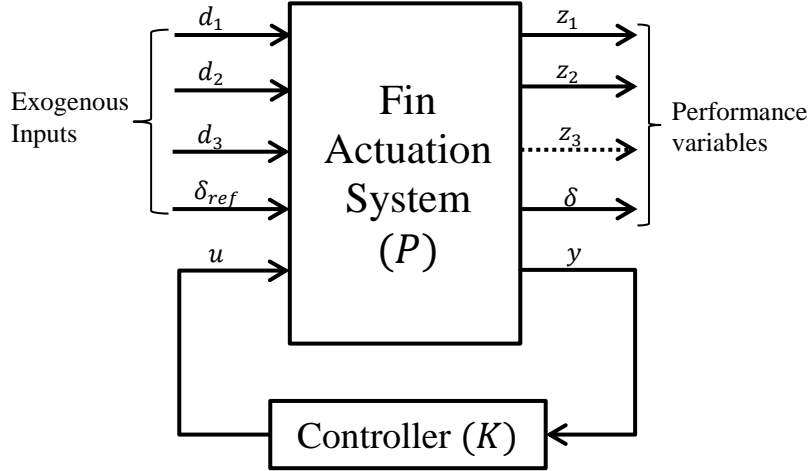


**Figure 44.** The plant in generalized plant notation

### 3.1.2.1. Weighting Function for Reference Signal $W_{ref}$

The reference command signal to the feedback system has a shape in frequency domain. According to the system requirements, the absolute value of system input  $\delta_{ref}$  will be maximum  $20^\circ$  in static condition (0 Hz) and will be  $\delta_{ref} = 1^\circ$  at 12 Hz. Using the previously stated RMS factor, the magnitude vs. frequency characteristics of the input signal is generated and stated in Figure 45. Note that the y-axis of the plot is the absolute magnitude and the unit is radians (not dB). The 0 Hz value is equal to  $\frac{20\pi}{180\cdot\sqrt{2}} = 0.247$ . The weighting function selected to be as first order (to keep the order of the controller minimum) and defined in equation (3.2). The function is obtained using frequency response fitting built-in function ‘magshape’ of MATLAB®.

$$W_{ref}(s) = \frac{0.0009275 \cdot s + 1.326}{s + 5.326} \quad (3.2)$$

This function is related to the exogenous input  $\delta_{ref}$ .

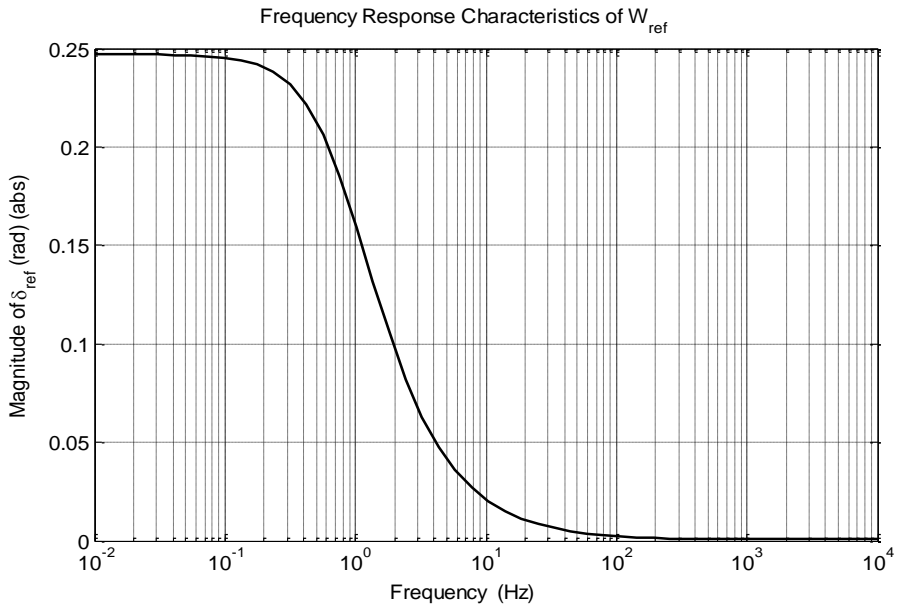


**Figure 45.** Magnitude plot of weighting function  $W_{ref}(s)$  in frequency domain

### 3.1.2.2. Weighting Function for Cogging Torque $W_{cog}$

The cogging torque is changing its direction but its magnitude is constant and  $T_{cog} = 17 \text{ N} \cdot \text{mm}$  as previously obtained in equation (2.3). During modeling, the unit for mass is kg, for angle rad, for current A and for length is mm. So,  $17 \text{ N} \cdot \text{mm} = 17 \cdot 10^3 \frac{\text{kg} \cdot \text{mm}^2}{\text{s}^2}$ . Hence  $W_{cog}(s) = 17000$  is defined as weighting function. This function is related to exogenous input  $d_1$ .

### 3.1.2.3. Weighting Function for Aerodynamic Loads $W_{aero}$

The aerodynamic load on the system is the hinge moment  $T_{hinge}$  and changes its magnitude and direction during the flight. However, to be on the safe side and satisfy the required robustness, the load will be assumed to be constant through all frequencies and has its maximum value during the flight. This value is calculated in section 2.1.3.1 and given in equation (2.19) as  $|T_{hinge}| \leq 283 \text{ N} \cdot \text{mm}$ . Hence,  $W_{aero}(s) = 283000$  is defined. This function is related to disturbance  $d_2$ .

### 3.1.2.4. Weighting Function for Sensor Noise $W_{sens}$

As mentioned in section 2.1.2.2, there may be noise in sensor, and this may cause to fault in the position data. The margin for this error in angular position measurement is  $\frac{2\pi}{2048}$  rad. Hence,  $W_{sens}(s) = \frac{2\pi}{2048}$  is defined.

### 3.1.2.5. Penalty for Deviation from Ideal System $W_{perf}$

Cost functions are used to penalize the system outputs to obtain required performance in closed loop system. In literature, generally error, the difference between the measured output and reference signal is penalized. This yields a bit more conservative result, because in this case the transfer function between the reference and the output is forced to be unity. Since, the desired closed loop

system behavior is a second order function with 12 Hz bandwidth, optimization of deviation from this characteristic is more important. In this manner, the penalizing cost function is shaped as a transfer function that has higher gain at low frequencies and very low gain at negligible high frequencies. The function is obtained as a first order transfer function and given in equation (3.3) . Magnitude of the frequency response curve of the function is given in Figure 46. Note that the y-axis of the plot is the absolute magnitude (not dB). Here, the corner frequencies and the static gain values dominantly affect the shape of the sensitivity function of feedback system. The final values obtained after many trial and error methods. The effects of weighting functions to performance and robustness of the controller will be discussed in the last chapter of this text.

$$W_{perf}(s) = \frac{0.2 \cdot s + 188.5}{s + 0.6283} \quad (3.3)$$

This function is related to the performance variable  $z_1$ .

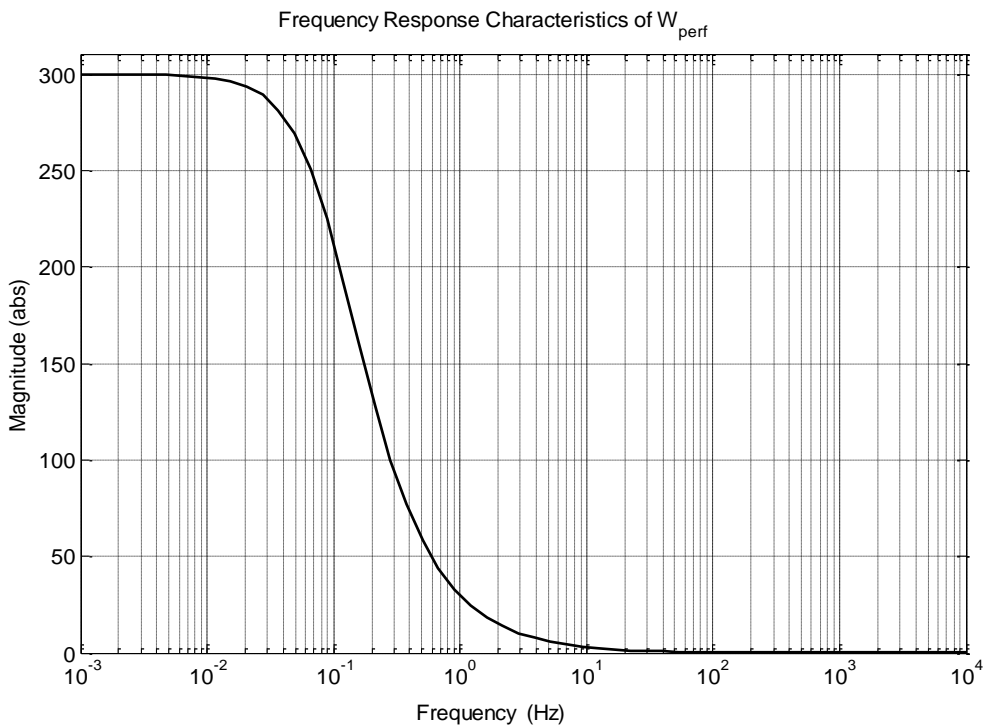


**Figure 46.** Magnitude plot of cost function  $W_{perf}(s)$  in frequency domain

### 3.1.2.6. Penalty for Controller Output $W_{act}$ (for Pure $H_2$ and $H_\infty$ Case)

As mentioned in section 3.1, the controller signal must be limited, such that its magnitude must be lower than 15 A. Since  $H_\infty$  algorithm minimizes the RMS value of the cost function, the penalty function for the controller signal is defined as constant at all frequencies  $W_{act}(s) = \frac{\sqrt{2}}{15}$ . The inverse of the penalty function determines the allowed RMS gain for the control signal. Output of this function defines the performance index  $z_2$ . In mixed controller design, this performance index is fed into  $H_\infty$  norm.

### 3.1.2.7. Penalty for Controller Output $W_{act2}$ (for Mixed $H_2/H_\infty$ Case)

The advantages of  $H_2/H_\infty$  mixed controller are previously discussed in section 1.4. The control system will be used in a mobile platform and the available energy for control effort is restricted. Therefore, the total energy of the control signal should be minimized. Although limiting of the maximum controller signal value also decreases the total energy, in mixed controller case an additional penalizing function can be defined. Using this function, it is possible to shape the control signal in frequency domain. In this manner, the allowable limits for current are defined to be low at more current demanding high frequencies and as three times higher in the unimportant low frequency region. The limiting value at high frequency is the same with  $W_{act}$  of section 3.1.2.6. These limits are shaped in frequency response and given in Figure 47. The reciprocal of this shape yields the desired weighting function and this transfer function is given in equation (3.4).

$$W_{act2}(s) = \frac{0.09428 \cdot s + 100}{s + 4243} \quad (3.4)$$

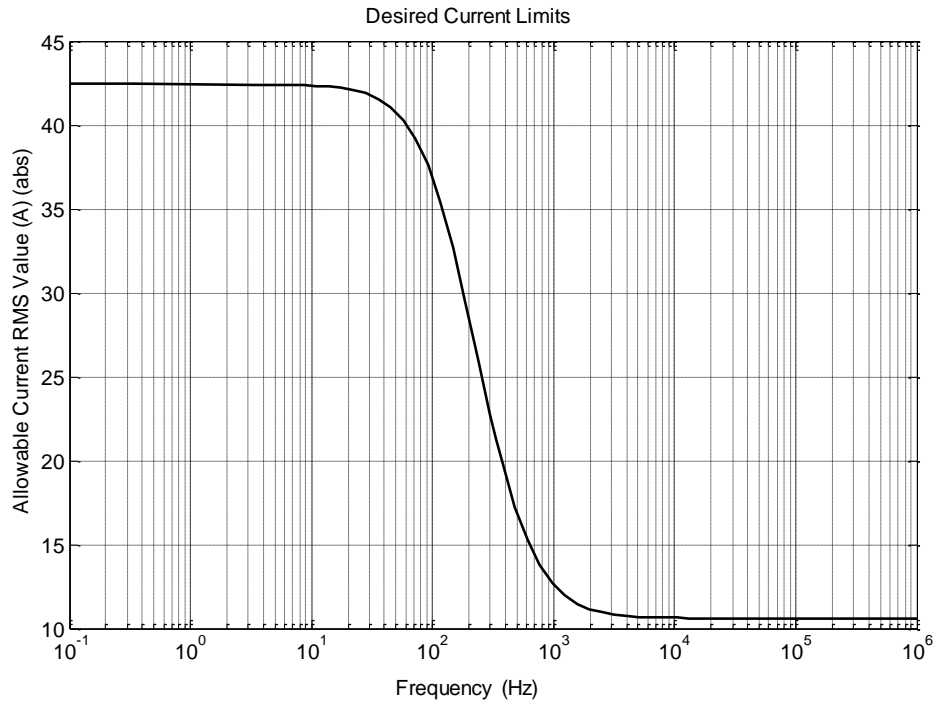


**Figure 47.** Inverse of  $W_{act2}(s)$  weighting function

Output of this function defines the performance index  $z_3$  and this weighting is used only in  $H_2/H_\infty$  mixed controller design to minimize the required energy. This performance index is fed into  $H_2$  norm.

### 3.1.3. Creation of Generalized Plant

The interconnections of the controller design scheme are given in Figure 26. After the determination of weighting functions in section 3.1.2, the generalized plant matrix  $P$  can be defined using MATLAB® built-in function ‘*sysic*’. Meanwhile in mixed  $H_2/H_\infty$  condition an additional weighting function will be used, two generalized plant matrices are created. The outputs of the ‘*sysic*’

command are given at APPENDIX A.1 in the form of generalized plant. The state space matrices of the generalized plant  $P_{fas}$  in the case of pure  $H_2$  and  $H_\infty$  control problem are given below with corresponding variables. There are 6 state space variables which determine the order of the generalized plant and equal to degree of the all weightings.

$$A_1 = \begin{matrix} & x_1 & x_2 & x_3 & x_4 & x_5 & x_6 \\ x_1 & -5.3680 & 0 & 0 & 0 & 0 & 0 \\ x_2 & 0 & -45.0217 & 0 & 0 & 0 & 0 \\ x_3 & 0 & 0.4348 & 0 & 0 & 0 & 0 \\ x_4 & -10.5682 & 0 & 0 & -106.6292 & -88.8264 & 0 \\ x_5 & 0 & 0 & 0 & 64 & 0 & 0 \\ x_6 & 0 & 0 & 0.1085 & 0 & -170.3778 & -0.6283 \end{matrix}$$

$$B_1 = \begin{matrix} & d_1 & d_2 & d_3 & \delta_{ref} & u \\ x_1 & 0 & 0 & 0 & 1 & 0 \\ x_2 & -8500 & 141442.7157 & 0 & 0 & 24000 \\ x_3 & 0 & 0 & 0 & 0 & 0 \\ x_4 & 0 & 0 & 0 & 0.00742 & 0 \\ x_5 & 0 & 0 & 0 & 0 & 0 \\ x_6 & 0 & 0 & 0 & 0 & 0 \end{matrix}$$

$$C_1 = \begin{matrix} & x_1 & x_2 & x_3 & x_4 & x_5 & x_6 \\ \delta & 0 & 0 & 0.0071 & 0 & 0 & 0 \\ z_1 & 0 & 0 & 0.0014 & 0 & -2.2207 & 12.2758 \\ z_2 & 0 & 0 & 0 & 0 & 0 & 0 \\ y & 186.7924 & 0 & -1 & 0 & 0 & 0 \end{matrix}$$

$$D_1 = \begin{matrix} & d_1 & d_2 & d_3 & \delta_{ref} & u \\ \delta & 0 & 0 & 0 & 0 & 0 \\ z_1 & 0 & 0 & 0 & 0 & 0 \\ z_2 & 0 & 0 & 0 & 0 & 0.0943 \\ y & 0 & 0 & -0.0031 & 0.1311 & 0 \end{matrix}$$

Note that these matrices satisfy the necessary conditions for the solvability of corresponding  $H_2$  and  $H_\infty$  robust controller problems given in section 1.3.3.1and 1.3.3.2.

In  $H_2/H_\infty$  mixed controller design step, since an additional weighting function is defined from first order, the corresponding transfer functions are changed. Therefore the updated state space matrices of the generalized plant for mixed robust controller synthesis are given below with corresponding variables. There are 7 state space variables which determine the order of the generalized plant and equal to degree of the all weightings. Note that due to weighting  $W_{act2}(s)$ , now the order of the plant is one time higher.

$$A_2 = \begin{matrix} & x_1 & x_2 & x_3 & x_4 & x_5 & x_6 & x_7 \\ x_1 & -5.3680 & 0 & 0 & 0 & 0 & 0 & 0 \\ x_2 & 0 & -4243 & 0 & 0 & 0 & 0 & 0 \\ x_3 & 0 & 0 & -45.02 & 0 & 0 & 0 & 0 \\ x_4 & 0 & 0 & 0.4348 & 0 & 0 & 0 & 0 \\ x_5 & 10.57 & 0 & 0 & 0 & -106.6 & -88.83 & 0 \\ x_6 & 0 & 0 & 0 & 0 & 64 & 0 & 0 \\ x_7 & 0 & 0 & 0 & 0.1085 & 0 & -170.4 & -0.6283 \end{matrix}$$

$$B_2 = \begin{array}{cccccc} & d_1 & d_2 & d_3 & \delta_{ref} & u \\ x_1 & 0 & 0 & 0 & 1 & 0 \\ x_2 & 0 & 0 & 0 & 0 & 16 \\ x_3 & -8500 & 141442.7157 & 0 & 0 & 24000 \\ x_4 & 0 & 0 & 0 & 0 & 0 \\ x_5 & 0 & 0 & 0 & 0.00742 & 0 \\ x_6 & 0 & 0 & 0 & 0 & 0 \\ x_7 & 0 & 0 & 0 & 0 & 0 \end{array}$$

$$C_2 = \begin{array}{ccccccc} & x_1 & x_2 & x_3 & x_4 & x_5 & x_6 & x_7 \\ \delta & 0 & 0 & 0.0071 & 0 & 0 & 0 & 0 \\ z_1 & 0 & 0 & 0.0014 & 0 & 0 & -2.2207 & 12.2758 \\ z_2 & 0 & 0 & 0 & 0 & 0 & 0 & 0 \\ z_3 & 0 & -18.75 & 0 & 0 & 0 & 0 & 0 \\ y & 0186.7924 & 0 & -1 & 0 & 0 & 0 & 0 \end{array}$$

$$D_2 = \begin{array}{ccccc} & d_1 & d_2 & d_3 & \delta_{ref} & u \\ \delta & 0 & 0 & 0 & 0 & 0 \\ z_1 & 0 & 0 & 0 & 0 & 0 \\ z_2 & 0 & 0 & 0 & 0 & 0.0943 \\ z_3 & 0 & 0 & 0 & 0 & 0.0943 \\ y & 0 & 0 & -0.0031 & 0.1311 & 0 \end{array}$$

To compare and simulate the controller responses, the overall plant with nonlinearities is modeled using SIMULINK® to tune the weightings used in the controller synthesis. According to the simulation results, weightings are updated and the controllers are revised. This procedure ended when the performance of the controller become satisfactory. The simulation block diagram used in the software is shown in Figure 49. The subsystems are expanded in Figure 48 and Figure 50. Here the response of the closed loop under the effect of uncertainties is compared with the ideal system response in time domain. The applied external torque to system is fed to plant as constant and hold at its maximum during the simulation. Also an artificial sensor noise is generated as a random binary signal.

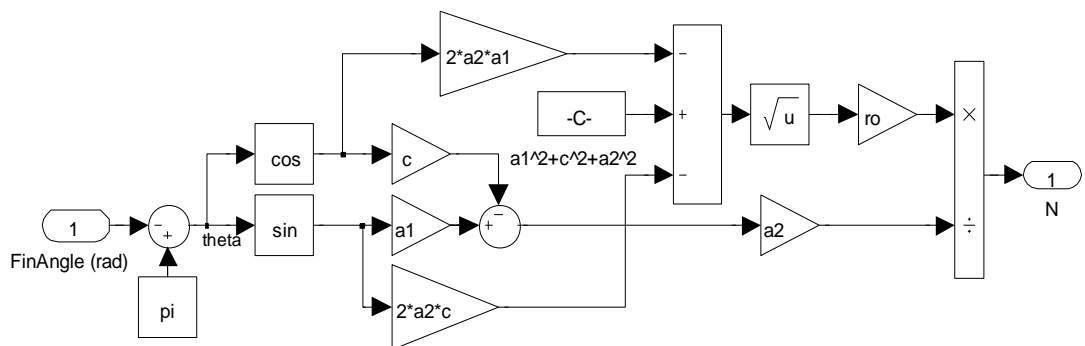


**Figure 48.** Subsystem to simulate the mechanism and calculation of gear ratio  $N$

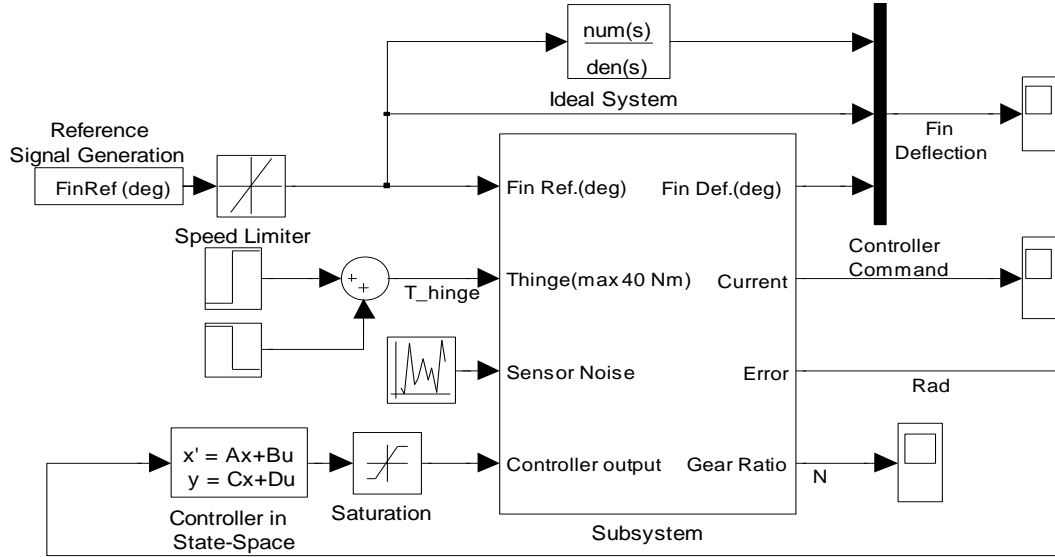


**Figure 49.** Outermost block diagram used in simulation

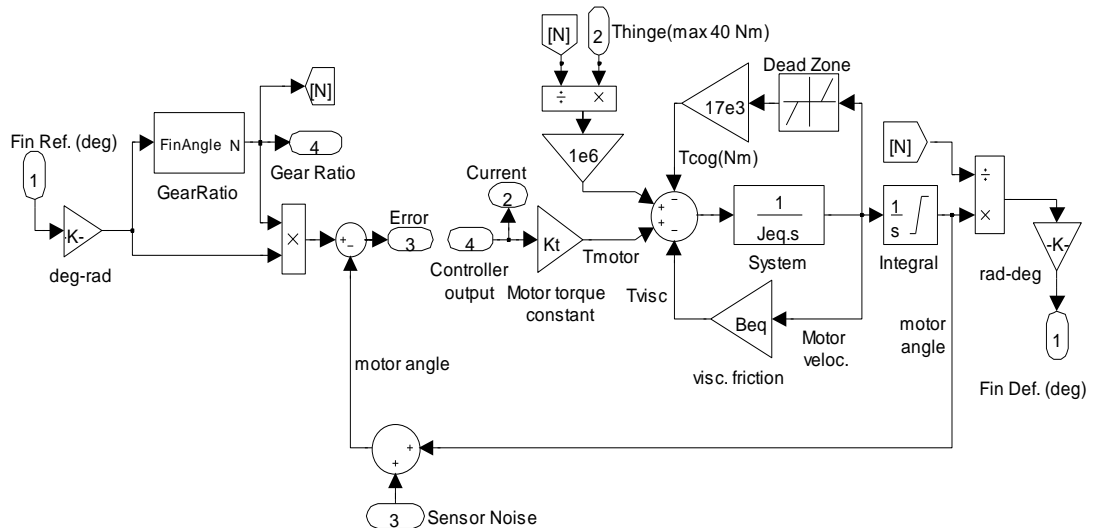


**Figure 50.** Expansion of subsystem in Figure 49, the fin actuation system plant

### 3.2. SYNTHESIS OF PURE ROBUST CONTROLLERS

When the generalized plant matrices are obtained, the controller design achieved using built-in functions of MATLAB®. To be able design a robust controller, the plant matrix should be constant and cannot include any uncertain parameter. The plant uncertainties are examined after the design of controller.

#### 3.2.1. $H_\infty$ Controller Synthesis

Using built-in command '*hinfsyn*', the corresponding  $H_\infty$  robust controller has been synthesized. Actually there is not a straightforward method to find the 'best' controller and optimization of controller is another research topic. The selection of the parameters on the weighting functions is

critical and affects the performance of the closed loop system. In this study, the weightings are not optimized and it is possible to obtain a controller that yields better performance and robustness. This condition will be evaluated on the final chapter of this text. Here, using the defined weightings, a stabilizing and robust controller is obtained by using Riccati equation method via the built-in command ‘*hinfsyn*’.

```
[Kinf, CLinf, GAM, INFO] = hinfsyn(Pfas, 1, 1, 'METHOD', 'ric', 'DISPLAY', 'on');
```

The obtained  $H_\infty$  controller in continuous time domain is given in equation (3.5).

$$K_\infty(s) =$$

$$\frac{8680 \cdot s^5 + 1.596 \cdot 10^6 \cdot s^4 + 1.365 \cdot 10^8 \cdot s^3 + 5.556 \cdot 10^9 \cdot s^2 + 9.687 \cdot 10^{10} \cdot s + 4.114 \cdot 10^{11}}{s^6 + 2007 \cdot s^5 + 9.831 \cdot 10^5 \cdot s^4 + 9.393 \cdot 10^7 \cdot s^3 + 4.465 \cdot 10^9 \cdot s^2 + 3.532 \cdot 10^9 \cdot s + 1.738 \cdot 10^{10}} \quad (3.5)$$

Corresponding  $H_\infty$  norm for the closed loop system is  $\gamma = 0.8180$ . Note that this value is lower than 1, according to small gain theorem the closed loop system robustly stable to uncertainties and disturbances that has defined via weighting functions.

Since the controller is obtained, now someone can check the ‘quality’ of the controller effort. Recall that, after some mathematical modeling effort the transfer function of the plant is obtained as given in equation (3.6) with  $J_{eq} = 4.6$ ,  $K_t = 48000$  with 5% uncertainty and  $B_{eq} = 207.1$  with 75% uncertainty.

$$G(s) = \frac{K_t}{s(J_{eq}s + B_{eq})} \quad (3.6)$$

To evaluate robust characteristics and robust performance of the feedback system, singular values and characteristics of the open loop gain  $L_\infty = G \cdot K_\infty$ , sensitivity function  $S_\infty = \frac{1}{1+L_\infty}$  and closed loop transfer function  $T_\infty = \frac{L_\infty}{1+L_\infty}$  can be checked, where  $G$  is the nominal transfer function of the plant given in equation (3.6). The singular values of  $L_\infty$  and  $S_\infty$  are given in Figure 52 and Figure 51. Note that the general shapes of these plots are well-matched with the typical functions that shown in Figure 42 and Figure 43. However, in both of the functions there is a peak at frequency 11 rad/s. This means that, a disturbance near to this frequency region can have dramatic effects at the closed response of the system.

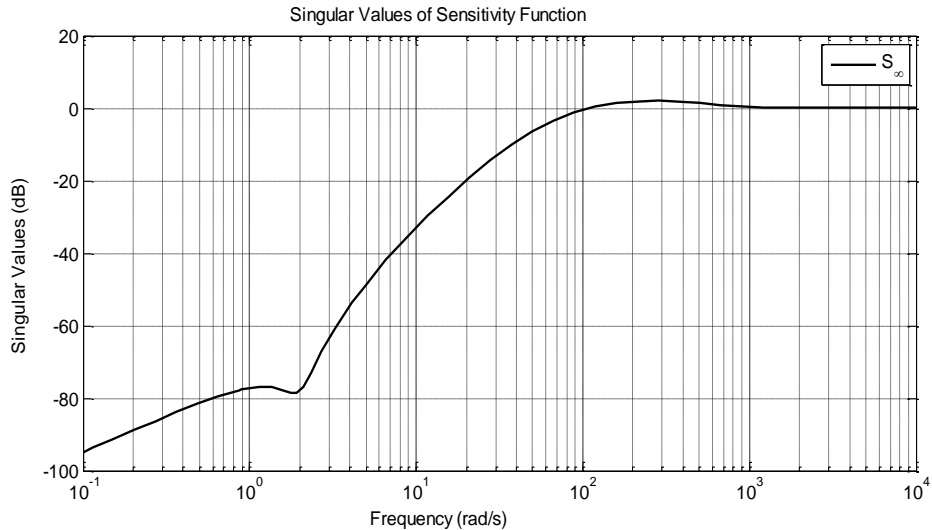


**Figure 51.** Singular value plot of the sensitivity function in  $H_\infty$  controlled case without uncertainty

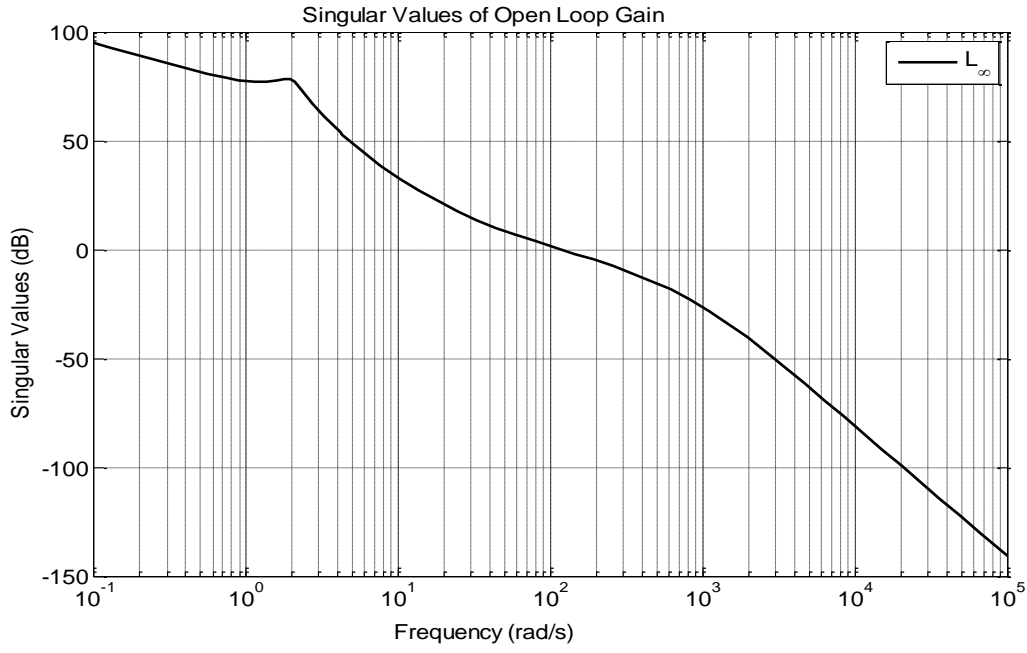


**Figure 52.** Singular value plot of the open loop gain in  $H_\infty$  controlled case without uncertainty

Recall that the expected bandwidth of the closed loop system is should be at least 12 Hz. This performance can be observed by looking Bode magnitude plot of  $T_\infty$ . As shown in Figure 53, the bandwidth of the feedback system is 30.5 Hz and this confirms that the required performance is satisfied. Another important observation from this figure is that, the closed loop behavior of the system is very similar to a typical second order system and this was the aim at the beginning of the design.

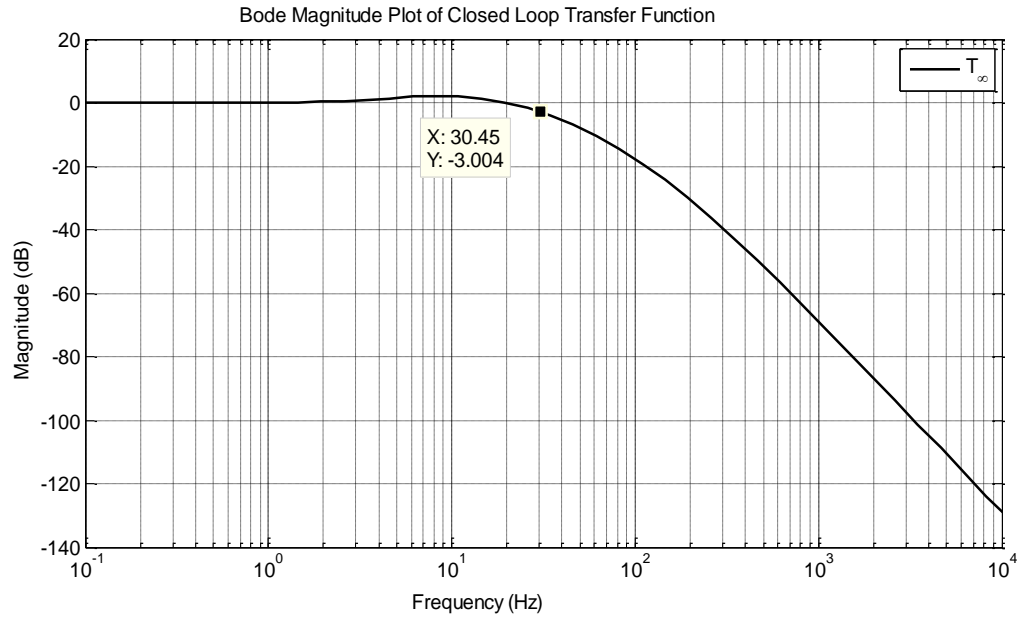


**Figure 53.** Bode plot of the closed loop response and corresponding bandwidth

The robustness and performance of the nominal plant is assessed for  $H_\infty$  controlled system until here. However, the system has parameter uncertainties and the effects of the variation of parameters should also be considered. The uncertainties are defined by using ‘*ureal*’ command. The effect of the parameter uncertainty to the robustness characteristics can be seen in Figure 54. As seen from the figure, higher frequency dynamics are not affected by the uncertainties. The uncertainties are dominant on lower frequency response of the feedback system but these effects are not dramatic, the singular values change only  $\pm 4\%$ .

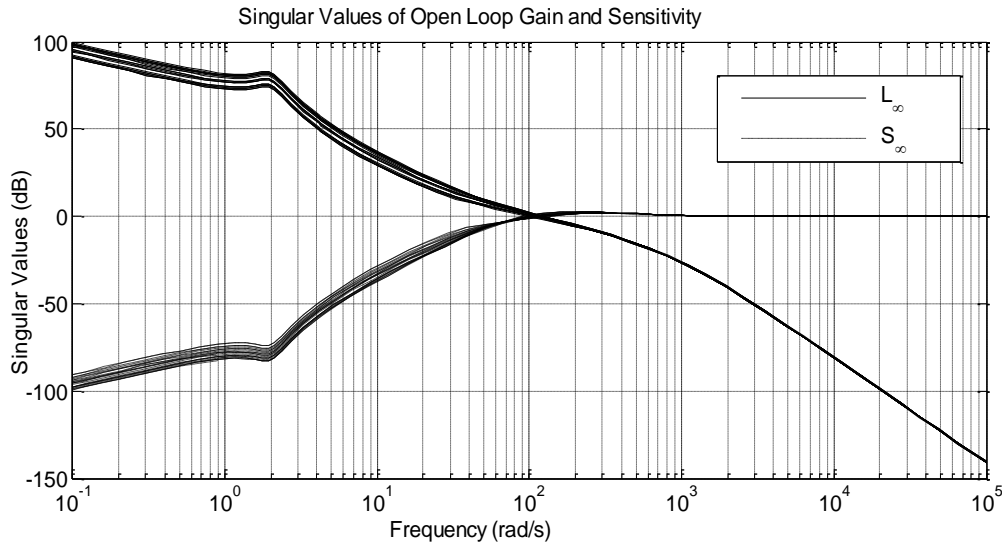


**Figure 54.** Effect of uncertainty to singular value plots

As a final analyze on the performance of the controller, the time domain characteristics of the plant with uncertainties can be checked to compare the results with the restrictions given in Table 8 by using the step response of the feedback system. By looking at Figure 55, it can be seen that settling time is about 0.11 seconds and the maximum percent over shoot is larger than 25%. In this manner the controller looks not to be good. On the contrary, the steady state error is minimized and near to 0.

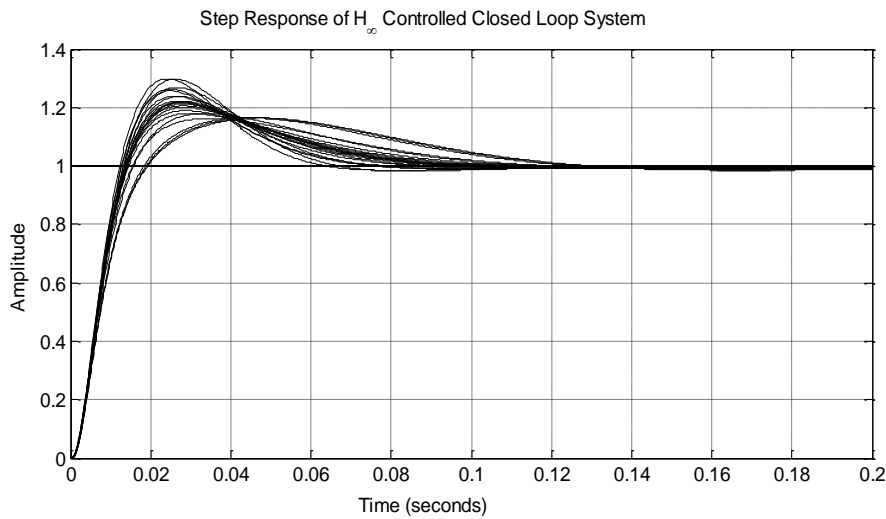


**Figure 55.** Step response of the closed loop system including parameter uncertainties

### 3.2.1.1. Simulation Results

The robustness of the controller is validated by using available analytical tools. Now, by using simulations; the effect of disturbances, especially the effect of aerodynamic loads, can be seen. Also it is possible to examine the changes in the control signal and the response of the closed loop system to different reference signals that has diverse magnitude and frequencies. Remember that the minimization of the control effort is also a consideration in the controller design problem. The simulations are achieved using the block diagrams given in section 3.1.3.

The simulation result of the controlled plant with  $40 \text{ N} \cdot \text{m}$  external torque and the previously mentioned sensor noise is given in Figure 56. Note that the reference step signal is shaped as a ramp. Because the fin actuation system cannot move faster than  $150^\circ/\text{s}$  and this is simulated by the ‘Rate Limiter’ block (see Figure 49). As seen from the figure, the closed loop system can successfully follow the reference signal which also includes a 1 Hz sine. The external aerodynamic load is applied at  $t = 0.5$  until  $t = 11.5 \text{ s}$ . These effect can be observed from the deviations at  $t = 0.5$  and  $t = 11.5 \text{ sec}$ . In Figure 57 the most critical section of the response is zoomed. Here there is an overshoot less than  $1^\circ (= 5\%)$  which is much less than theoretical step response that given in Figure 55. Actually the reference signal here is ramp not an ideal step and the external load applied to the system decreases the amplitude of the overshoot. Also note that there exists a low frequency oscillation around the steady state value. The reason of this phenomenon is the cogging torque that described in section 2.1.3.2.

The characteristics of the control signal can be observed from Figure 58. Note that the control signal reaches to its maximum as  $12 \text{ A}$  at  $t = 4 \text{ s}$  where the torque is opposite to direction of fin deflection. Note that the maximum value is smaller than  $15 \text{ A}$  as desired.

The simulated response of the feedback system to  $12 \text{ Hz}$  sinusoidal signal with amplitude  $\pm 1^\circ$  is shown in Figure 59. The simulation achieved under the effect of external torque disturbance and sensor noise. Note that the feedback system performs well to follow the high frequency reference signal.

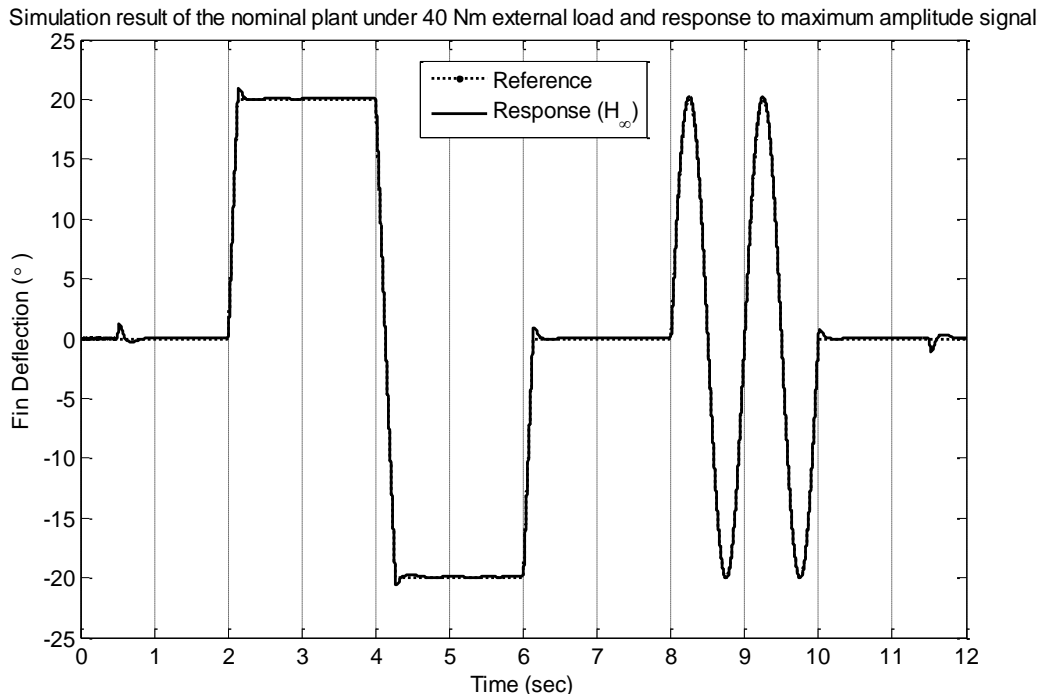


**Figure 56.** Simulation response of the feedback system under external  $40 \text{ N.m}$  disturbance

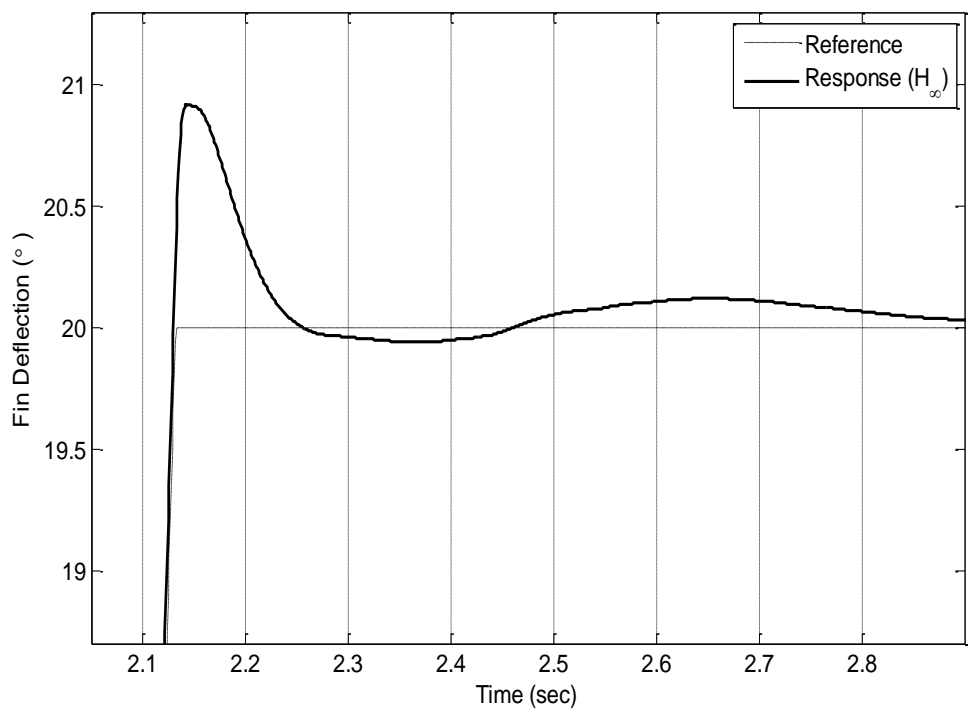


**Figure 57.** Zooming of Figure 56

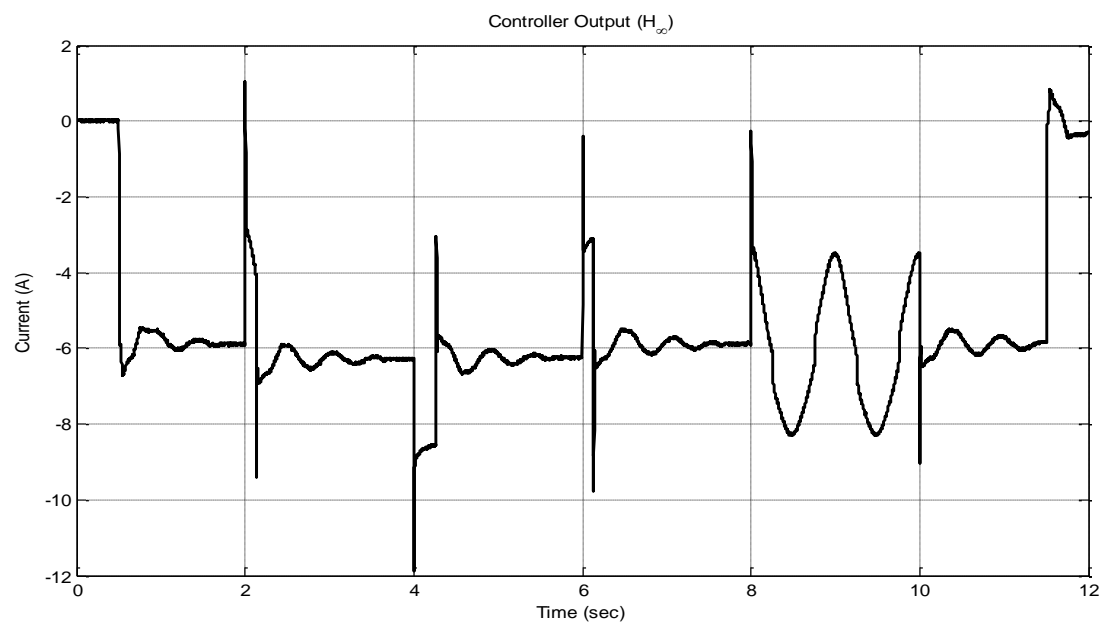


**Figure 58.** Command generated by the  $H_{\infty}$  controller

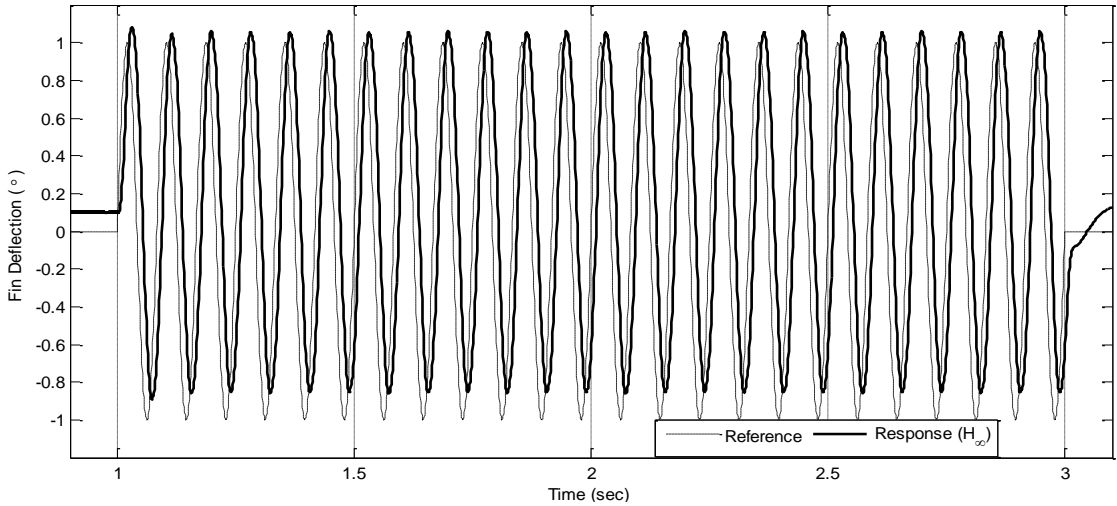


**Figure 59.** Simulated response of  $H_\infty$  controlled plant to 12 Hz sinusoidal reference signal

### 3.2.2. $H_2$ Controller Synthesis

In previous section  $H_\infty$  controller is designed. To compare the performance and robustness characteristics, an  $H_2$  controller is also defined by using the same weightings and generalized plant off section 3.2.1. The controller is designed by using MATLAB® command ‘*h2syn*’.

```
[K2, CL2, GAM2, INFO2] = h2syn(Pfas, 1, 1);
```

The obtained  $H_2$  controller in continuous time domain is given in equation (3.7)

$$K_2(s) = \frac{3702 \cdot s^5 + 7.060 \cdot 10^5 \cdot s^4 + 6.252 \cdot 10^7 \cdot s^3 + 2.689 \cdot 10^9 \cdot s^2 + 5.076 \cdot 10^{10} \cdot s + 2.026 \cdot 10^{11}}{s^6 + 1915 \cdot s^5 + 8.111 \cdot 10^5 \cdot s^4 + 7.944 \cdot 10^7 \cdot s^3 + 3.903 \cdot 10^9 \cdot s^2 + 2.238 \cdot 10^{10} \cdot s + 1.234 \cdot 10^{10}} \quad (3.7)$$

Corresponding minimized  $H_2$  norm of the closed loop system is 5.5843.

To evaluate robust characteristics and robust performance of the feedback system, singular values and characteristics of the open loop gain  $L_2 = G \cdot K_2$ , sensitivity function  $S_2 = \frac{1}{1+L_2}$  and closed loop transfer function  $T_2 = \frac{L_2}{1+L_2}$  can be checked, where  $G$  is the nominal transfer function of the plant given in equation (3.6). The singular values of  $L_2$  and  $S_2$  are given in Figure 60 and Figure 61. Note that the general shapes of these plots are well-matched with the typical functions shown in Figure 42 and Figure 43. At a first glance, the clearest difference from  $H_\infty$  case is that the peaks in the plot are removed.

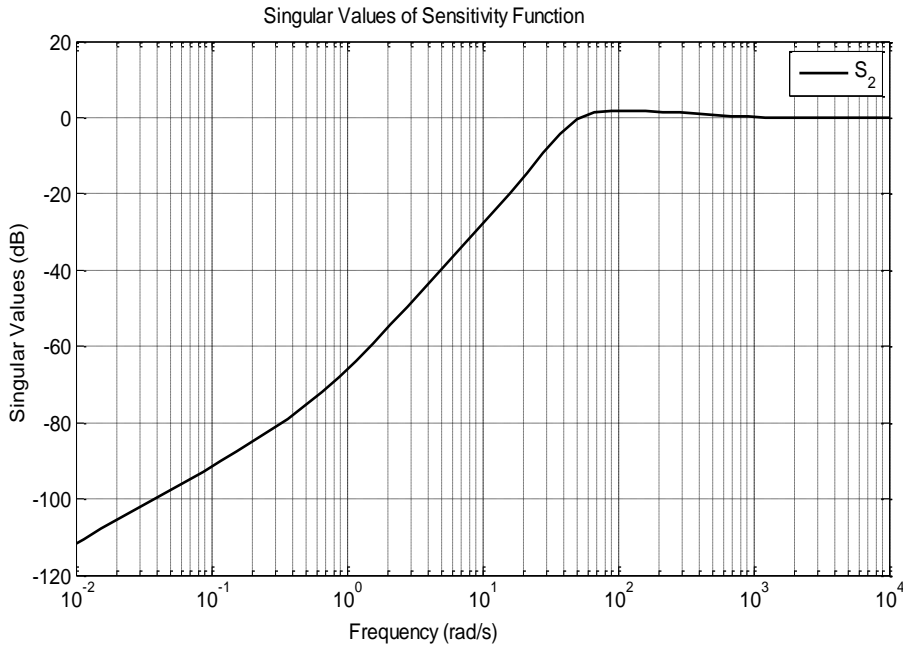


**Figure 60.** Singular value plot of the sensitivity function in  $H_2$  controlled case without uncertainty

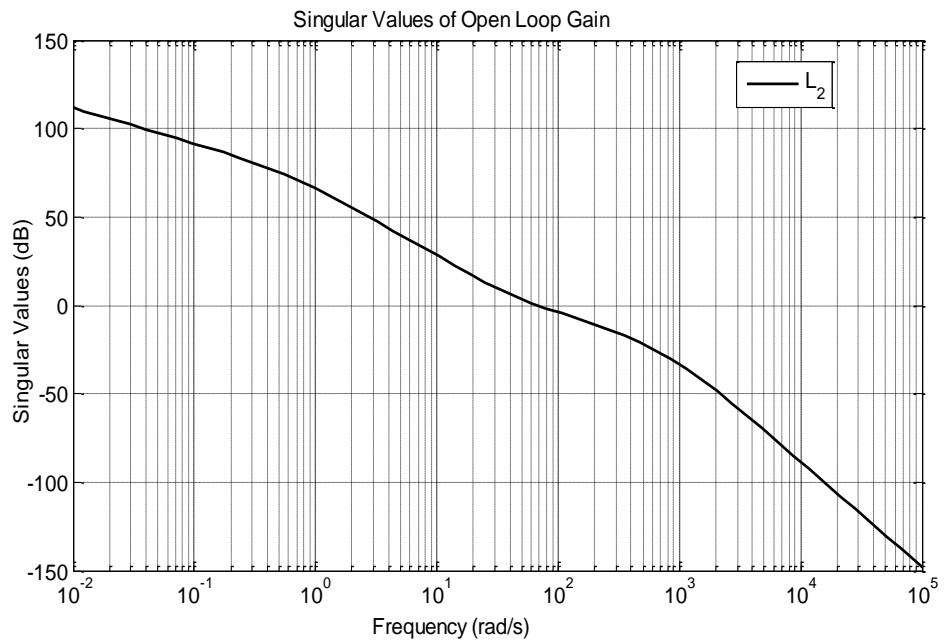


**Figure 61.** Singular value plot of the open loop gain in  $H_2$  controlled case without uncertainty

Bandwidth of the closed system can be described by looking Bode magnitude plot of  $T_2$ . As shown in, the bandwidth of the feedback system is 6.6 Hz and this is not sufficient for performance.

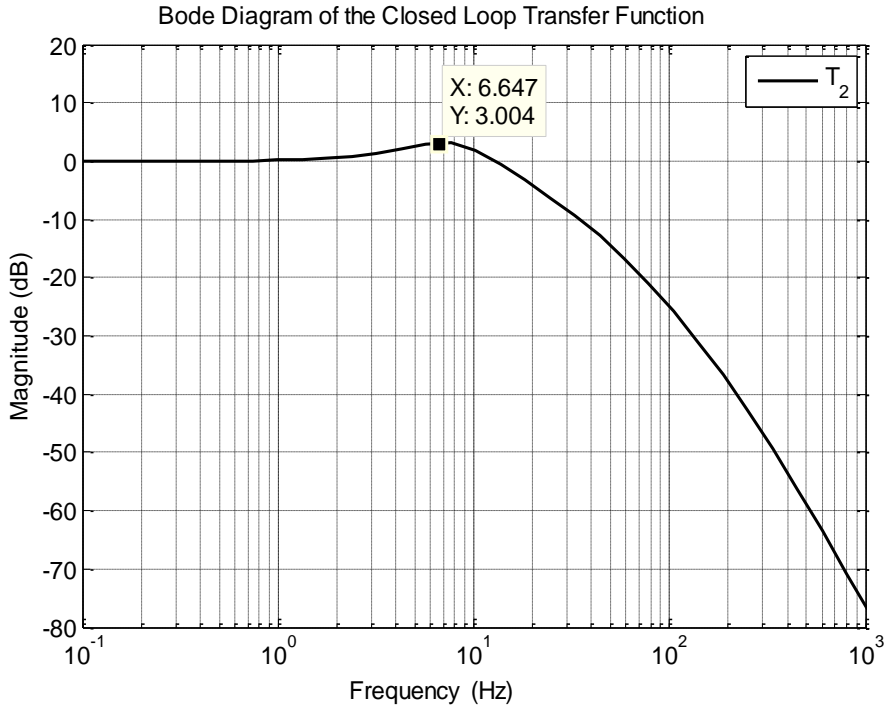


**Figure 62.** Bode plot of the closed loop response and corresponding bandwidth

Robustness to uncertainties can be evaluated over Figure 63 . Similar to  $H_\infty$  case, higher frequency dynamics are not affected by the uncertainties. The uncertainties are dominant on lower frequency response of the feedback system but these effects are not dramatic, the singular values change only  $\pm 5\%$ .

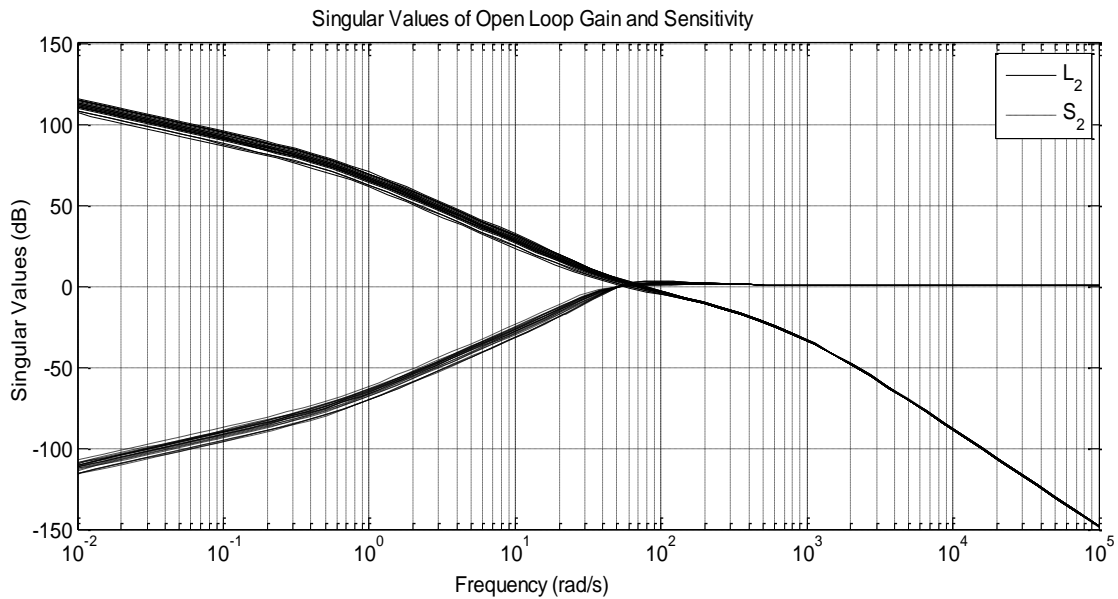


**Figure 63.** Effect of uncertainty to singular value plots

Analysis in time domain can be achieved via the step response of the feedback system with parameter uncertainties. By looking at Figure 64, it can be seen that settling time is about 0.18 seconds which is larger than  $H_\infty$  curve and the maximum percent over shoot is larger than 35%. In this manner, this controller is even worse than the predesigned  $H_\infty$  controller. Similar to  $H_\infty$  case, the steady state error is minimized and near to 0.

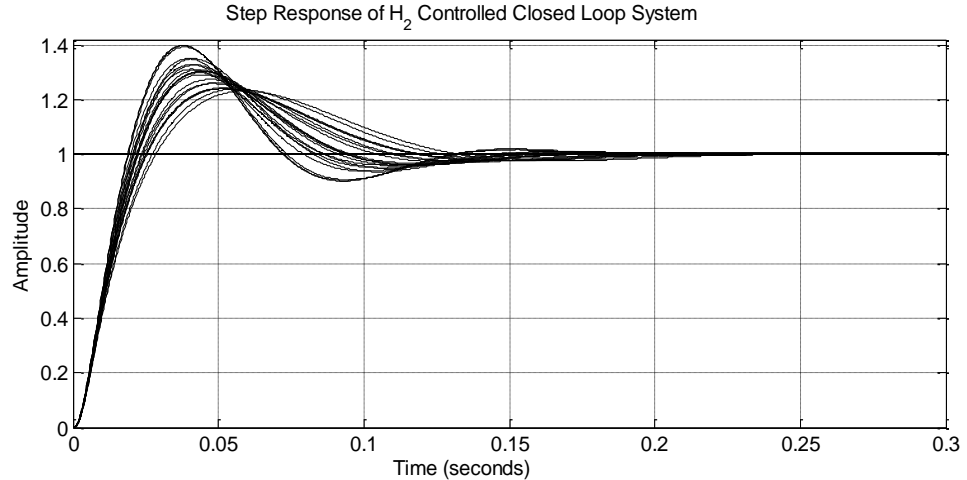


**Figure 64.** Step response of the closed loop system including parameter uncertainties

### 3.2.2.1. Simulation Results

Using the same conditions of section 3.2.1.1,  $H_2$  controlled system is simulated. The simulated response to the same reference signal is given in Figure 65. As seen from the figure, although the closed loop system can successfully follow the reference signal the performance is worse than  $H_\infty$  case. In Figure 66, the most critical section of the response is zoomed. Here there is an over shoot more than  $2^> 10\%$  which is much higher than  $H_\infty$  controlled case. The effect of cogging can also be seen in this figure. Note that the amplitudes of oscillations are much higher than the previous controller.

According to response outputs, one can easily claim that  $H_2$  controller is worse than  $H_\infty$  case. Therefore the use of  $H_2$  is not a good choice in performance manner. Although this comment is true, the main advantage of the  $H_2$  method is that; it minimizes the energy of the control signal. To observe this, the current drained from the source and fed into plant by controller is plotted on Figure 67. The maximum value of the current is smaller than 9 A and the peaks on the current are removed. Also note that the control signal is smoother than  $H_\infty$  case.

The simulated response of the feedback system to 12 Hz sinusoidal signal with amplitude  $\pm 1^\circ$  is shown in Figure 68. Here the feedback system cannot track the high frequency reference signal, because the bandwidth of the system is low as shown in Figure 62.

Simulation result of the nominal plant under 40 Nm external load and response to maximum amplitude signal

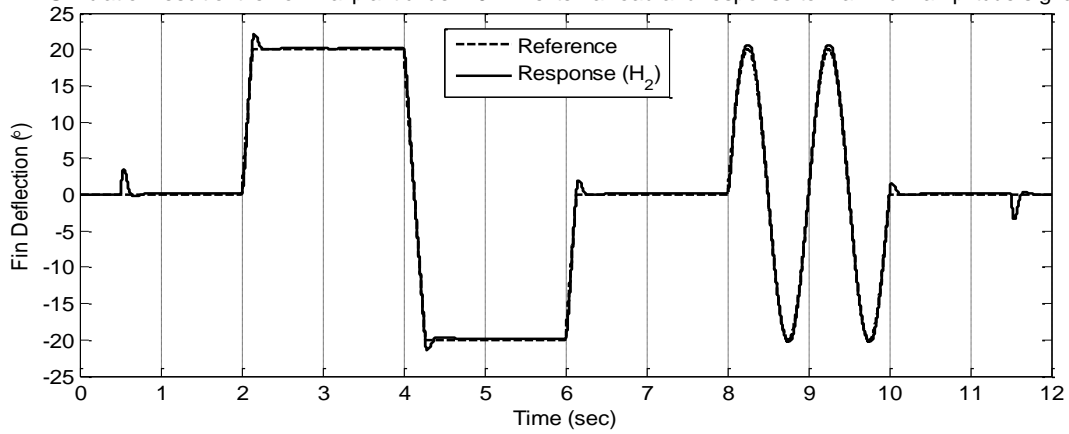


**Figure 65.** Simulation response of the feedback system under external 40 N.m disturbance

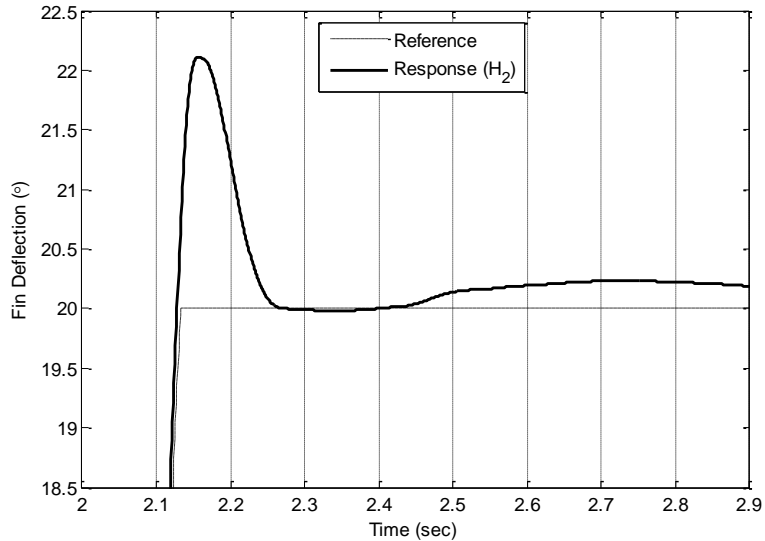


**Figure 66.** Zooming of Figure 65

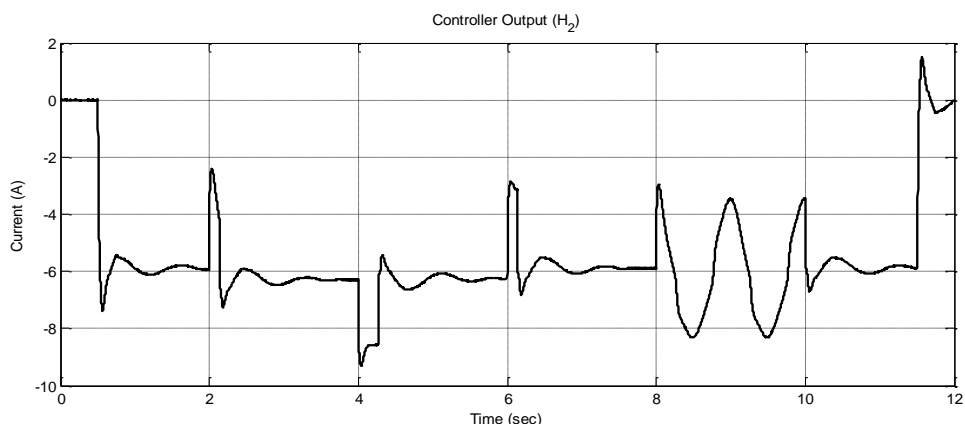


**Figure 67.** Command generated by the  $H_2$  controller

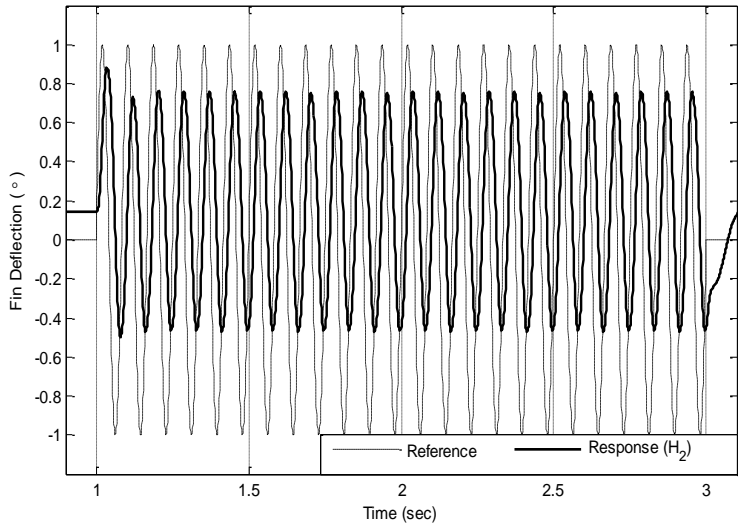


**Figure 68.** Simulated response of  $H_2$  controlled plant to 12 Hz sinusoidal reference signal

### 3.3. $H_2/H_\infty$ MIXED CONTROLLER SYNTHESIS

In section 3.2, pure  $H_\infty$  and  $H_2$  controller are designed. According to simulations,  $H_\infty$  controller is good at performance and robustness,  $H_2$  controller is good at minimizing the consumed energy for control effort. By synthesizing  $H_2/H_\infty$  mixed controller, one can combine the best properties of these two methods. In this context, using an additional weight  $W_{act2}(s)$  and defining the generalized plant, the mixed controller can be designed by using built-in function ‘*h2hinfsyn*’.

For problem definition of  $H_2/H_\infty$  mixed control, please refer to equation (1.16). To have a stable and robust closed loop characteristics,  $H_\infty$  norm of the mixed controller should be less than 1, i.e.  $\gamma_o < 1$ . The tradeoff criteria  $\alpha = 0.1$  and  $\beta = 0.9$  are selected. It is possible assign different values for these factors. These parameters define the ‘mixing ratio’ of two controllers. The sum of the ratios are not to be  $\alpha + \beta = 1$ . If this sum differ from 1, the algorithm scales the factors to 1. Similar to selection of weightings, the relevant values were not achieved immediately. Initially they assigned as  $\alpha = \beta = 1$  and further configured during the controller design process by the help of examination of simulations and analysis.

The mixed controller is generated by using the following command:

```
h2hinfsyn(MIXP,1,1,1,[0.1 0.9],'Display','On','DKMAX',0,'HINFMAX',0.99)
```

Here to obtain a strictly proper controller, option ‘DKMAX’ assigned to zero. Maximum allowable value for  $H_\infty$  norm of the closed loop system is defined as 0.99. The obtained  $H_2$  controller in continuous time domain is given in equation (3.8). Note that the order of the controller is one times greater than the previous controllers due to additional order of  $W_{act2}(s)$ .

$$K_{mix}(s) = \frac{8828s^6 + 4.556 \cdot 10^7 \cdot s^5 + 6.773 \cdot 10^9 \cdot s^4 + 4.96 \cdot 10^{11} \cdot s^3 + 1.483 \cdot 10^{13} \cdot s^2 + 2.058 \cdot 10^{14} \cdot s + 8.221 \cdot 10^{14}}{s^7 + 3857 \cdot s^6 + 5.139 \cdot 10^6 \cdot s^5 + 3.058 \cdot 10^9 \cdot s^4 + 3.067 \cdot 10^{11} \cdot s^3 + 1.543 \cdot 10^{13} \cdot s^2 + 5.521 \cdot 10^{13} \cdot s + 5.12 \cdot 10^{13}} \quad (3.8)$$

The characteristics of this controller will be evaluated at section 4.1 by comparing its robustness and performance characteristics with previously generated controllers. Corresponding minimized  $H_2$  norm of the closed loop system is 9.85 which is higher than pure  $H_2$  case. Since the solution restricted to obtain  $\gamma_{opt} \leq 0.99$ , the reached  $H_\infty$  norm of the closed loop system is 0.99. If this value is less than 1, system is robust and it should be near to 1 to guarantee performance.

The features of mixed controller will be given in the final chapter of this text by comparing with the previously obtained controllers. The step response of the controlled system with uncertainty is given in Figure 69. As seen from the figure, in the worst case, the maximum percent overshoot value is less than 9% and the settling time is 0.17 s. Here the settling time value is better than  $H_2$  case and the maximum over shoot value is the best of all.

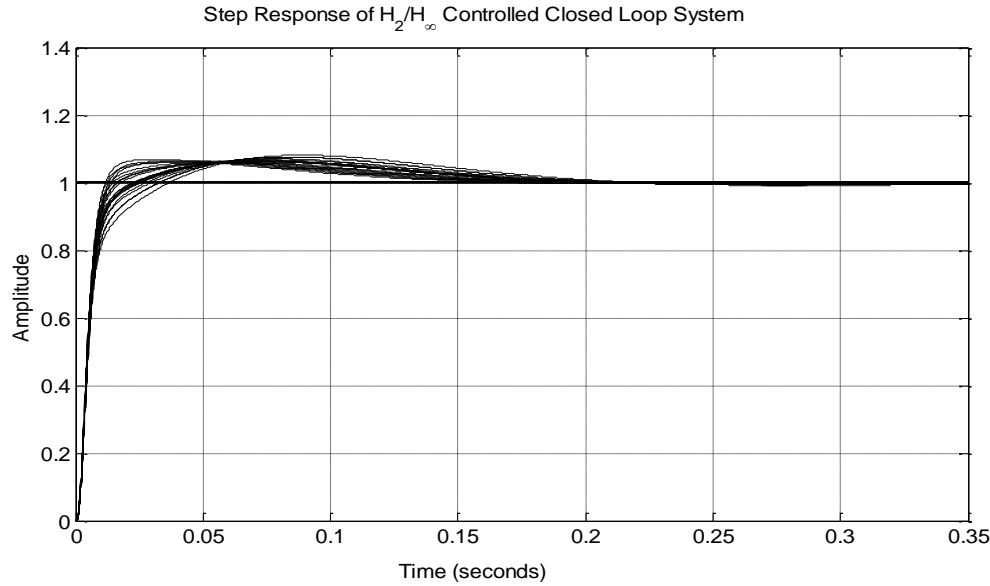


**Figure 69.** Step response of the closed loop system including parameter uncertainties

## CHAPTER 4.

### DISCUSSION, CONCLUSION AND RECOMMENDATIONS

A lot of control methods are available at the present time. In this work, the objective is to compare the mixed  $H_2/H_\infty$  type controllers with pure  $H_2$  and  $H_\infty$  type controllers and confirming the theoretical results on a physical system. To design a controller, after the identification of system is accomplished, first the requirements of the feedback system are defined. Then three different types of robust controllers are synthesized using the same weighting functions. Although the experiments show that none of the designed controllers can exactly meet the initial performance specifications; the performance of mixed  $H_2/H_\infty$  type controller shows the best performance in the manner of both minimization of the energy of the control signal and tracking of the reference signal under disturbances. This case is attained from the discussions presented in the following section.

#### 4.1. COMPARISON OF THE CONTROLLERS

##### 4.1.1. Comparison via Analytical Methods

Generated  $H_2$  and  $H_\infty$  controllers are discussed in section 3.2. In this part the performance and robustness properties of the simple controllers are compared with the  $H_2/H_\infty$  mixed controller using the available analysis methods. The responses are also compared by the ideal second order system determined in equation (3.1).

The nominal sensitivity functions of three different systems are given in Figure 70. It is obvious that the  $H_2/H_\infty$  mixed controlled plant has a sensitivity function behavior that passes through between  $H_2$  and  $H_\infty$  controlled systems and obviously satisfies the required robustness shape that given in Figure 42.

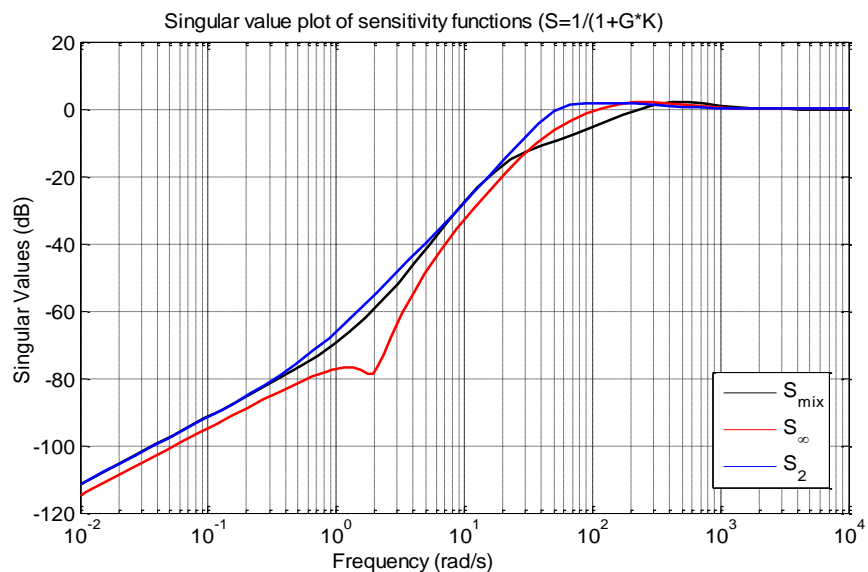


**Figure 70.** Comparison of sensitivity functions

The open loop characteristics are compared on Figure 71. As seen from the figure, the characteristic of the  $H_2/H_\infty$  mixed controlled plant is similar to  $H_2$  control in low frequency region and similar to  $H_\infty$  control in high frequency region. This property makes possible to remove the peaks that appear on  $H_\infty$  control case. Since the higher frequency region is very similar to  $H_\infty$  case, the robustness of the mixed controller to sensor noise and unmodeled dynamics is better than  $H_2$  case.

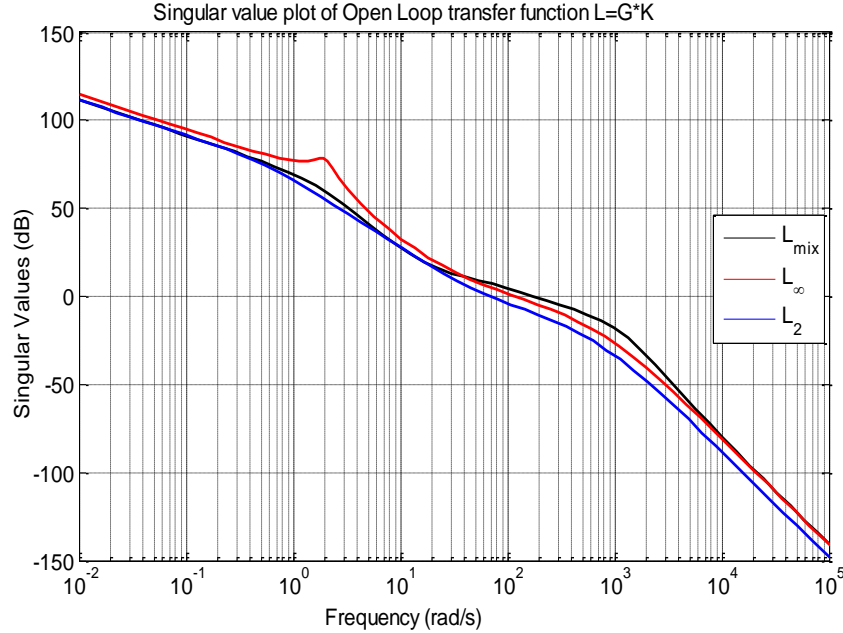


**Figure 71.** Comparison of open loop transfer functions

The singular value plots of the three different controllers are given in Figure 72. Note that, the  $H_2/H_\infty$  mixed controller converges to  $H_2$  at low frequency and to  $H_\infty$  at high frequency region.

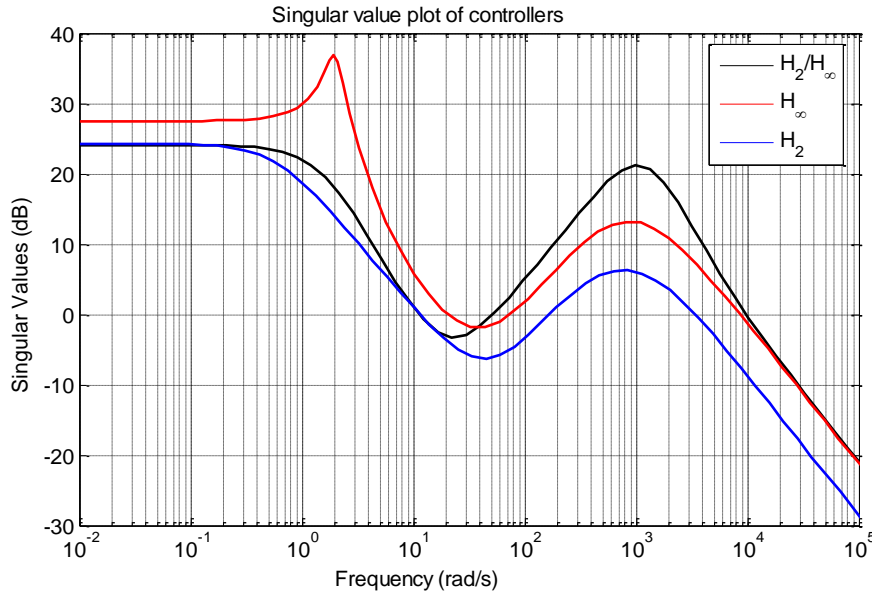


**Figure 72.** Comparison of controllers

To evaluate the effect of uncertainties, singular value plot of uncertain closed loop transfer functions (i.e. complementary sensitivity functions) are plotted in Figure 73. If the singular value is less than 1, the system is robustly stable (bounded input to system generates bounded output). Although there are some regions where the singular value are larger than 1, according to the figure,  $H_2/H_\infty$  mixed type controller has the best robustness property among of all controllers covered. Because in the other type of controllers, the areas where singular value are higher than 1 is wider. Also the hump over to value 1 reaches much higher values in  $H_2$  and  $H_\infty$  case. Generally, in a closed loop system response, if the singular value is away from 1, the tracking performance of the system decreases.

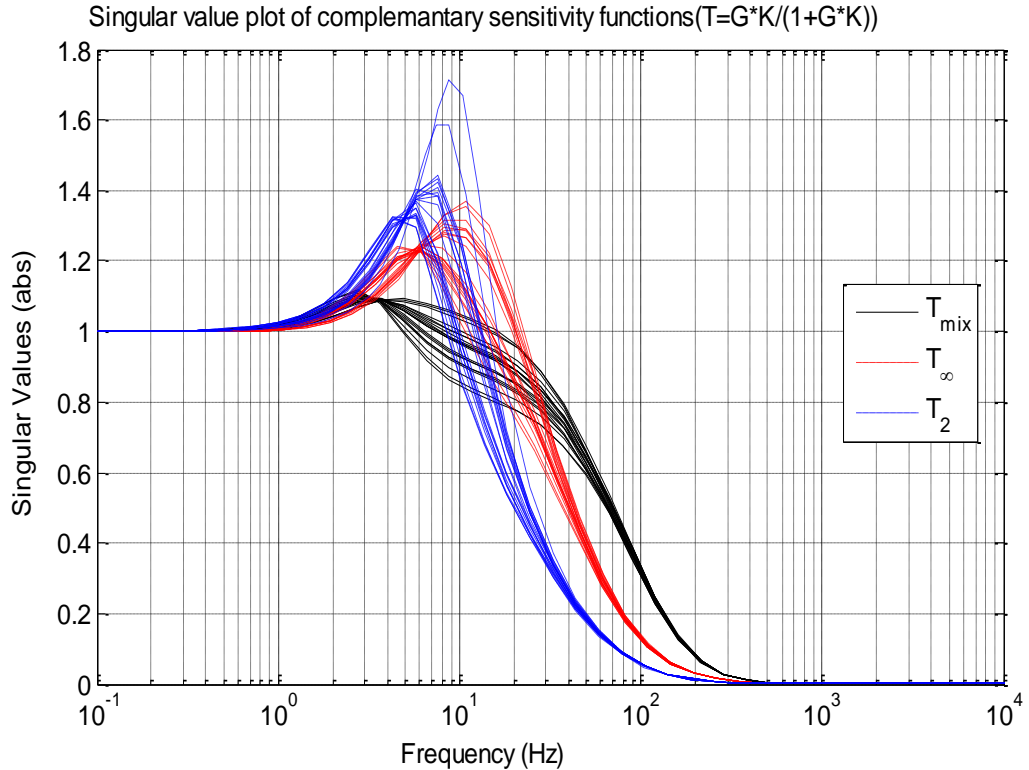


**Figure 73.** Comparison of complementary singular values

In Figure 74, the Bode plot of closed loop transfer functions are given together with the ideal function. Note that the bandwidth of the  $H_2/H_\infty$  mixed controller is 42.4 Hz and larger than the previous controllers.

To evaluate the time domain performance of the systems, the step response of the nominal plants are plotted together and given in Figure 75. It is obvious that, all of the robust controlled systems are faster than ideal system in rise time manner. All of the closed loop systems have zero steady state error. The least overshoot occurs in  $H_2/H_\infty$  mixed controller case and the amount of overshoot is 5%.

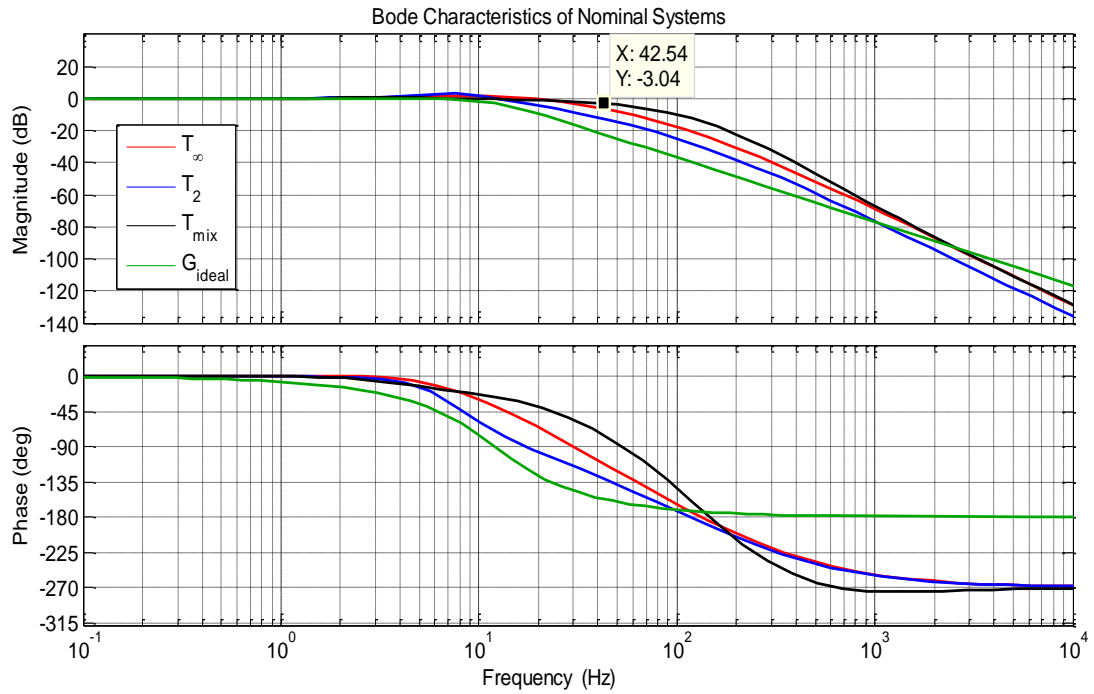


**Figure 74.** Bode plot of closed loop transfer functions with corresponding bandwidth

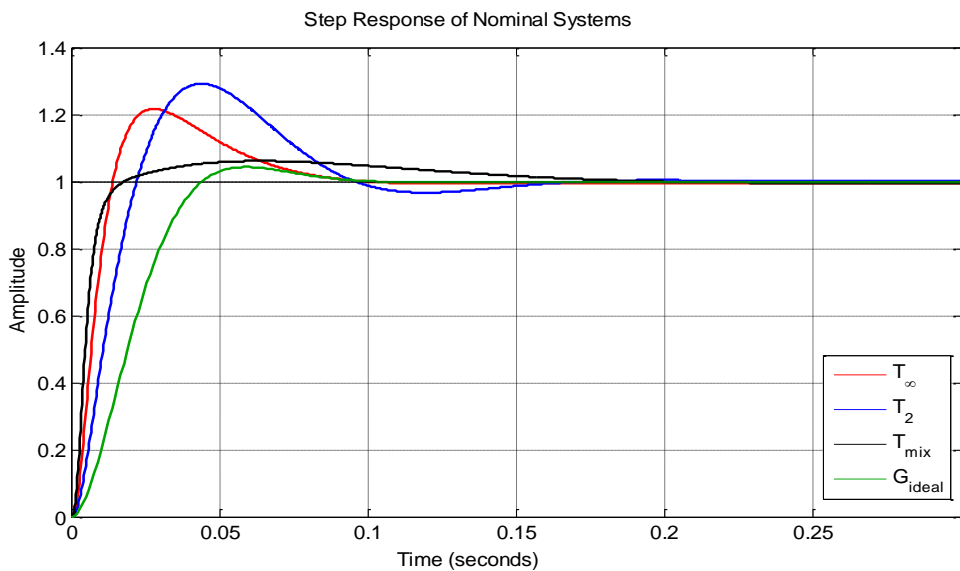


**Figure 75.** Comparative step response characteristics

According to the requirements given in section 3.1, the closed loop system should be able to follow  $\pm 1^\circ$  sinusoidal reference signal at 12 Hz. This case is tested using uncertain transfer functions and the results are provided in Figure 76. As seen from the figure, the requirement is best achieved by mixed controller. In  $H_2/H_\infty$  mixed controller case, the uncertainties in the plant causes less deviations from the nominal plant relative to other type of controllers.

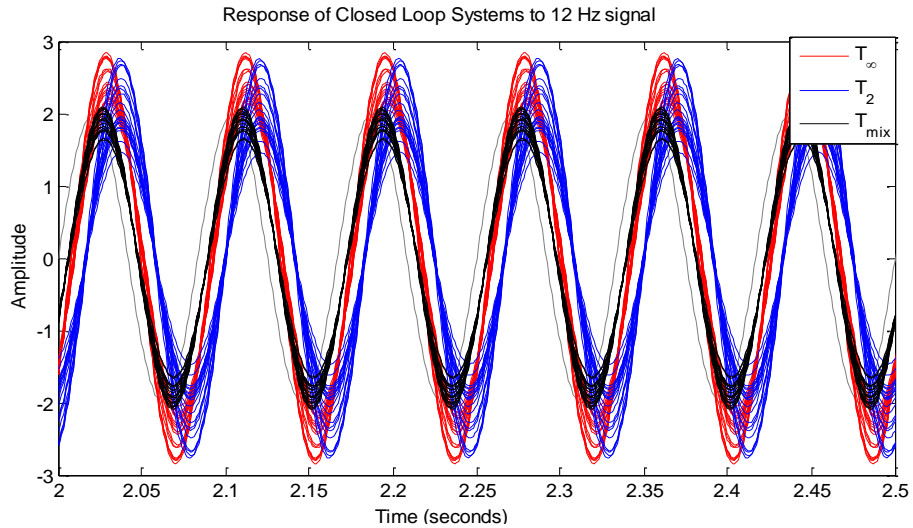


**Figure 76.** Frequency response comparison

Until this point, the characteristics that can be shown by graphics are analyzed. As a final step, the comparisons related to numerical values are considered. The poles of the nominal closed loop transfer functions are listed below. All of the poles have negative real parts, therefore the systems are stable. The most *dominant poles* (the pole nearest to imaginary axis) determine the relative stability of the systems. Hence,  $H_2/H_\infty$  controlled system has the best dominant pole characteristics. Another observation from the poles is that, although the locations of farthest poles are different, the lower order dynamics of the different systems are similar, because the locations of the poles with smaller real values are near.

$$\begin{aligned} T_\infty &\rightarrow \{-5.99; -39.36 \pm 22.10i; -53.36 \pm 53.19i; -130.69; -341.32; -1388.63\} \\ T_2 &\rightarrow \{-5.32; -29.19 \pm 40.25i; -53.31 \pm 53.31i; -59.69; -341.31; -1388.63\} \\ T_{mix} &\rightarrow \{-6.23; -16.53 \pm 15.15i; -53.51 \pm 53.23i; -333.90; -736.18 \pm 443.89; -1949.55\} \end{aligned}$$

The robust stability of the uncertain closed loop systems can be checked via the built-in function '*robuststab*' of MATLAB®. The function can be run using the following script.

```
[stabmarg,destabunc,Report] = robuststab(sys)
```

The function returns the structure '*stabmarg*' with the fields given in Table 9.

**Table 9.** Stabmarg fields descriptions

Field	Description
<i>LowerBound</i>	Lower bound on stability margin, positive scalar. If greater than 1, then the uncertain system is guaranteed stable for all values of the modeled uncertainty. If the nominal value of the uncertain system is unstable, then <i>stabmarg.UpperBound</i> and <i>stabmarg.LowerBound</i> both are equal to 0.
<i>UpperBound</i>	Upper bound on stability margin, positive scalar. If less than 1, the uncertain system is not stable for all values of the modeled uncertainty.
<i>DestabilizingFrequency</i>	The critical value of frequency at which instability occurs, with uncertain elements closest to their nominal values. At a particular value of uncertain elements (see <i>destabunc</i> below), the poles migrate across the stability boundary (imaginary-axis in continuous-time systems, unit-disk in discrete-time systems) at the frequency given by <i>DestabilizingFrequency</i> .

If the robust stability margin exceeds 1, the uncertain system is stable for all values of its model uncertainty [38]. The returned parameter ‘*report*’ describes the output of the script as text.

For these three different cases, the obtained results on the ‘*stabmarg*’ are the same except numerical differences at the order of  $10^{-5}$ . The function generates that:

*LowerBound: 3.644*

*UpperBound: 3.644*

*DestabilizingFrequency: 0 rad/s*

The lower and upper bounds here states that the closed loop system can tolerate up to 364.4% of the modeled uncertainty. The destabilizing combination occurs near to 0 rad/s. Here, stability robustness margins are greater than 1, therefore the uncertain system is robustly stable to modeled uncertainty.

Although the stability robustness margins are the same for three different cases, the sensitivities with respect to uncertain elements are different. The output argument ‘*report*’ gives the following results:

- The sensitivity of  $H_\infty$  controlled plant with respect to uncertain element  $B_{eq}$  is 100% and  $K_t$  is 70%. This means increasing  $B_{eq}$  by 25% leads to a 25% decrease in the margin and increasing  $K_t$  by 25% leads to 18% decrease in the margin.
- The sensitivity of  $H_2$  controlled plant with respect to uncertain element  $B_{eq}$  is 100% and  $K_t$  is 0%. This means increasing  $B_{eq}$  by 25% leads to a 25% decrease in the margin and increasing  $K_t$  do not lead to any change in the margin.
- The sensitivity of  $H_2/H_\infty$  controlled plant with respect to uncertain element  $B_{eq}$  is 100% and  $K_t$  is 70%. This means increasing  $B_{eq}$  by 25% leads to a 25% decrease in the margin and increasing  $K_t$  by 25% leads to 18% decrease in the margin. This characteristic is the same with  $H_\infty$ .

The results obtained in this part shows that, the  $H_2/H_\infty$  mixed robust controller can perform better than pure controllers and it is also robust to defined uncertainties at least as  $H_\infty$  controller. The performance and robustness of the controllers under the disturbances and external effects will be analyzed by using simulations in the next section.

#### 4.1.2. Comparison via Simulation Results

There are available tools to analyze the disturbance rejection and noise suppression characteristics of the closed loop systems. However, since the simulation of model is built, the effects of the external disturbances can be checked by using this more easily. Using the simulation model and conditions covered in previous chapters, the response of three different feedback systems are drawn together in Figure 77. Due to the frequency responses characteristics can be separated well at higher order frequencies, the reference command includes a sine signal with  $\pm 1^\circ$  at 12 Hz.

At a first glance to Figure 77, one can obviously see that the amount of maximum overshoot is the lowest in  $H_2/H_\infty$  mixed controller case. The detailed view of the response to  $20^\circ$  rise is shown on Figure 78 and it is clear that the overshoot of the mixed controller is lower and rise times are almost the same. In Figure 79, response to 12 Hz sinusoidal input is zoomed. As seen in the plot, the performance of  $H_\infty$  controller is better than others and  $H_2/H_\infty$  mixed controller shows better performance than  $H_2$  controller.

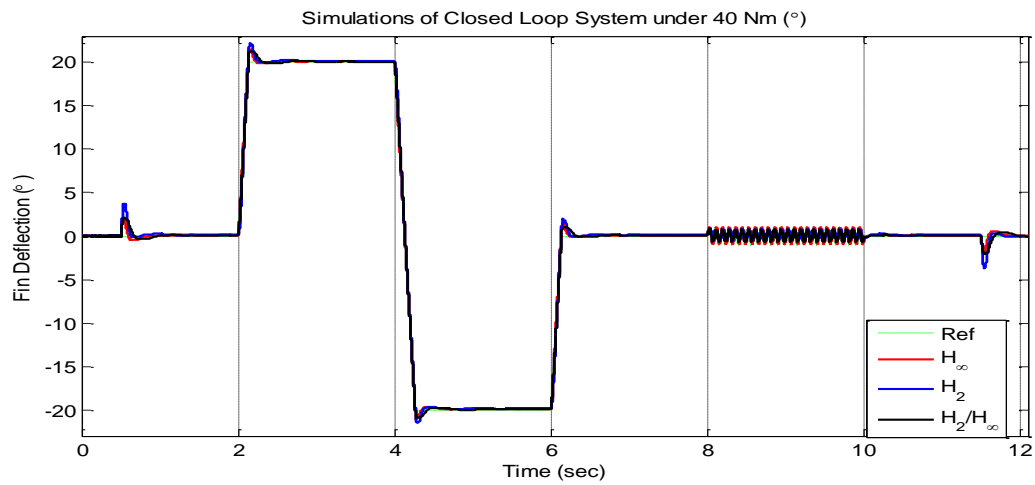


**Figure 77.** Simulated response of closed loop systems.

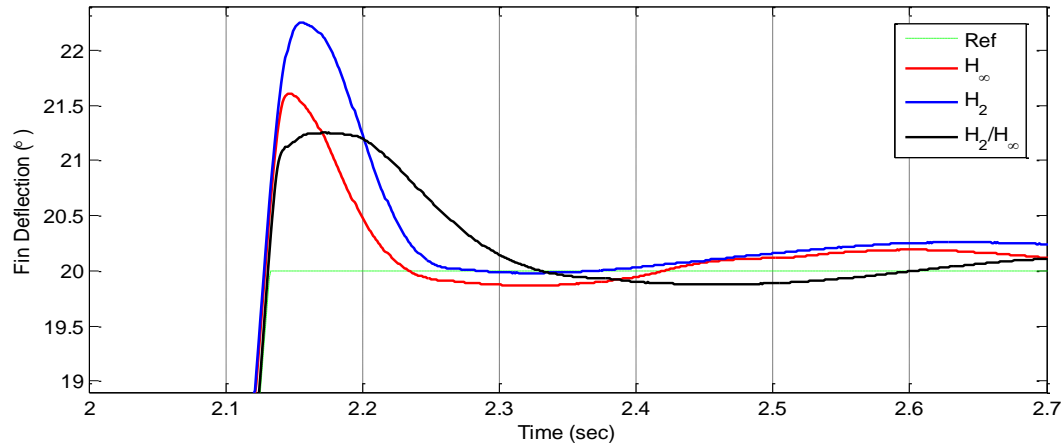


**Figure 78.** Detailed view of responses to ramp input

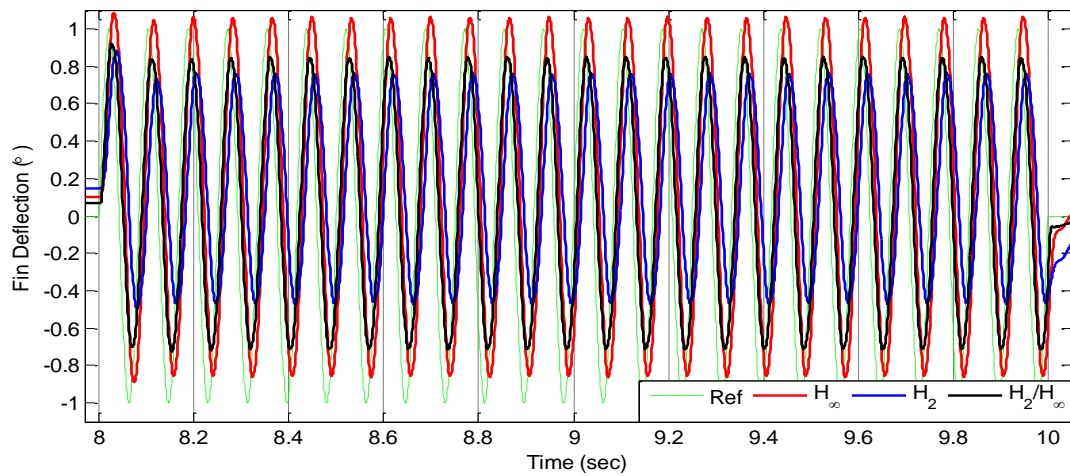


**Figure 79.** Detailed view to sinusoidal input

#### 4.1.3. Experimental Results

Up to this point the synthesized controllers are analyzed and calculations have been achieved. The generated controller matrices are discretized using ‘zero order hold’ method and uploaded to a real time experimental system using MATLAB® xPC Target module. There is an active controlled torque applying system connected onto fin shaft as an experimental set-up. This experimental set-up can be seen on the figure at APPENDIX A.6. Using this torque generating system, a constant  $40 N \cdot m$  load is applied in positive direction and the performances of the controllers are tested. Two types of reference commands are fed into system. The first type of signal includes a high amplitude ( $\pm 20^\circ$ ) sine with 1 Hz frequency and second one includes a high frequency (12 Hz) with  $\pm 1^\circ$  amplitude.

The responses of the real system for three different types of controllers are plotted together in Figure 80 and Figure 82. The most critical sections of the responses are zoomed to show details in Figure 81 and Figure 83. In the light of these experiments, one can claim that, the  $H_2/H_\infty$  mixed type controller has the best tracking performance among of all. Because, as seen from Figure 81, the  $H_2/H_\infty$  mixed type controller has the least overshoot value. Another important observation from the same figure is that,  $H_2$  controller has got a steady state error however the others have not. In Figure 80, it can be seen that all of the controllers can follow the sinusoidal input at 1 Hz. However,  $H_2$  controller yields some overshoots. To see the overshoots and prevent saturations on positions, the geometric limits on the mechanism are removed, during the experiments. So, the fin deflection capability is higher than  $\pm 23^\circ$ .

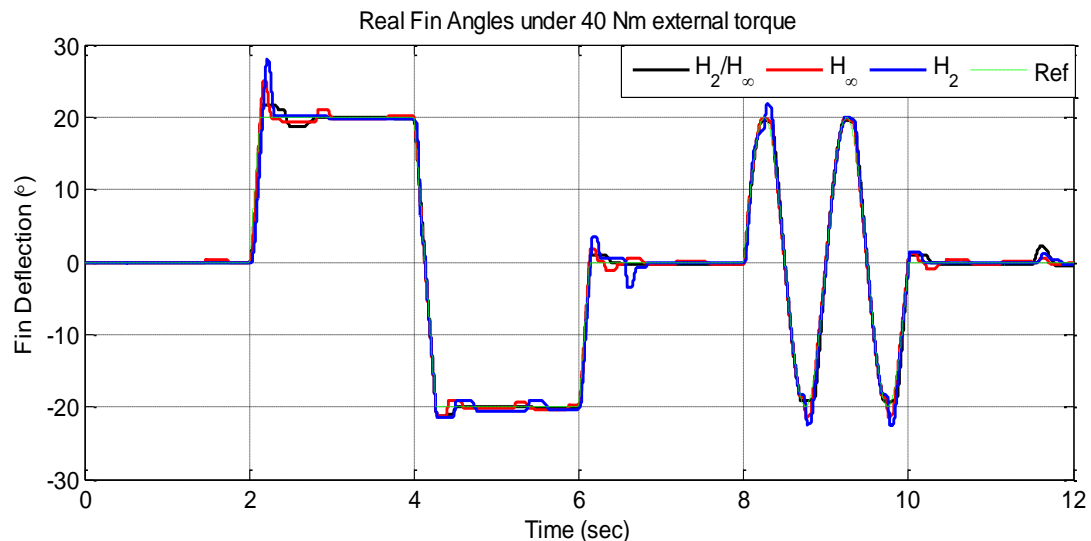


**Figure 80.** Command tracking performance of real system

In Figure 82, responses to a reference signal that has 12 Hz sinusoidal components are shown. The detailed view on Figure 83 shows that, all of the controllers are unsuccessful at the following of a fast sine. The  $H_2$  controlled system even cannot create a remarkable deflection at the fin. In spite of the generated deflection are not large enough to follow an  $1^\circ$  reference, the  $H_2/H_\infty$  mixed controller acquires the best response and reaches to  $-0.5^\circ$  and  $+0.2^\circ$ .

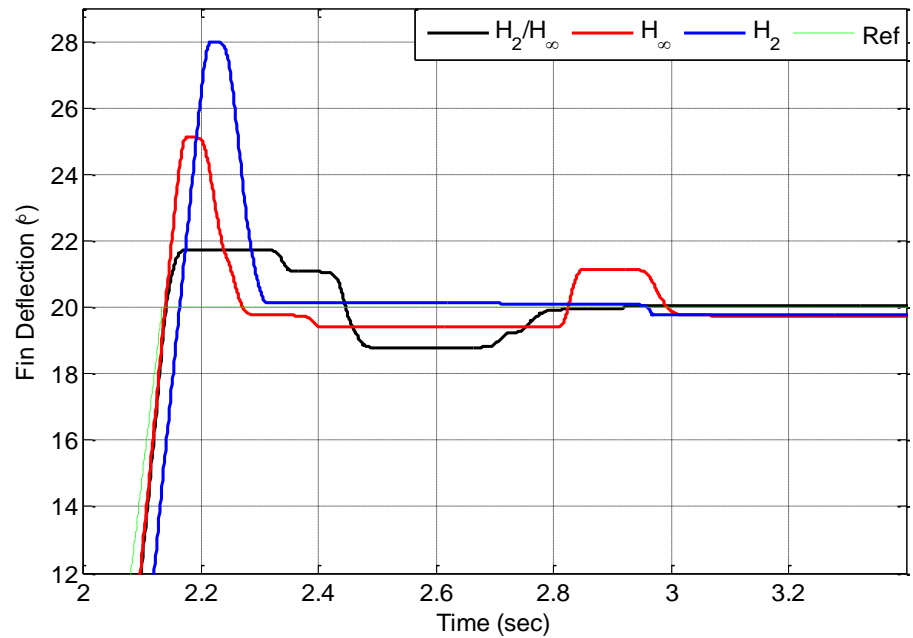


**Figure 81.** Detailed view of Figure 80

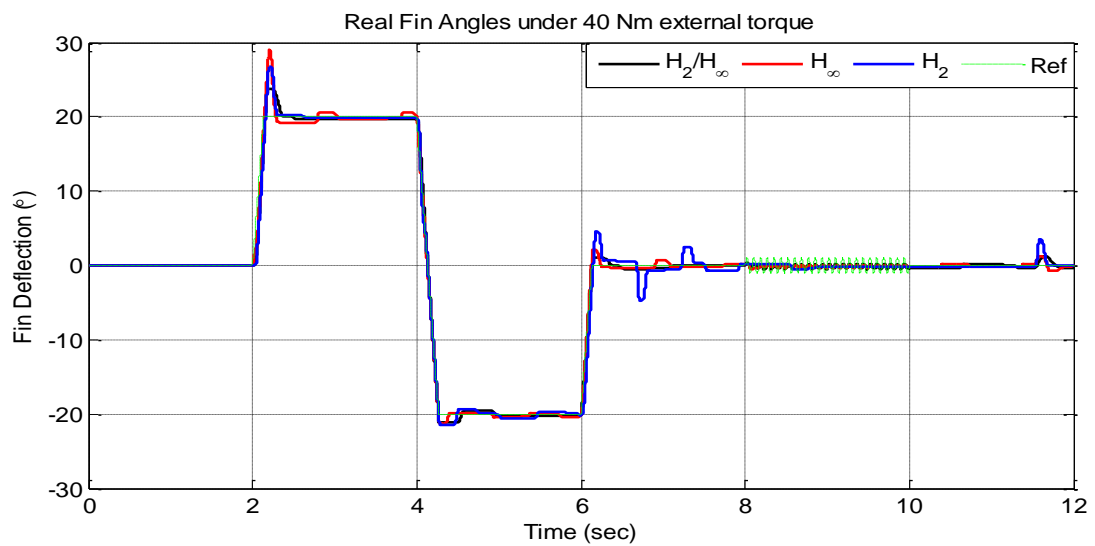


**Figure 82.** Response to higher frequency input of real system

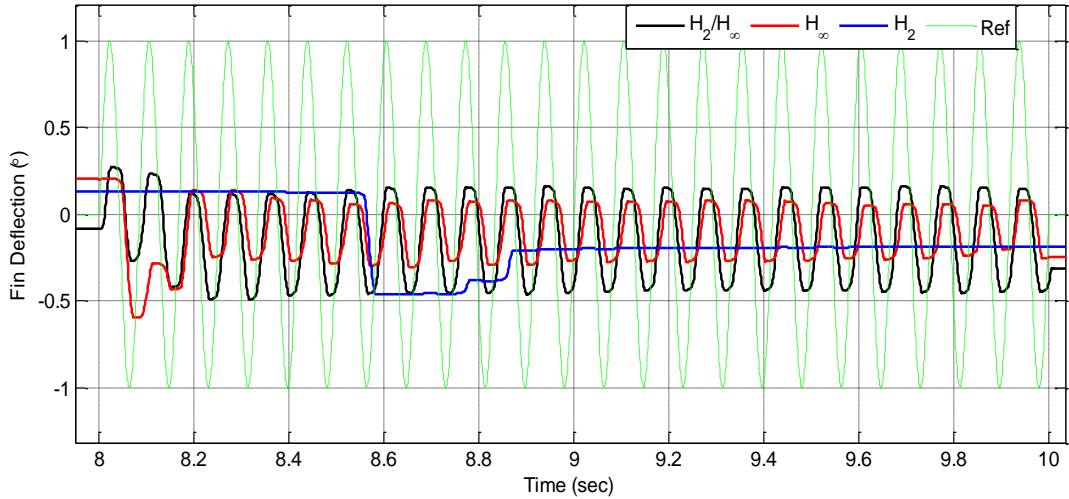


**Figure 83.** Detailed view of Figure 82

Some important observations about the controllers can be obtained by inspection of the controller commands. The generated signals by the controllers are the currents to the motor and given in Figure 84 and Figure 86. At a first glance, one can see that the current consumed by the  $H_2/H_\infty$  mixed controller is less than pure  $H_\infty$  and higher than  $H_2$ . The detailed view on Figure 85 shows that, while the other controllers cause to a saturation on the current to follow step input,  $H_2/H_\infty$  mixed controller does not create any saturation and the maximum level of the current is lower than 15 A. Due to this saturation, pure controllers cause more overshoot and settling time.

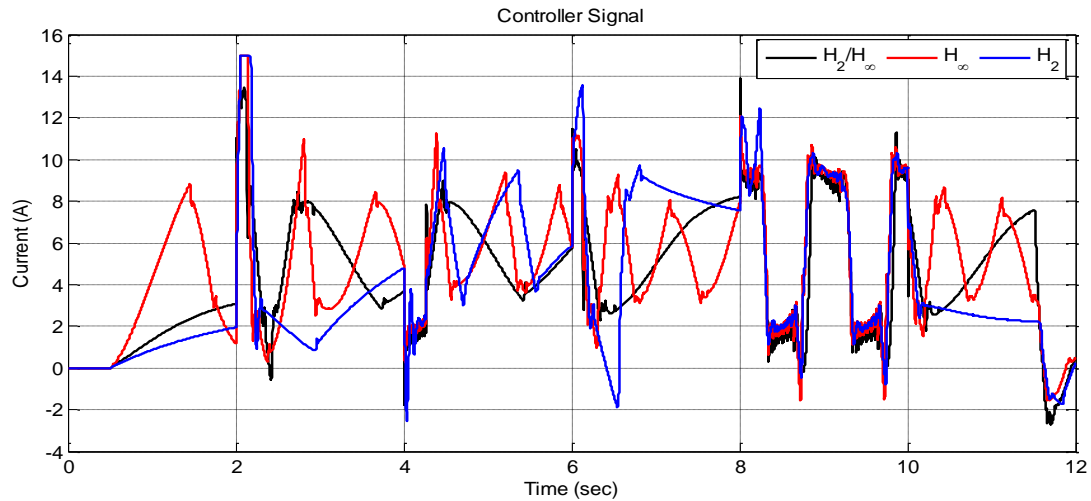


**Figure 84.** Controller command during the reference tracking given in Figure 80

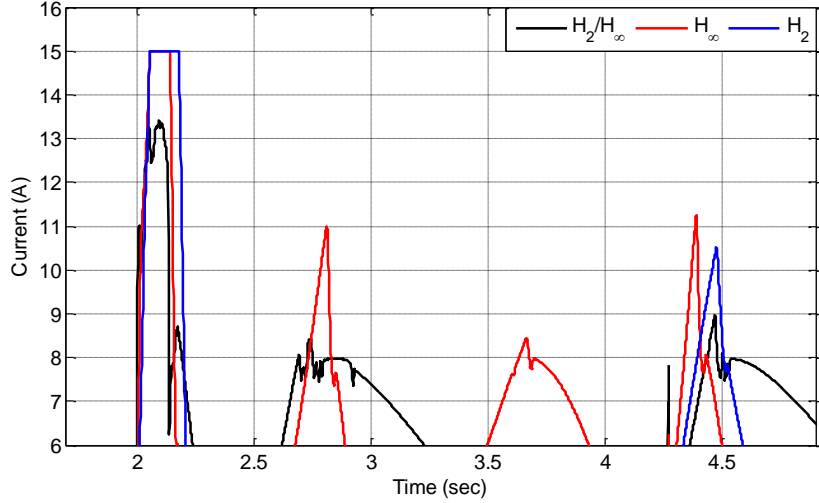


**Figure 85.** Detailed view of Figure 84

Another important feature about the command signals can be observed from Figure 87. In the case of high frequency reference tracking,  $H_2$  controller consumes less power than others, but the consumed power is not enough to generate required deflection. The same figure also shows that the current commands of  $H_2/H_\infty$  mixed and pure  $H_\infty$  are slightly differs, however their tracking performances differ in observable amount, as previously mentioned.

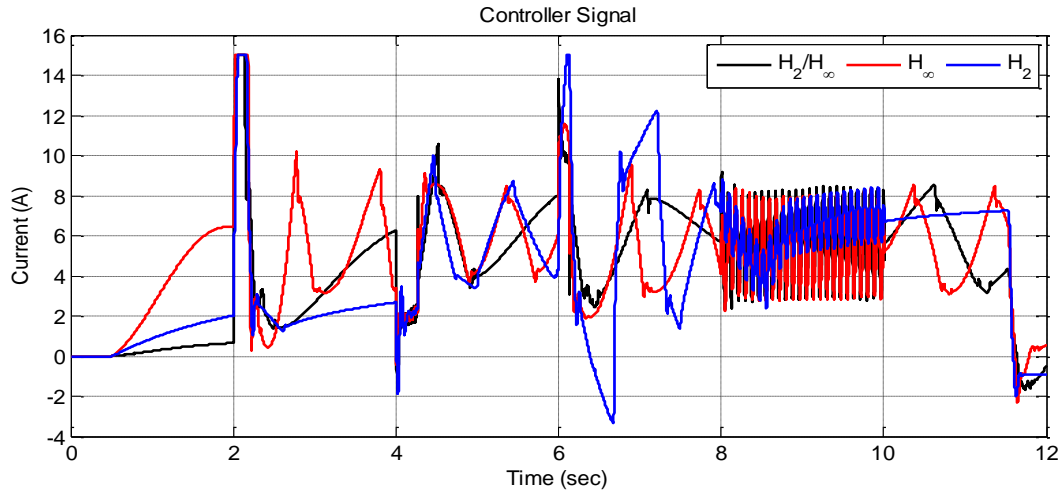


**Figure 86.** Controller command during the reference tracking given in Figure 82

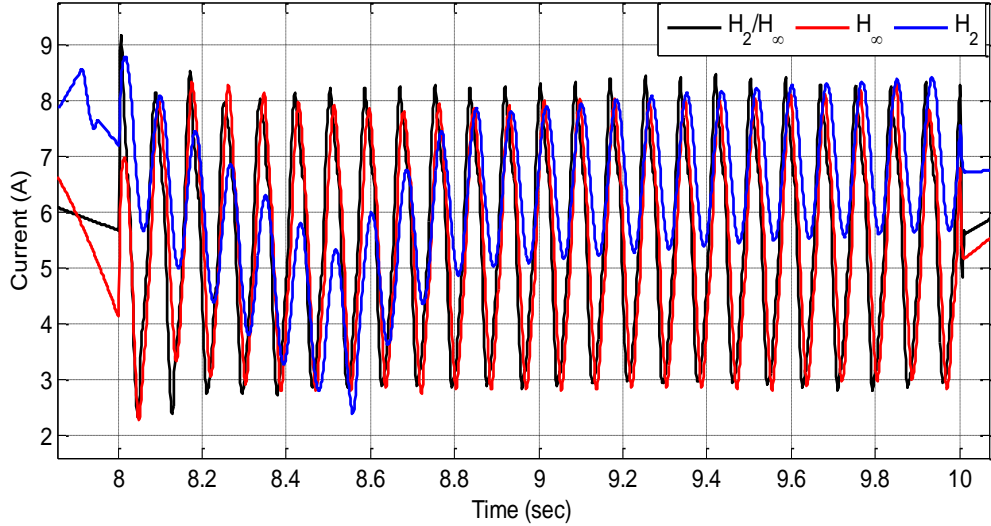


**Figure 87.** Detailed view of Figure 86

#### 4.2. CONCLUSION

The obtained results in section 4.1 shows that the robustness of the  $H_2/H_\infty$  type multiobjective controller is as good as  $H_\infty$  controller and performs better than a pure  $H_2$  and  $H_\infty$  controller. Because it ensures wider bandwidth, less overshoot and better command tracking. These properties are summarized in Table 10.

**Table 10.** Summary of comparison of controllers

Closed Loop Performances	$H_2$ Controlled	$H_\infty$ Controlled	$H_2/H_\infty$ Controlled
$H_2$ norm	5.58	6.67	9.85
$H_\infty$ norm	1.17	0.82	0.99
Bandwidth	6.7 Hz	30.4 Hz	42.4 Hz
Overshoot	35%	25 %	9%
Settling Time	0.18 sec	0.11 sec	0.17 sec

Using this  $H_2/H_\infty$  mixed robust control technique it is possible to obtain a closed loop performance that resides between the frequency response characteristic of the pure  $H_2$  controlled and  $H_\infty$  controlled systems. In this study, the plant is a specially designed fin actuation system and the general behavior of this system is not far away from a linear system due to its geometry and design. Here the robust controller techniques are preferred especially to overcome plant uncertainties and external disturbances rather than the nonlinearities. Although none of the synthesized controllers do not yields the required performance, it is shown that implementation of an  $H_2/H_\infty$  type mixed controller creates substantial gain especially in performance. One can easily comment that; in the case of a highly nonlinear plant and existence of modeling errors due to neglected higher order dynamics, the influence of an  $H_2/H_\infty$  mixed controller will be more valuable. According to results of this study; it is possible to remove ‘peaky’ regions in the frequency response characteristics via mixed controller. Hence, the  $H_2/H_\infty$  mixed control technique will be more contributing in control of plants which have some resonant and humped regions in their frequency responses. In this manner, though the plant of this thesis is not a good example to see these contributions of the  $H_2/H_\infty$  mixed control, nonetheless it is obvious that this technique causes some advantages in performance and robustness behavior of the closed loop system.

In contrast to mentioned advantages, design of a mixed controller requires much more effort than pure robust controller. Because, the mixed controller synthesis procedure includes more configuration parameters than pure robust controller case. Additionally, the characteristic and performance of  $H_2/H_\infty$  mixed controller is more sensitive to selection of weighting functions. Another issue about the mixed controller is that, it is implementation for simulation and experiments is a bit harder due to calculation of large numbers in state space matrices. The main observation is that, the simulations of mixed controllers take more time than pure  $H_2$  and  $H_\infty$  cases.

In robust controller design, maybe the most important point is the selection and definition of weightings. For example, the order of weightings describes the order of controllers and if the order of the controller increases, the applicability of controller to real system decreases. The frequency response shape of the weightings is important to tune the properties and performance of the closed loop system. However, for precisely tuning of the closed loop characteristics the higher order weighting functions may be required. Another important point about the weightings is that, their characteristics should be a projection of the real system and these characteristics are strictly dependent to the system parameters. Therefore, in some situations the degree of freedom on the change of the weighting parameters can be very narrow due to restrictions on the system. For example, some criteria on the controller performance may require higher order weighting functions and at the same time the order of the controller is wanted to be small. In such conditions, design of an  $H_2/H_\infty$  mixed type controller can be a good alternative.

In conclusion, the  $H_2/H_\infty$  mixed type controller is a good alternative method to obtain robust and well performed controller, especially when the system has peaks on its frequency response and the weightings cannot be optimized due to strict restrictions on the plant. Although, the fin actuation system of this thesis do not exactly have these properties, use of  $H_2/H_\infty$  mixed controller still creates enhancements on the closed loop performance and robustness properties of pure robust controllers.

### 4.3. FUTURE WORKS

In this work, although some remarkable performance developments are obtained using  $H_2/H_\infty$  controllers, one can claim that it is possible to find a pure  $H_\infty$  or other type of robust controller for this system. In this point, an important point about the controller is that, the final values of weightings and design parameters used here are not the ‘optimized’ values. For example the tradeoff criteria of equation (1.16) (i.e. the mixing ratios  $\alpha$  and  $\beta$ ) are selected by applying some trial and error methods. Similarly the used weightings are selected to be as first order and the parameters inside the functions are configured in this manner (1.17). Optimization of the design parameters is another topic and may be achieved as a further work. Another issue about  $H_2/H_\infty$  mixed type of controllers is that, their performance and robustness characteristic strictly depends on the weightings and optimization techniques used. If the compared  $H_2$  and  $H_\infty$  controllers are optimized such that they yield very similar closed loop behavior, the design of mixed  $H_2/H_\infty$  controller become infeasible. Because, mixed  $H_2/H_\infty$  technique produces a closed loop behavior such that it passes between two pure robust controllers. In this manner, for this plant, one can obtain a ‘better’ controller using the weightings provided in APPENDIX A.2 as MATLAB® scripts.

The experiments covered in this study are limited to some special case and also the torque disturbance to the system applied as constant. However in a real system, a fin actuation system is exposed to random torque and wind gust disturbances. As a future experimental study, the system performance can be tested against random torque.

## REFERENCES

- [1] Özkan B., Özgören M.K., Mahmetyazıcıoğlu G., "An Overview of Missile Control Systems," in *5th Ankara International Aerospace Conference*, Ankara, 2009.
- [2] Ogata, K., Modern Control Engineering, New Jersey, Prentice Hall Inc., 4th ed., 2002.
- [3] Grimble, M.J., Robust Industrial Control Systems-Optimal Design Approach for Polynomial Systems, John Wiley & Sons Ltd., 1st ed., 2006.
- [4] Green M., Limebeer D.J.N, Linear Robust Control, London, Prentice Hall Int., 1st ed., 1994.
- [5] Doyle J., Francis B., Tannenbaum A., Feedback Control Theory, California, Macmillan Publishing Co., 1st ed., 1990.
- [6] Bibel J. E., Malyevac D.S., "Guidelines for the Selection of Weighting Functions for H-infinity Control," NSWC, Dahlgren, Virginia, 1992.
- [7] Wise K., Lavretsky E., "Robust and Adaptive Control Workshop Lecture Notes," in *18th IFAC World Congress*, Milano, 2011.
- [8] Doyle J., Glover K., Khargonekar P.P., Francis B.A., "State Space Solutions to Standard H2 and  $H\infty$  Control Problems," *IEEE Trans. on Automatic Control*, vol. 34, no. 8, pp. 831-847, 1989.
- [9] Zhou K., "Comparison Between H2 and  $H\infty$  Controllers," *Trans. on Automatic Control*, vol. 37, no. 8, pp. 1261-1265, 1992.
- [10] Ullauri J. C., Mixed H2/ $H\infty$  Optimization with Multiple  $H\infty$  Constraints, M.Sc. Thesis, Air Force Institute of Technology, Ohio, 1994.
- [11] Kusnierek J., Application of Mixed H2/ $H\infty$  Optimization, M. Sc. Thesis, Air Force Institute of Technology, Ohio, 1991.
- [12] Gahinet P., Nemirovski A., Laub A.J., Chilali M., "LMI Control Toolbox User's Guide for Use with Matlab," Mathworks Inc., Natick, MA, 1995.
- [13] Zhou K., Doyle J.C., Glover K., Robust and Optimal Control, New Jersey, Prentice Hall, 1st ed., 1995.
- [14] Megretski A., "Multivariable Control Systems Lecture Notes," Massachusetts Institute of Technology Open Course Ware, - Spring 2004. [Online]. Available: <http://ocw.mit.edu/courses/electrical-engineering-and-computer-science/6-245-multivariable-control-systems-spring-2004/>. [Accessed 7 July 2012].
- [15] Bernstein D.S., Haddad W.M., "LQG Control with an  $H\infty$  Performance Bound - A Riccati Equation Approach," *IEEE Trans. on Automatic Control*, vol. 34, no. 3, pp. 293-305, 1989.
- [16] Zhou K., Doyle J., Glover K., Bodenheimer B., "Mixed H2 and  $H\infty$  control," in *American Control Conference*, San Diego, California, 1990.
- [17] Rotea M.A., Khargonekar P.P., "H2 Optimal Control with an  $H\infty$  Constraint: The State Feedback

- Case," *Automatica*, vol. 27, no. 2, pp. 307-316, 1991.
- [18] Khargonekar P., Rotea M. A., "Mixed H<sub>2</sub>/H <sub>$\infty$</sub>  Control: A Convex Optimization Approach," *IEEE Trans. on Automatic Control*, vol. 36, no. 7, pp. 824-837, 1991.
- [19] Zhou K., Glover K., Bodenheimer B., Doyle J., "Mixed H<sub>2</sub> and H <sub>$\infty$</sub>  Performance Objectives I: Robust Performance Analysis," *IEEE Trans. on Automatic Control*, vol. 39, no. 8, pp. 1564-1574, 1994.
- [20] Zhou K., Glover K., Bodenheimer B., Doyle J., "Mixed H<sub>2</sub> and H <sub>$\infty$</sub>  Performance Objectives II: Optimal Control," *IEEE Trans. on Automatic Control*, vol. 39, no. 8, pp. 1575-1587, 1994.
- [21] Chilali M., Gahinet P., "H <sub>$\infty$</sub>  Design with Pole Placement Constraints: An LMI Approach," *IEEE Trans. on Automatic Control*, vol. 41, no. 3, pp. 358-367, 1996.
- [22] Wu J.L., Lee T.T., "A new method for mixed H<sub>2</sub>/H <sub>$\infty$</sub>  control with regional pole constraints," *Optim. Control Appl. Meth.*, vol. 24, pp. 139-152, 2003.
- [23] Scherer C., "Mixed H<sub>2</sub> H <sub>$\infty$</sub>  Control," *Trends in Control: A European Perspective*, vol. of the special contributions to the ECC, 1995.
- [24] Nonami K., Sivrioglu S., "Active Vibration Control Using LMI-Based Mixed H<sub>2</sub>/H <sub>$\infty$</sub>  State and Output Feedback Control with Nonlinearity," in *35th Conference on Decision and Control*, Kobe, 1995.
- [25] Yoo C.H., Young C.L., Sang Y.L., "A Robust Controller for an Electro-Mechanical Fin Actuator," in *American Control Conference*, Boston, Massachusetts, 2004.
- [26] Popov A., Less Conservative Mixed H<sub>2</sub>/H <sub>$\infty$</sub>  Controller Design Using Multi-Objective Optimization, Project Work, Technische Universität Hamburg-Harburg, Hamburg, 2005.
- [27] Bensenouci A., Ghany A.M.A., "Mixed H <sub>$\infty$</sub> /H<sub>2</sub> with Pole Placement Design of Robust LMI-Based Output Feedback Controllers for Multi-Area Load Frequency Control," in *The Int. Conference on Computer as a Tool*, Warsaw, 2007.
- [28] Alazard D., Fezans N., Imbert N., Carpentier B., "Mixed H<sub>2</sub>/H <sub>$\infty$</sub>  Control Design for Mechanical Systems: Analytical and Numerical Developments," in *AIAA Guidance, Navigation and Control Conference and Exhibit*, Honolulu, Hawaii, 2008.
- [29] Akbar S. A., Singh A.K., Datta K.B., "Study of Response and Robustness Measures of Mixed H<sub>2</sub>/H <sub>$\infty$</sub> , LQG and H <sub>$\infty$</sub>  Controllers for Continuous Time Singularly Perturbed Systems," *Elektrika*, vol. 11, no. 2, pp. 7-15, 2009.
- [30] Türkay S., Akçay H., "Multi-Objective Control of Full-Vehicle Suspensions a Case Study," in *18th IFAC World Congress*, Milano, 2011.
- [31] Özkan B., Dynamic Modeling, Guidance and Control of Missiles, Ph.D. Thesis: METU, Ankara, Turkey, 2005.
- [32] Söderström T., Stoica P., System Identification, Cambridge, Prentice Hall Int., 1st ed., 1989.
- [33] Y. Zhu, Multivariable System Identification for Process Control, Eindhoven, Elsevier Sc. & Tech. Books, 1st ed., 2001.

- [34] Babuska R., Fuzzy Modeling for Control, Boston, Kluwer Academic Publishers, 1st ed., 1998.
- [35] Madoyan A., Design and Comparison of Mixed  $H_\infty/H_2$  Controller For AMB System, M.Sc.Thesis, Lappeenranta University of Technology,Lappeenranta, 2009.
- [36] Fortuna L., Frasca M., Optimal and Robust Control Advanced Topics with MATLAB, Florida, CRC Press, 1st ed., 2012.
- [37] Akmeşe A., Aerervoelastic Analysis and Robust Controller Synthesis for Flutter Suppresion of Air Vehicle Control Actuation Systems, Ph.D. Thesis: METU,Ankara,Turkey, 2006.
- [38] Balas G.,Chiang R.,Packard A.,Safonov M., "Robust Control Toolbox User's Guide for Use with Matlab," Mathworks Inc., 2012.
- [39] Rotstein H.,Sznajer M., Idan M., "H<sub>2</sub>/H<sub>∞</sub> Filtering Theory and an Aerospace Application," *Int. Journal of Robust and Nonlinear Control*, vol. 6, pp. 347-366, 1996.
- [40] Özkan B., "Gerçek Zamanlı Denetim Sistemlerinde Örnekleme Sıklığının Belirlenmesi," in *Otomatik Kontrol Ulusal Toplantısı*, İstanbul (in Turkish), 2009.
- [41] Lublin L.,Athans M., "Linear Quadratic Control," in *The Control Handbook*, CRC Press Inc., 1st ed.,1996, pp. 635-650.

## APPENDIX

### A.1. State Space Matrices of Generalized Plants

Pfas =

A =

	x1	x2	x3	x4	x5	x6
x1	-5.368	0	0	0	0	0
x2	0	-45.02	0	0	0	0
x3	0	0.4348	0	0	0	0
x4	10.57	0	0	-106.6	-88.83	0
x5	0	0	0	64	0	0
x6	0	0	0.1085	0	-170.4	-0.6283

B =

	d1	d2	d3	dref	u
x1	0	0	0	1	0
x2	-8500	1.414e+05	0	0	2.4e+04
x3	0	0	0	0	0
x4	0	0	0	0.00742	0
x5	0	0	0	0	0
x6	0	0	0	0	0

C =

	x1	x2	x3	x4	x5	x6
dRad	0	0	0.007072	0	0	0
z1	0	0	0.001414	0	-2.221	12.28
z2	0	0	0	0	0	0
y	186.8	0	-1	0	0	0

D =

	d1	d2	d3	dref	u
dRad	0	0	0	0	0
z1	0	0	0	0	0
z2	0	0	0	0	0.09428
y	0	0	-0.003068	0.1311	0

MIXP =

A =

	x1	x2	x3	x4	x5	x6	x7
x1	-5.368	0	0	0	0	0	0
x2	0	-4243	0	0	0	0	0
x3	0	0	-45.02	0	0	0	0
x4	0	0	0.4348	0	0	0	0
x5	10.57	0	0	0	-106.6	-88.83	0
x6	0	0	0	0	64	0	0
x7	0	0	0	0.1085	0	-170.4	-0.6283

B =

	d1	d2	d3	dref	u
x1	0	0	0	1	0
x2	0	0	0	0	16
x3	-8500	1.414e+05	0	0	2.4e+04
x4	0	0	0	0	0

```

x5      0      0      0      0.00742      0
x6      0      0      0      0      0
x7      0      0      0      0      0

C =
    x1      x2      x3      x4      x5      x6      x7
dRad   0      0      0  0.007072      0      0      0
z1     0      0      0  0.001414      0      -2.221  12.28
z2     0      0      0      0      0      0      0
z3     0  -18.75      0      0      0      0      0
Y     186.8      0      0      -1      0      0      0

D =
    d1      d2      d3      dref      u
dRad   0      0      0      0      0
z1     0      0      0      0      0
z2     0      0      0      0  0.09428
z3     0      0      0      0  0.09428
Y     0      0  -0.003068  0.1311      0

```

## A.2. Alternative Weightings to Generate Better Controller

```

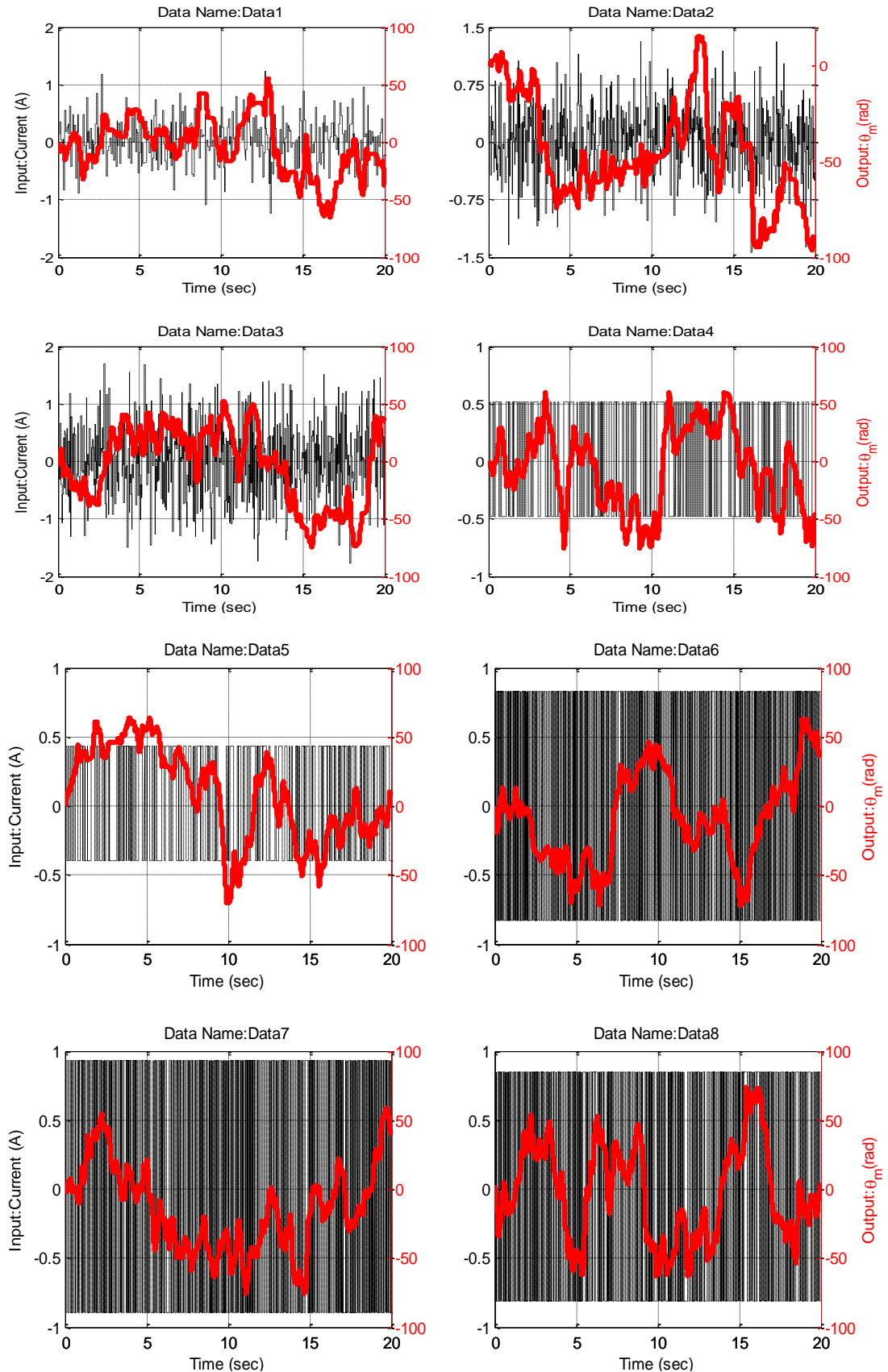
%Reference signal shape - Wref
Kref=(20*pi)/(180*sqrt(2)); %max 20 deg
wcref=0.01*2*pi;           %decrease after 0.1 Hz
Wref=zpk([],-wcref,Kref*wcref); %first order TF

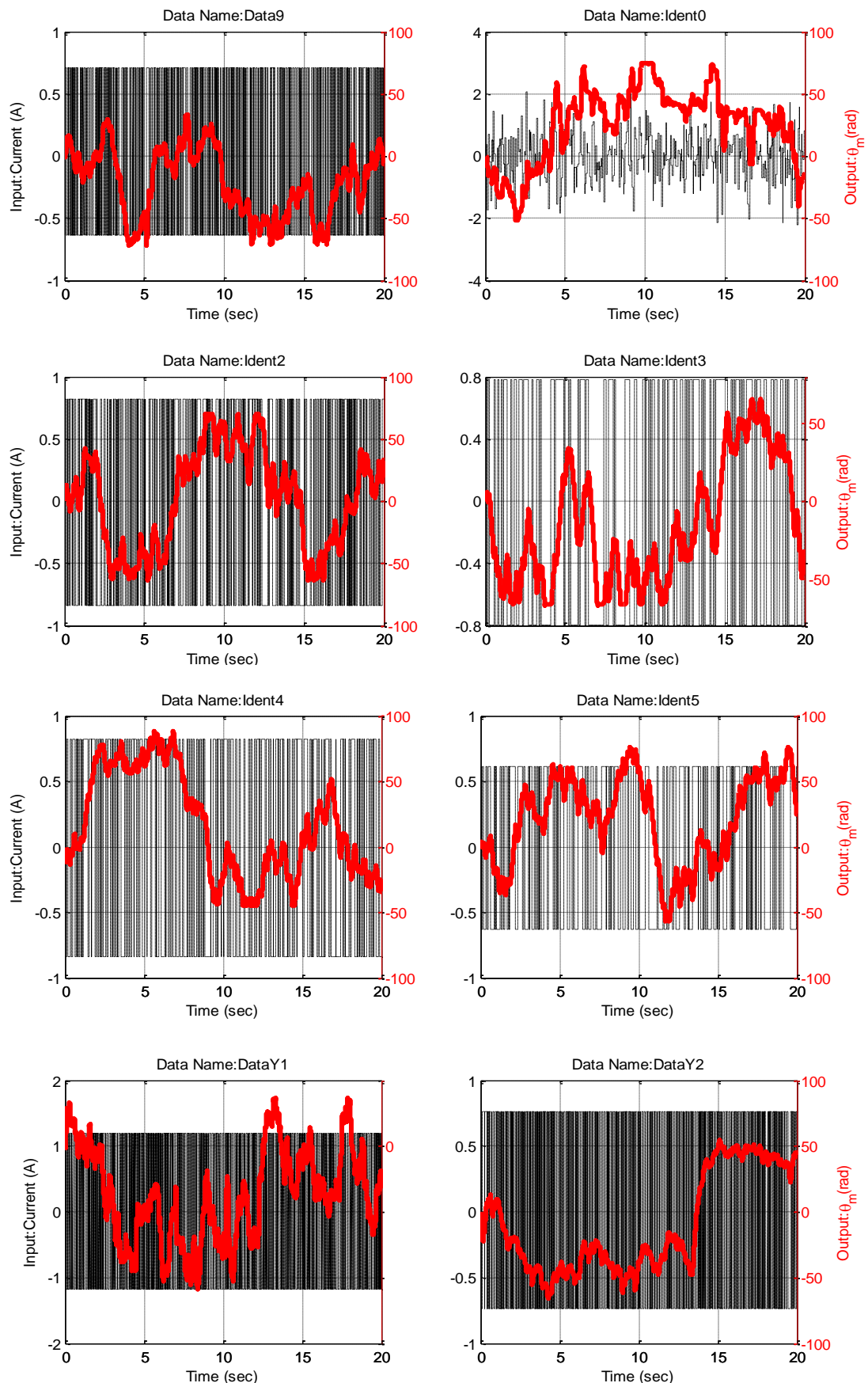
%Penalty for deviation from ideal system - Wperf
Kp=0.2;                   %penalty for large frequencies
w2p=350*2*pi/Kp;          %w_o=.5 Hz
w1p=100*2*pi*0.001;       %penalty for small frequencies
Wperf=zpk(-w2p,-w1p,Kp);

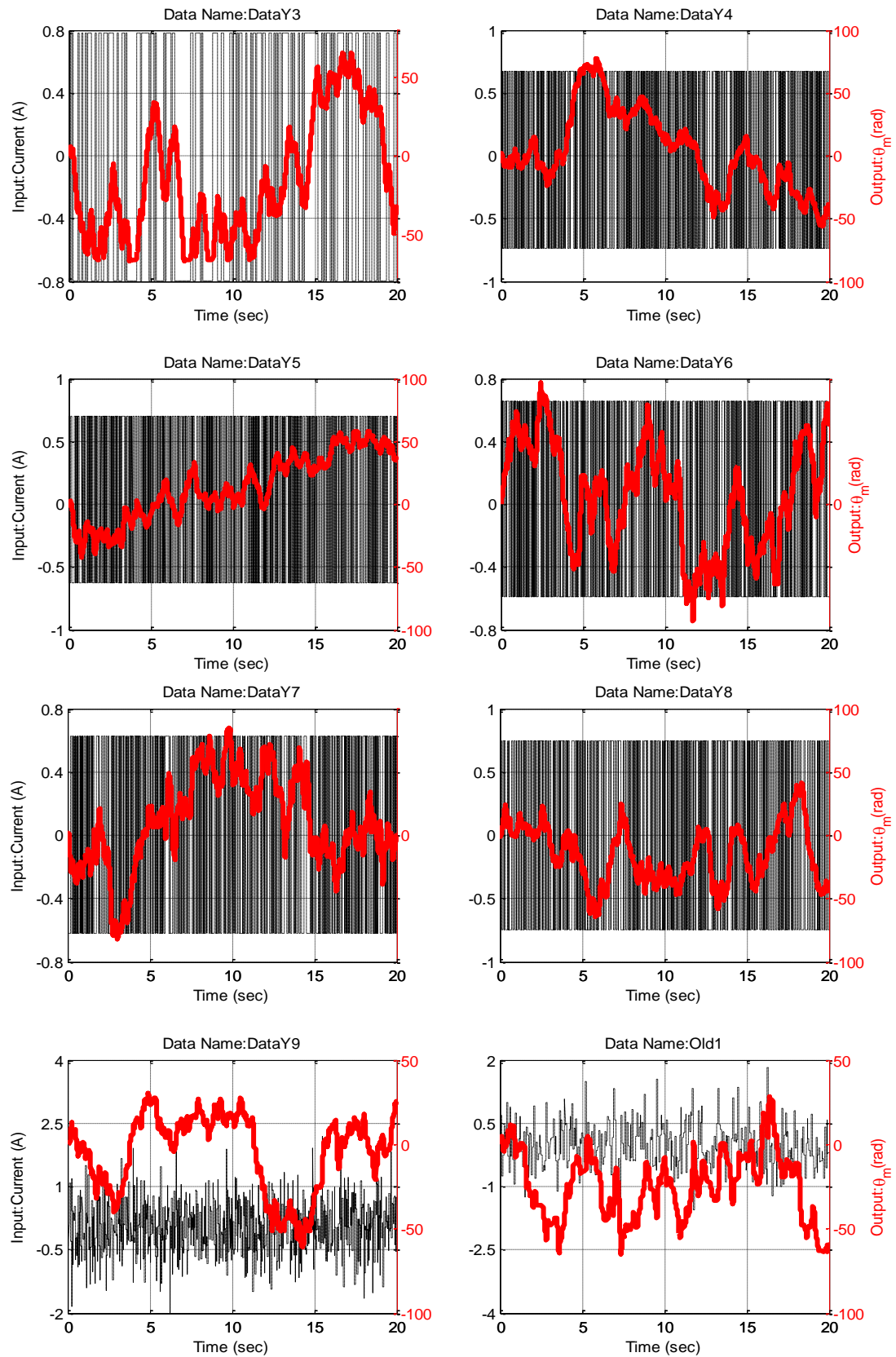
%Penalty for control signal - Wact
A=sqrt(2)/15;
Ka=A/5;
w2a=10*2*pi*A;
w1a=10*2*pi*Ka;
Wact=zpk(-w2a,-w1a,Ka);

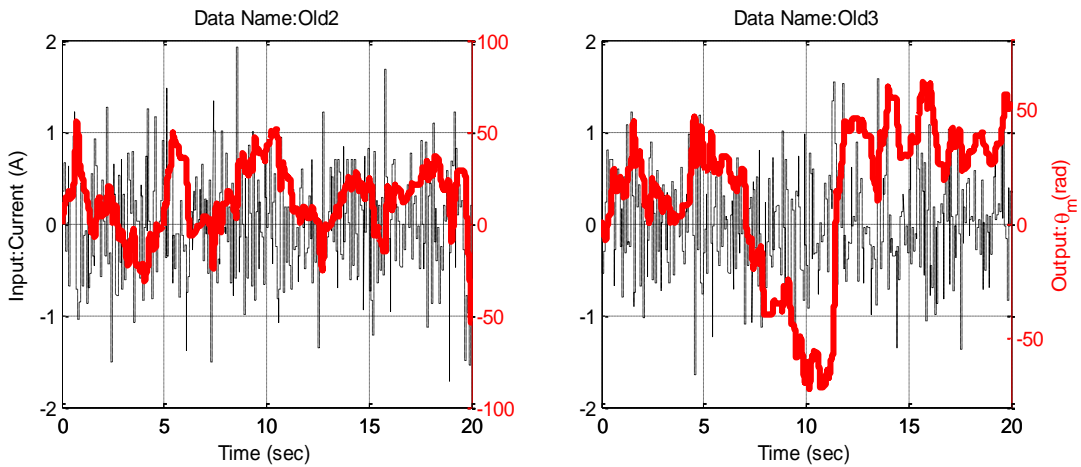
```

### A.3. System Identification Input-Outputs in Time Domain





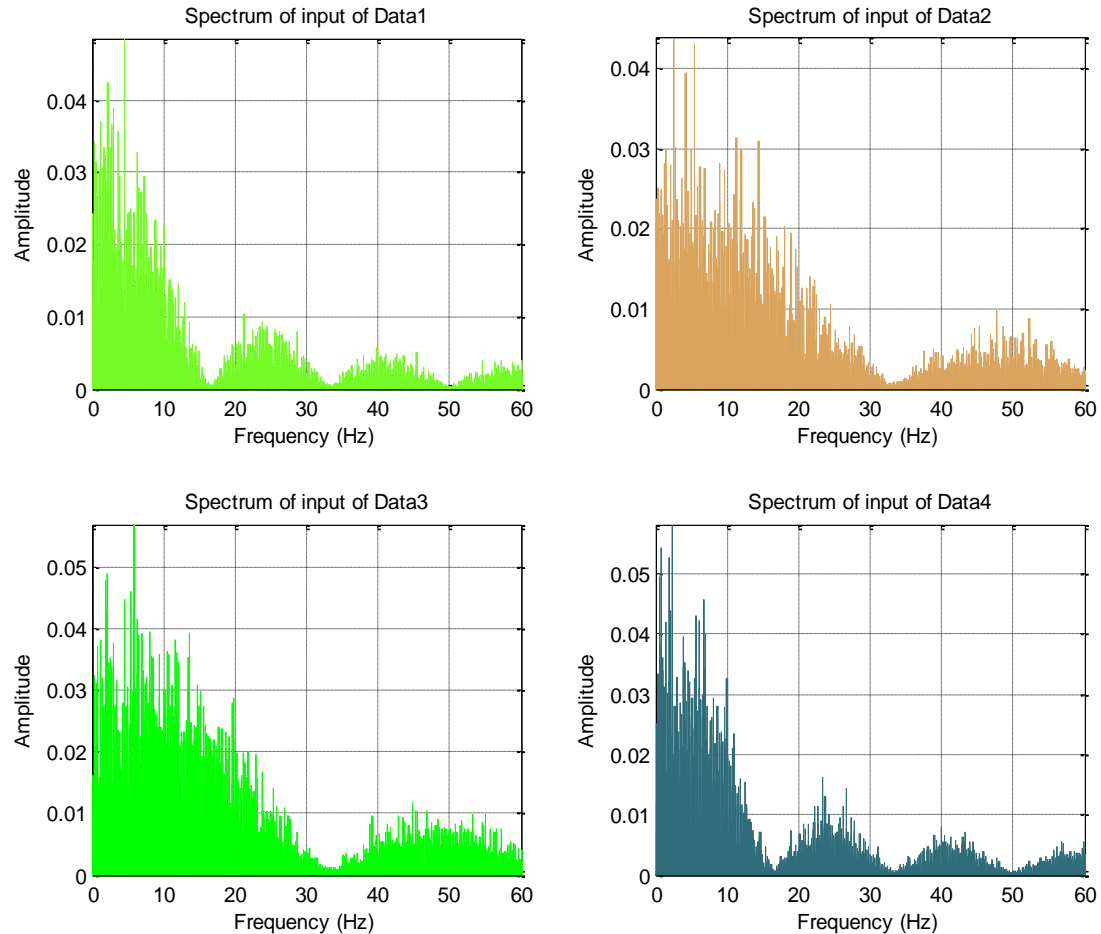


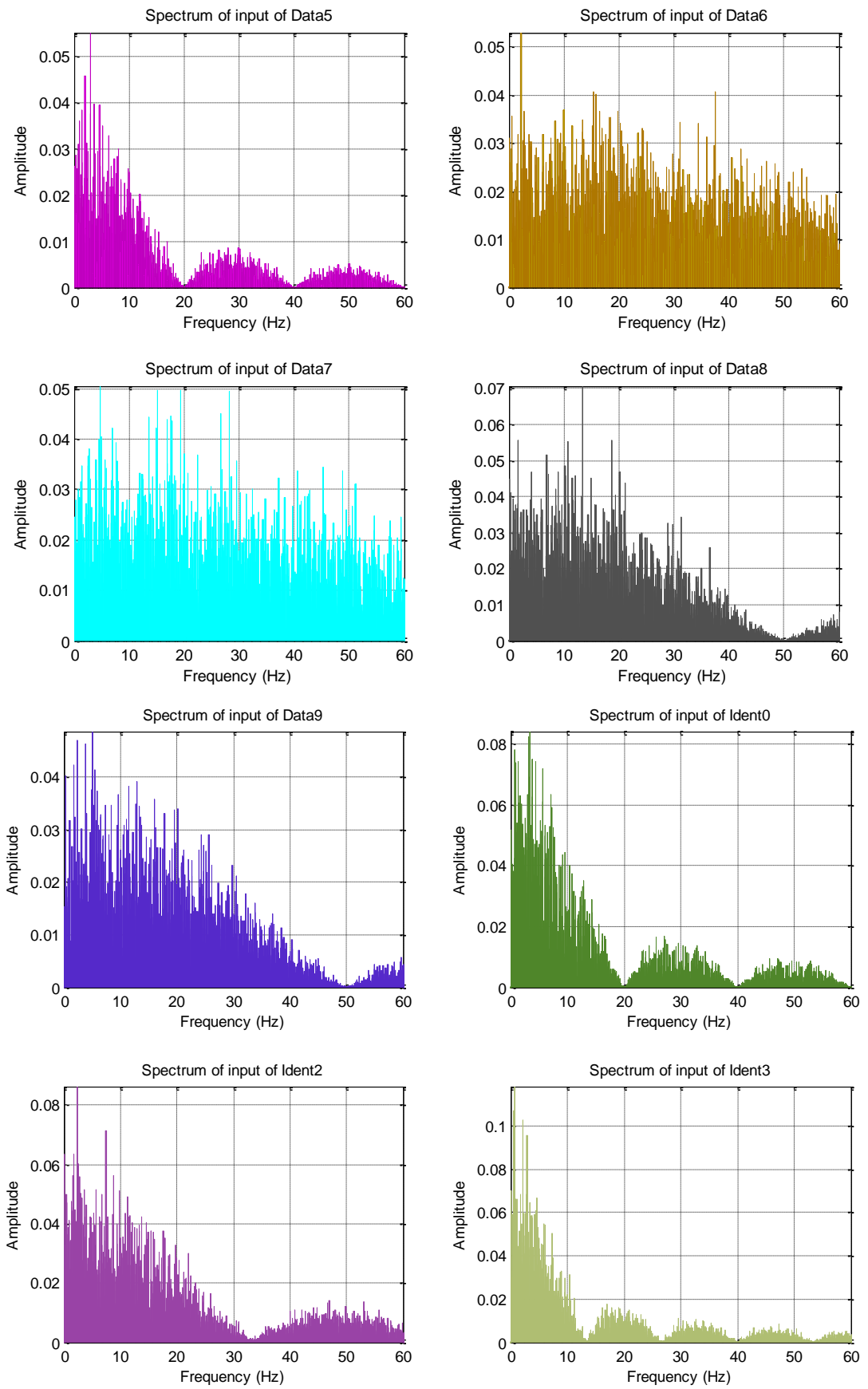


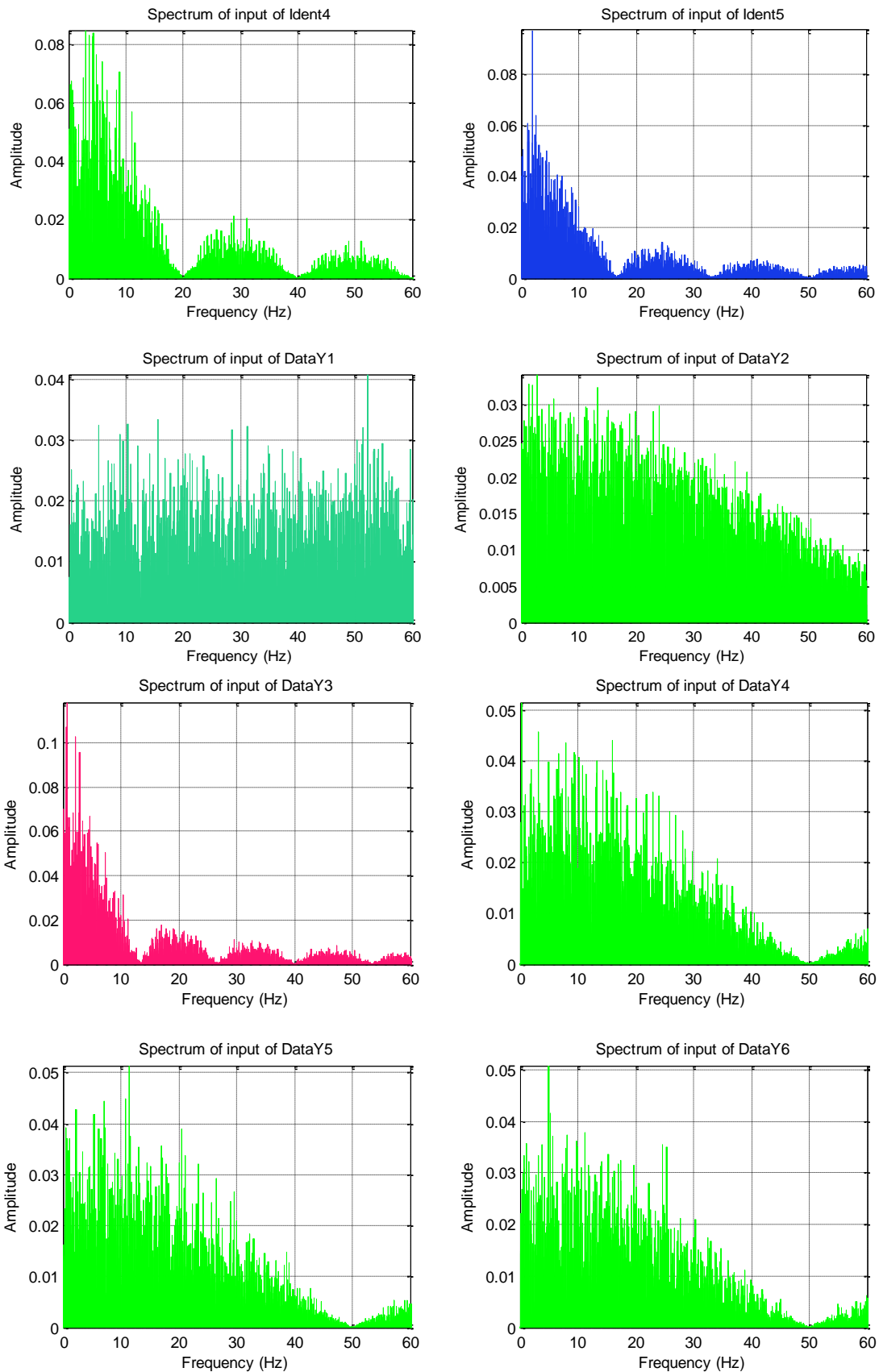
**Figure 88.** System identification of input-outputs in time domain

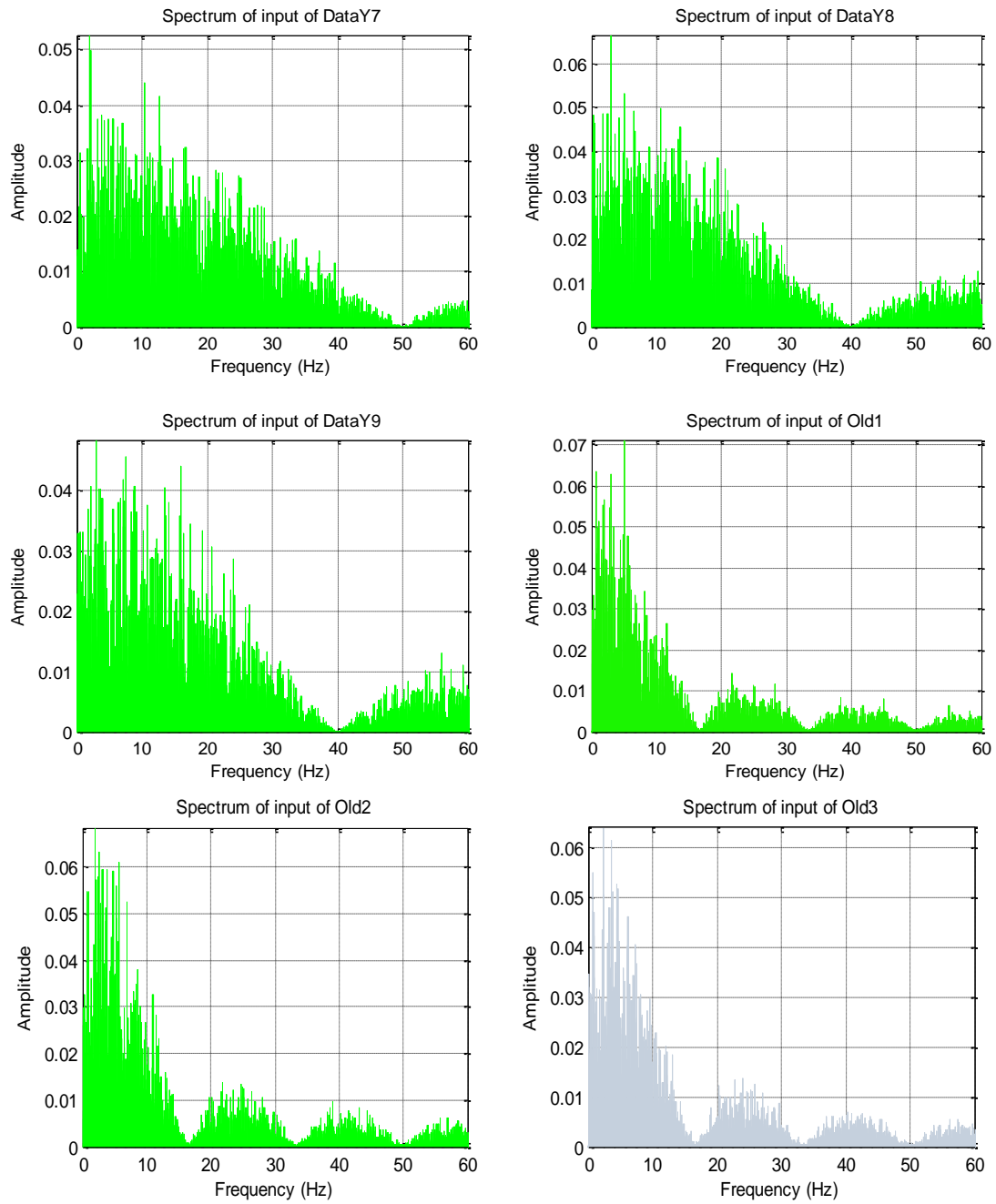
#### A.4. Frequency Spectrum of Input Signals

Frequency domain transfer function fits to all data sets yields VAF compatibility greater than 90%. The green-colored datasets give VAF compatibility larger than 70% in time domain at the same time.



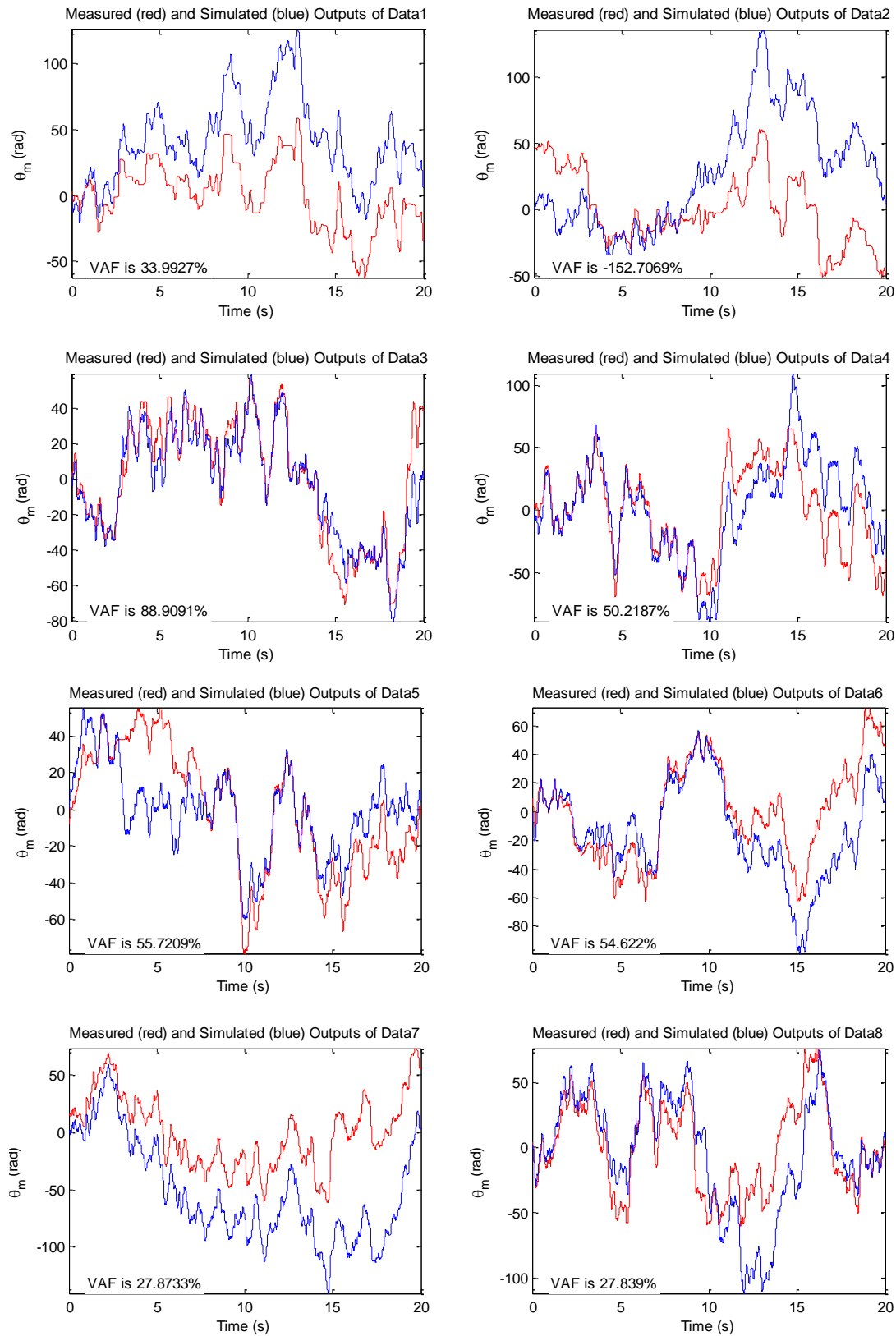


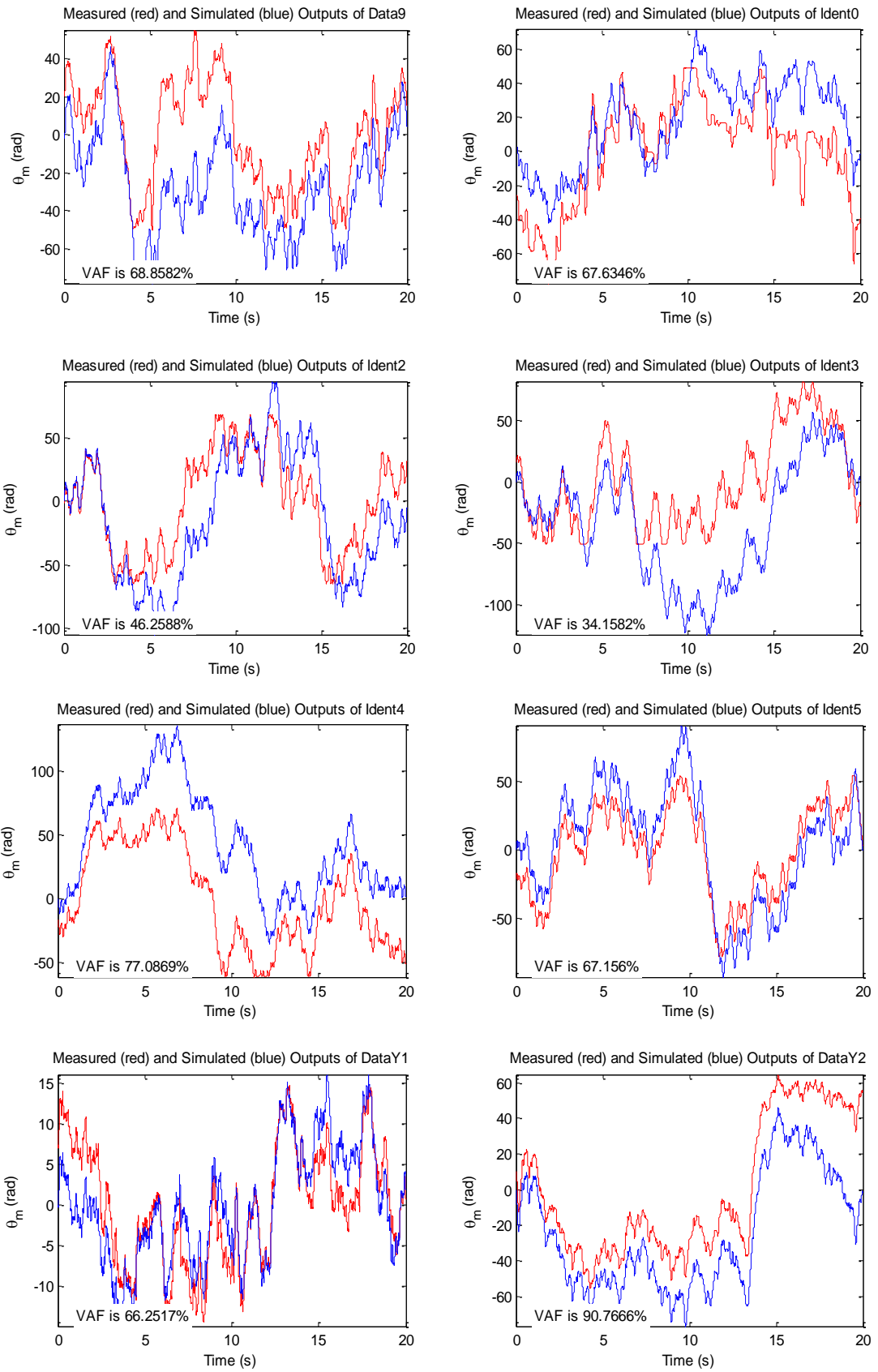


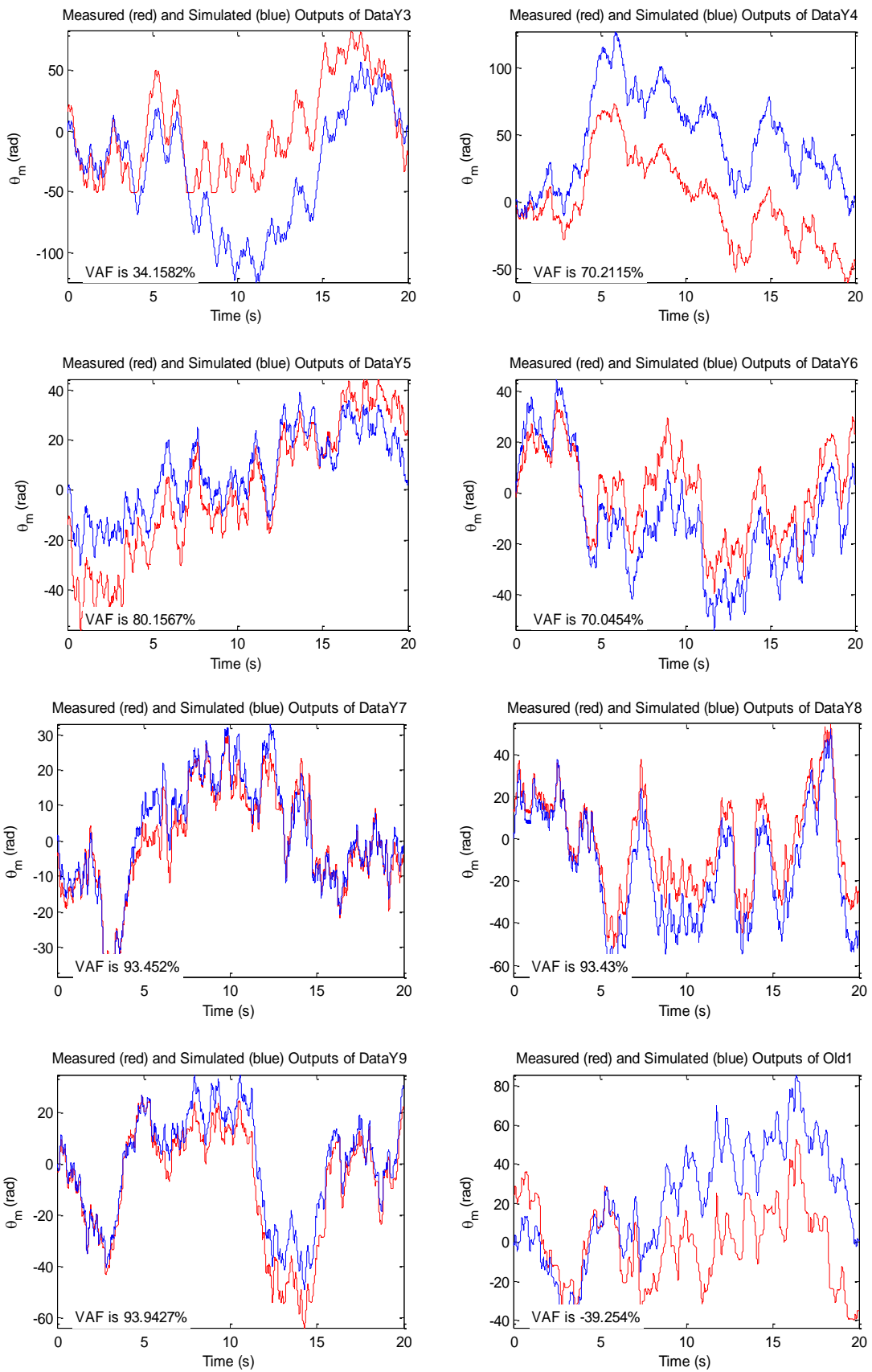


**Figure 89.** Frequency spectrum of input signals.

### A.5. Time Domain Comparison of Bode Estimations







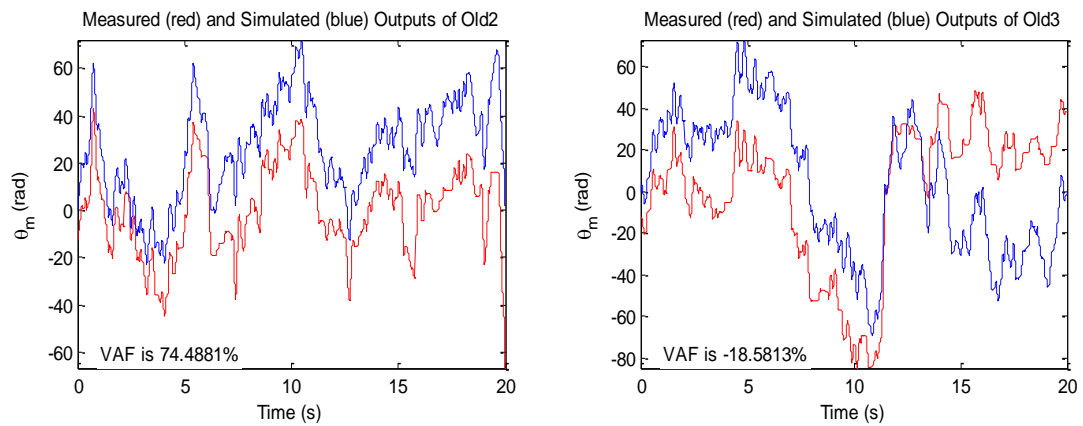


**Figure 90.** Time domain comparison of estimation results.

#### A.6. Photo of the System

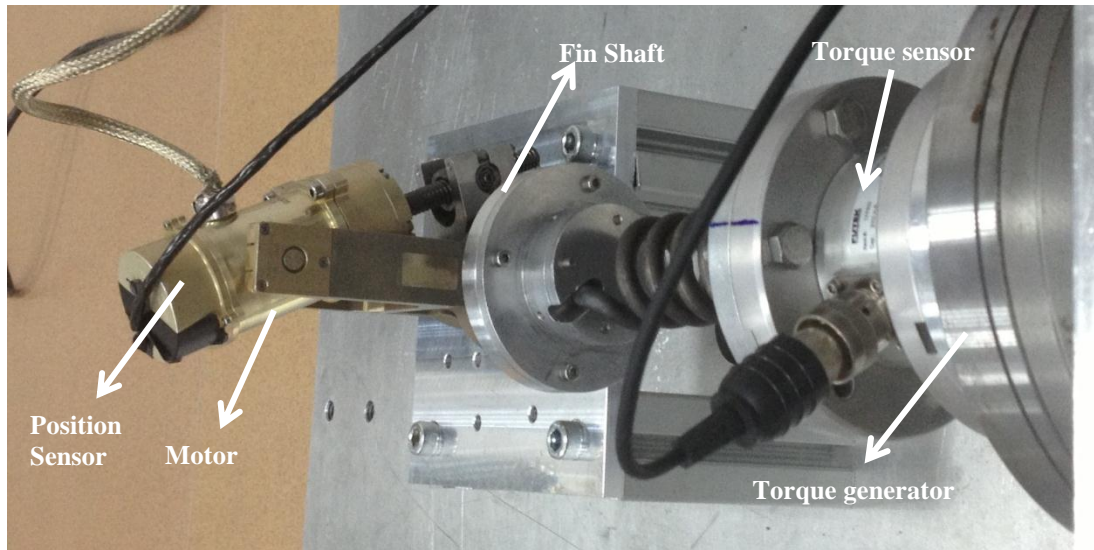


**Figure 91.** Photo of the experimental set up including the plant